NOTICE

The quality of this microform is heavily dependent upon the quality of the original thesis submitted for microfilming. Every effort has been made to ensure the highest quality of reproduction possible.

If pages are missing, contact the university which granted the degree.

Some pages may have indistinct print especially if the original pages were typed with a poor typewriter ribbon or if the university sent us an inferior photocopy.

Reproduction in full or in part of this microform is governed by the Canadian Copyright Act, R.S.C. 1970, c. C-30, and subsequent amendments.

AVIS

La qualité de cette microforme dépend grandement de la qualité de la thèse soumise au microfilmage. Nous avons tout fait pour assurer une qualité supérieure de reproduction.

S'il manque des pages, veuillez communiquer avec l'université qui a conféré le grade.

La qualité d'impression de certaines pages peut laisser à désirer, surtout si les pages originales ont été dactylographiées à l'aide d'un ruban usé ou si l'université nous a fait parvenir une photocopie de qualité inférieure.

La reproduction, même partielle, de cette microforme est soumise à la Loi canadienne sur le droit d'auteur, SRC 1970, c. C-30, et ses amendements subséquents.

Canada

HIGHER ORDER QCD CORRECTIONS

TO

PROCESSES WITH POLARIZED PARTICLES

by

Basim Kamal

A Thesis submitted to the Faculty of Graduate Studies and Research in partial fulfillment of the requirements of the degree of Doctor of Philosophy.

Department of Physics

McGill University

Montreal, Quebec

Canada

April 1995

National Library
of Canada

Acquisitions and
Bibliographic Services Branch

395 Wellington Street
Ottawa, Ontario
K1A 0N4

Bibliothèque nationale
du Canada

Direction des acquisitions et
des services bibliographiques

395, rue Wellington
Ottawa (Ontario)
K1A 0N4

Your file Votre référence

Our file Notre référence

ISBN 0-612-08119-2

Canada

To my parents and Rammie

Abstract

QCD higher order corrections (HOC) to three processes are considered: (i) Direct photon production in longitudinally polarized hadron-hadron collisions with numerical applications to proton-proton collisions; (ii) lepton-pair production in transversely polarized hadron-hadron collisions with numerical applications to proton-proton collisions; (iii) heavy quark pair production by polarized and unpolarized photons. The HOC to all three processes are found to be significant. Processes (i) and (ii) are shown to be sensitive probes of the proton's polarized gluon distribution and the transversity distributions, respectively. The asymmetries are found to exhibit perturbative stability. Process (iii) is considered as a background to $\gamma\gamma \rightarrow H^* \rightarrow b\bar{b}$ (standard model). As well, top-quark production not too far above threshold is considered.

Résumé

Dans le cadre de CDQ, des corrections d'ordre supérieur (COS) pour trois réactions sont considérées: (i) Production directe de photons provenant des collisions des hadrons polarisés longitudinalement avec des applications numériques aux collisions proton-proton; (ii) production des paires de leptons provenant de la collision de hadrons polarisés transversalement, avec des applications numeriques aux collisions proton-proton; (iii) production des paires des quarks lourds par des photons polarisés et non-polarisés. Pour chacune de ces trois réactions on trouve des COS substantielles. On montre que les réactions (i) et (ii) sont des détecteurs sensibles dans le proton des distributions de gluons polarisés et de transversités respectivement. On trouve que les asymétries sont characterisées par une stabilité perturbative. Réaction (iii) est considerée comme un fond au $\gamma\gamma \to H^* \to b\bar{b}$ (modèle standard). On considere aussi la production de top-quarks prés de seuil.

Original Contributions to Knowledge

In chapter 3, we present the first complete calculation of HOC to large-p_T direct photon production in polarized hadron-hadron collisions, with numerical applications to proton-proton collisions, and examine it as a probe of the proton's polarized gluon distribution. In chapter 4, we present complete next-to-leading order analytical results for the production of lepton-pairs in transversely polarized hadron-hadron collisions (transverse Drell-Yan), determined for the first time using *dimensional methods*, with numerical applications to proton-proton collisions. This process is examined as a probe of the proton's transversity distributions. In chapter 5, we present the first complete analytical results, and numerical applications as well, for the production of heavy-quark pairs in polarized and unpolarized photon-photon collisions in next-to-leading order. This process is considered as a background to the process $\gamma\gamma \to H^* \to b\bar{b}$. As well, top-quark production, not too far above threshold is considered. Various useful information is presented in the appendixes, including a novel counterterm relevant to dimensional reduction and novel parameterizations of the proton's polarized parton distributions.

Acknowledgments

I would like to express great thanks and indebtedness to my supervisor, Prof. A.P. Contogouris, not only for suggesting these projects, but also for many careful teachings and very fruitful collaboration in addition to his essential supervision. Secondly, I thank Z. Merebashvili for his excellent collaboration. I give thanks to F.V. Tkachov and S. Papadopoulos for their help in the early stages of this work. Also, I am greatful to Professors Margolis, Sharp and Svec for all their help, as well as all the other professors who gave me an excellent education at McGill. I would like to thank J. Zhang for many lengthy discussions and the other graduate students in room 345. Last, but not least, I thank my father for all his help and my mother for her encouragement.

Contents

List of Figures

Chapter 1

Introduction

Over the past two decades, the search for a theory of strong interactions has spawned Quantum Chromodynamics (QCD) as the only plausible theory explaining such interactions. It is the strong force which binds quarks to form hadrons and is responsible for holding nuclei together. The only fundamental fermions which feel the strong force are the quarks. As in Quantum Electrodynamics (QED), the theory of electromagnetic interactions, there are no "action at a distance" forces. It is possible to describe interactions as occurring via the interchange of gauge bosons: the *gluon* in QCD, the *photon* in QED. Both the gluon and the photon are required to be massless due to local gauge invariance.

The weak interactions, on the other hand, are mediated by massive vector bosons, the Z^0 and $W^{\pm}$. Local gauge invariance normally requires all vector bosons to be massless. For the weak interactions, the masses come about via the Higgs mechanism. The Higgs ground state is not symmetric under SU(2)×U(1) gauge transformations. This is known as *spontaneous symmetry breaking* by the ground state. Since we must apply perturbation theory about the ground state, we now generate masses for the Z^0 and $W^{\pm}$ fields. In the quantum theory, spontaneous symmetry breaking implies a nonzero vacuum expectation value. The success of the electroweak theory thus

necessitates the existence of the (still undiscovered) Higgs boson, which is massive and has spin 0. The Higgs mass is not fixed by the standard model, but the LEP data imply[1]

$$m_H > 58 \text{ GeV}. \tag{1.1}$$

We label quarks by their flavor: u (up), d (down), s (strange), c (charm), b (bottom), t (top - recently discovered[2]), and for every quark there is an antiquark. Quarks possess an additional quantum number, *color* (red, green, or blue), which the leptons do not possess. It is this color which is responsible for the strong force. The additional degree of freedom that color provides helps ensure that the Pauli Principle is satisfied for baryons such as the Δ^{++}, whose ground state would otherwise be a symmetric 3-quark state in violation of the Pauli Principle.

Since the strong force is color independent we may impose SU(3) local gauge invariance on the QCD Lagrangian density. The SU(3) group is non-Abelian since its generators are non-commuting. This non-Abelian nature leads to gluon-gluon couplings. There are no photon-photon couplings in QED since its Lagrangian density posesses only U(1) local gauge invariance, and the U(1) group is Abelian.

Both QCD and the electroweak theory are *renormalizable* gauge theories. By renormalizable, we mean that it is possible to absorb the infinities associated with diagrams into physical quantities, like the coupling and the mass. This is possible since such infinities arise from a finite number of configurations (i.e. vertex, self energy graphs). Hence, one may introduce general counterterms, whose form is valid to all orders of perturbation theory.

In QCD, due to the gluon-gluon interaction, the coupling approaches zero as the energy scale of the process, Q^2, increases (i.e. as the quark separation decreases) and

vice-versa, provided that the number of flavors is less than or equal to 16 (which is the case at presently attainable energies). This property of the coupling approaching zero with increasing Q^2 is known as *asymptotic freedom*. As a result, we may apply perturbation theory for large Q^2 in QCD. It is believed that quarks may not be observed in isolation. One expects this since the coupling increases as the quark separation increases.

In this thesis we apply perturbative QCD to calculate higher order corrections (HOC) to certain processes with polarized particles. In QCD, the HOC are very important since they are usually quite large, and sometimes new features develop beyond leading order. As well, in polarized hadron-hadron collisions, the perturbative stability of the asymmetry is of great interest for the determination of the polarized parton distributions. Inclusion of HOC also increases stability against changes in the scale parameters and against process dependences of the parton distributions.

In the remaining part of the Introduction, we first present certain basic elements of QCD, the parton model and hadronic structure. We also discuss recent experimental developments and future prospects in spin physics. In chapter 2, we examine and present estimates of the proton's polarized parton distributions. Then, we give the relevant background on regularization and renormalization, in order to make the subsequent chapters clear. In chapter 3, we present the first complete calculation of HOC to large-p_T direct photon production in polarized hadron-hadron collisions, with numerical applications to proton-proton collisions, and examine it as a probe of the proton's polarized gluon distribution. In chapter 4, we present complete next-to-leading order analytical results for the production of lepton-pairs in transversely polarized hadron-hadron collisions (transverse Drell-Yan), determined for the first time using *dimensional methods*, with numerical applications to proton-proton colli-

sions. This process is examined as a probe of the proton's transversity distributions. In chapter 5, we present the first complete analytical results, and numerical applications as well, for the production of heavy-quark pairs in polarized and unpolarized photon-photon collisions in next-to-leading order. This process is considered as a background to the process $\gamma\gamma \to H^* \to b\bar{b}$. As well, top-quark production, not too far above threshold is considered. Various useful information is presented in the appendixes, including a novel counterterm relevant to dimensional reduction and novel parameterizations of the proton's polarized parton distributions.

1.1 Quantum Chromodynamics

We may infer the structure of QCD from SU(3) local gauge invariance. The free Lagrangian is

$$\mathcal{L}_0 = \bar{\psi}_k^\alpha (i\gamma^\mu \partial_\mu - m_k)\psi_k^\alpha \tag{1.2}$$

with the ψ_k^α ($\bar{\psi}_k^\alpha$) being the quark (antiquark) fields of color α ($= 1, 2, 3$) and flavor k ($= 1, \ldots, N_f$) with N_f the number of flavors. Here, m_k is the mass of a quark of flavor k. Throughout, we assume the standard convention of summation over repeated indices (of all types).

The gauge invariant Lagrangian is required to be invariant under the infinitesimal transformation

$$\psi_k^\alpha(x) \to [\delta^{\alpha\beta} + i\epsilon_a(x)T_a^{\alpha\beta}]\psi_k^\beta(x), \tag{1.3}$$

with $T_a \equiv \lambda_a/2$ ($a = 1, \ldots, 8$) the SU(3) generators and $\epsilon_a(x)$ a space-time dependent infinitesimal. The λ_a are the Gell-Mann matrices; therefore, the T_a satisfy the relation

$$[T_a, T_b] = i f_{abc} T_c, \tag{1.4}$$

where f_{abc} is the antisymmetric SU(3) structure constant. The gauge invariant Lagrangian is found to take the form

$$\mathcal{L}_{\rm GI} = \bar{\psi}^a_k(i\gamma^\mu\partial_\mu - m_k)\psi^a_k + g(\bar{\psi}^\alpha_k\gamma_\mu T^{\alpha\beta}_a\psi^\beta_k)G^\mu_a - 1/4\ G^a_{\mu\nu}G^{\mu\nu}_a. \tag{1.5}$$

where g is the strong unit charge. In order to preserve gauge invariance, we had to replace the regular derivative in (1.2) by the *covariant derivative*,

$$D_\mu = \partial_\mu - igT_aG^a_\mu. \tag{1.6}$$

and introduce the eight gauge fields G^a_μ with the SU(3) transformation properties

$$G^a_\mu \rightarrow G^a_\mu + 1/g\ \partial_\mu\epsilon_a - f_{abc}\epsilon_bG^c_\mu. \tag{1.7}$$

In addition, we introduced the field strength tensor defined by

$$G^a_{\mu\nu} = \partial_\mu G^a_\nu - \partial_\nu G^a_\mu + gf_{abc}G^b_\mu G^c_\nu. \tag{1.8}$$

We can see from (1.5) that there are terms cubic and quartic in G, which lead to the 3-gluon and 4-gluon vertices, respectively.

There are other subtleties involved though. Using a covariant gauge, $\partial^\mu G^a_\mu = 0$, we have the freedom to write the free wave equation for G^a_μ as

$$[g^{\nu\mu}\Box^2 - (1 - 1/\xi)\partial^\nu\partial^\mu]G^a_\mu = 0. \tag{1.9}$$

The *gauge parameter*, ξ, determines the gauge: $\xi = 1$ for the Feynman gauge (which we generally use in our calculations), $\xi = 0$ for the Landau gauge, etc ... . As a result, we must add to the Lagrangian a gauge fixing term defined by[3]

$$\mathcal{L}_{gf} = -1/2\xi\ (\partial^\mu G^a_\mu)^2. \tag{1.10}$$

By including a set of "ghost" fields, η^a ($a = 1, \ldots, 8$), known as the Faddeev-Popov[4] ghosts, we may cancel unphysical contributions occuring in closed gluon loops. We thus add a ghost term to the Lagrangian.

$$\mathcal{L}_{\text{ghost}} = \partial^\mu \bar{\eta}^a \overbrace{(\partial_\mu \delta^{ac} - g f_{abc} G^b_\mu)}^{\equiv D^{ac}_\mu} \eta^c. \tag{1.11}$$

The ghost-field technique is useful in calculating higher order corrections since the ghost field interacts only with gluons (not quarks), leading to a gluon-ghost vertex. The final QCD Lagrangian is given by

$$\mathcal{L} = \mathcal{L}_{\text{GI}} + \mathcal{L}_{\text{gf}} + \mathcal{L}_{\text{ghost}} \tag{1.12}$$

where the various parts are given by (1.5), (1.10) and (1.11).

In order to obtain the Feynman rules, we must second quantize. We may either use the path integral approach[5] or the canonical operator formalism.[6] In the path integral approach, the fermion and ghost fields are treated as Grassman numbers (mutually anticommuting). In the canonical approach, they are mutually anticommuting field operators. Having added $\mathcal{L}_{\text{gf}}$ and $\mathcal{L}_{\text{ghost}}$ to $\mathcal{L}_{\text{GI}}$, the classical Lagrangian (1.12) is no longer gauge invariant under the transformations (1.3), (1.7). After quantization, we may ask if the full quantum Lagrangian posesses any particular symmetry.

Fortunately, the final quantum Lagrangian *is* invariant under the local gauge transformations

$$\begin{aligned}
\psi^\alpha_k(x) &\rightarrow [\delta_{\alpha\beta} - i\hat{\epsilon} g T^a_{\alpha\beta} \eta^a_2] \psi^\beta_k(x) \\
G^a_\mu &\rightarrow G^a_\mu - \hat{\epsilon} D^{ab}_\mu \eta^b_2 \\
\eta^a_1 &\rightarrow \eta^a_1 - i\hat{\epsilon} \frac{1}{\xi} \delta^\mu G^a_\mu \\
\eta^a_2 &\rightarrow \eta^a_2 + \frac{1}{2} \hat{\epsilon} g f^{abc} \eta^b_2 \eta^c_2
\end{aligned} \tag{1.13}$$

where

$$\eta^a \equiv (\eta_1^a + i\eta_2^a)/\sqrt{2} \tag{1.14}$$

and we have made the ansatz

$$\epsilon^a(x) = -g\hat{\epsilon}\eta_2^a(x). \tag{1.15}$$

The transformation (1.13) is known as the BRS[7] (Becchi-Rouet-Stora) transformation.

1.2 General Structure and Spin Structure of Hadrons

We use the *parton model*[8,9,10] (PM) in calculating cross sections for high energy collisions involving hadrons. We call the constituents (quarks and gluons) of the hadrons *partons*. The PM asserts that during scattering processes we may treat the partons of each of the hadrons involved as noninteracting particles sharing the parent hadron's momentum. These partons interact with the partons of *other* hadrons and with incident leptons and photons. Examples of such processes to be considered in this thesis are: *the Drell-Yan process* – the production of lepton pairs, and *direct photon production* (at large momentum transfer) – the production of photons not created by secondary decay processes, both in hadron–hadron collisions.

The PM is justified through the *impulse approximation*, according to which, the time scale on which colliding partons interact is much shorter than the time scale on which partons belonging to the same hadron interact. If Q is taken as the large momentum transfer of the process, then interactions between colliding partons occur on a time-scale of order $1/Q$, decreasing with increasing Q. It can be shown that, due to relativistic time dilation and parton confinement, interactions between partons belonging to the same hadron occur on a much longer time-scale. Therefore, we

assume that any given subprocess will involve only one parton from a particular hadron and that the other partons are merely "spectators". The PM also arises as the first term in the operator product expansion for processes such as deep-inelastic scattering.

We may formulate the PM mathematically by considering the contribution of the subprocess $a(x_a P_A) + b(x_b P_B) \rightarrow c(P_C/z) + x$ to the process $A(P_A) + B(P_B) \rightarrow C(P_C) + X$, where the small letters represent partons, the capital letters represent observed particles (x, X are arbitrary sets of final products), and where x_a, x_b, z denote momentum fractions. Since we work at high energy scales, initial state partons and hadrons are taken as *massless*.

The differential of the inclusive cross section, at energy scale Q^2, is given by

$$d\sigma = \sum_{abc} \int_0^1 \frac{dx_a}{x_a} \frac{dx_b}{x_b} \frac{dz}{z^2} F_{a/A}(x_a, Q^2) F_{b/B}(x_b, Q^2) \mathcal{D}_{C/c}(z) d\hat{\sigma}_{abc} + (1 - \delta_{ab})[A \leftrightarrow B], \tag{1.16}$$

where $d\hat{\sigma}_{abc}$ is the differential of the subprocess cross section, the $F_{i/I}(x_i, Q^2)$ are the *parton momentum distributions* defined by

$$F_{i/I}(x_i, Q^2) = x_i f_{i/I}(x_i, Q^2) \tag{1.17}$$

with $f_{i/I}(x_i, Q^2)$ being the *probability density* for finding parton i with momentum $x_i P_I$ in hadron I which has momentum P_I. The function $\mathcal{D}_{C/c}(z)$ is the *parton fragmentation function* representing the probability density for parton c to fragment into particle C with momentum fraction z. If $c = C$, then $\mathcal{D}_{C/c}(z) = \delta(1 - z)$ and c need not be a parton. Similarly, if $a = A$ or $b = B$.

In this thesis, we are interested in processes with *polarized* beam and target, so we consider the polarization of the partons *as well as* their momentum fraction (with respect to the parent hadron) in calculating cross sections and asymmetries.

To obtain from (1.16) the differential of the corresponding *longitudinally* polarized cross section for the process $\vec{A} + \vec{B} \rightarrow C + X$ (i.e. longitudinally polarized beam and target), we make the substitutions

$$\begin{aligned} d\sigma &\rightarrow \Delta d\sigma \equiv 1/2\,[d\sigma(++) - d\sigma(+-)], \\ d\hat{\sigma} &\rightarrow \Delta d\hat{\sigma} \equiv 1/2\,[d\hat{\sigma}(++) - d\hat{\sigma}(+-)], \\ F(x,Q^2) &\rightarrow \Delta F(x,Q^2) \equiv F^{+/+}(x,Q^2) - F^{-/+}(x,Q^2), \end{aligned} \tag{1.18}$$

since, by parity conservation and time reversal invariance,

$$d\hat{\sigma}(-\pm) = d\hat{\sigma}(+\mp), \qquad F^{\pm/-} = F^{\mp/+}, \tag{1.19}$$

where the $+,-$ signs in $d\sigma(+\pm)$ represent the *hadronic* helicities of A, B, respectively, and in $d\hat{\sigma}(+\pm)$ they represent the *partonic* helicities of a, b. In $F^{\pm/+}$, the first sign represents the parton helicity and the second sign represents its parent hadron's helicity – these are the longitudinally polarized momentum distributions. We may similarly substitute

$$f(x,Q^2) \rightarrow \Delta f(x,Q^2) \equiv f^{+/+}(x,Q^2) - f^{-/+}(x,Q^2) \tag{1.20}$$

for the longitudinally polarized densities. The explicit representations of the unpolarized quantities are:

$$\begin{aligned} d\sigma &= 1/2\,[d\sigma(++) + d\sigma(+-)] \\ d\hat{\sigma} &= 1/2\,[d\hat{\sigma}(++) + d\hat{\sigma}(+-)] \\ F(x,Q^2) &= F^{+/+}(x,Q^2) + F^{-/+}(x,Q^2). \end{aligned} \tag{1.21}$$

Now suppose hadrons A, B are *transversely* polarized, i.e. we have the process $A_\uparrow + B_\uparrow \rightarrow C + X$; the up-arrows indicating transverse polarization with respect to

some fixed spin directions S_A, S_B. Then, all the argumentation used to go from unpolarized to longitudinally polarized reactions holds for transversely polarized processes as well. We simply make the substitutions.

$$\Delta \to \Delta_T, \qquad + \to \uparrow, \qquad - \to \downarrow \tag{1.22}$$

everywhere. Analogously, we call

$$\Delta_T F(x, Q^2) = x \Delta_T f(x, Q^2) \tag{1.23}$$

the *transversity* momentum distributions and $\Delta_T f(x, Q^2)$ the transversity densities. The $f_{i/I}^{\uparrow\uparrow/\uparrow\downarrow}(x, Q^2)$ represent the probability of quark i having the same (opposite) transversity as hadron I (gluons cannot be transversely polarized). The transversity operator

$$T_p(s) = \gamma_5 \not{s} \tag{1.24}$$

has the property

$$T_p(s) u(p, \pm s) = \pm u(p, \pm s) \tag{1.25}$$

with

$$s \cdot p = 0, \qquad s^2 = -1, \qquad s^\mu = (0, \mathbf{s}) \quad \text{(in rest frame of } p\text{)}, \tag{1.26}$$

where $\mathbf{s}$ is transverse to p. Since s is invariant under boosts along p, the transversity operator (and transversity eigenvalue) is also invariant under such boosts. In general, the operator $(1 + \gamma_5 \not{s})/2$ projects out the spinor pointing in the $\mathbf{s}$ direction in the rest frame of p.

Originally, in the *naive* PM, the gluons played no role and the distributions $F_{i/I}$ were merely functions of the scaling variable x. But, due to gluon radiative corrections and the presence of a gluon distribution, scaling is violated and the parton distributions are seen to vary as functions of both x and Q^2.

Figure 1.1: Deep-inelastic scattering.

In general, one needs to know the polarized momentum distributions for arbitrary Q^2. If they are known for some value of $Q^2 = Q_0^2$, they may be evolved to any value of Q^2 (see Sect. 2.3.2). For the unpolarized distributions, various parameterized forms already exist as a function of x and Q^2. Therefore, given the polarized distributions at some Q_0^2, we have all the means necessary to compute cross sections in hadronic collisions at any value of Q^2.

There are also non-parton model, *higher twist*, contributions, in which the hadron as a whole interacts. They drop off as $\sim 1/Q$ and are expected to be negligible for most of the Q considered in this work. There are also many great uncertainties associated with their determination. Hence we do not consider them.

Deep inelastic scattering (DIS) of polarized leptons off a polarized hadron target serves as a good means to determine a hadron's longitudinally polarized parton structure. This process was first studied in detail in the experiment of the European Muon Collaboration (EMC)[11] (combined with earlier SLAC data[12]), in which leptons (μ^+) polarized longitudinally were scattered off a longitudinally polarized proton target.

To see how this experiment leads to a determination of the spin dependent proton

structure function, consider the high energy inclusive reaction (Fig. 1.1):

$$\mu^+(k) + \mathrm{p}(P) \rightarrow \mu^+(k') + X, \qquad k \equiv (E, \mathrm{k}),\ k' \equiv (E', \mathrm{k}'). \tag{1.27}$$

The virtual photon 4-momentum is $q = k - k'$. The initial proton state will be denoted by $|P, s\rangle$, where P is the proton 4-momentum and s is a 4-vector denoting the proton spin, satisfying $s \cdot P = s^2 + 1 = 0$.

The differential of the inclusive cross section for the process (1.27) has the form[3,13]:

$$d\sigma = \frac{\alpha^2}{(q^2)^2} L^{\mu\nu} W_{\mu\nu} \frac{d^3\mathrm{k}'}{EE'}. \tag{1.28}$$

Here $L_{\mu\nu}$ is the lepton tensor, describing the interaction of the virtual photon with the muon. In general, it is given by the expression ($\not{k} \equiv k^\mu \gamma_\mu$)

$$L_{\mu\nu} = \frac{1}{2}\mathrm{Tr}[(\not{k}' + m_m)\gamma_\mu(\not{k} + m_m)\gamma_\nu] + 2im_m\varepsilon_{\mu\nu\rho\sigma}q^\rho(s_m)^\sigma, \tag{1.29}$$

where m_m is the muon mass and s_m is a 4-vector denoting the initial muon spin. $W_{\mu\nu}$ is the hadronic tensor, which parameterizes in a general way the structure of the nucleon: it is given by the formal expression[3]

$$W_{\mu\nu} = \frac{1}{2\pi}\int d^4\xi e^{iq\cdot\xi}\langle P, s|[J_\mu(\xi), J_\nu(0)]|P, s\rangle. \tag{1.30}$$

$J_\mu(x)$ is the electromagnetic current operator, given by

$$J_\mu(x) = \sum_q e_q \bar{\psi}_q(x)\gamma_\mu\psi_q(x), \tag{1.31}$$

where the sum runs over all quark flavors and the $\psi_q(x)$ are the corresponding quark fields. We may express the hadronic tensor as follows:

$$W_{\mu\nu} = W^S_{\mu\nu} + iW^A_{\mu\nu}. \tag{1.32}$$

$W^S_{\mu\nu}$ is a real symmetric tensor which describes the process (1.27) with unpolarized μ^+ and **p**. Taking into account Lorentz invariance, parity conservation and current conservation, $W^S_{\mu\nu}$ takes the form

$$m_p W^S_{\mu\nu} = \left(-g_{\mu\nu} + \frac{q_\mu q_\nu}{q^2}\right) F_1 + \left(P_\mu - q_\mu \frac{P\cdot q}{q^2}\right)\left(P_\nu - q_\nu \frac{P\cdot q}{q^2}\right)\frac{F_2}{P\cdot q}, \qquad (1.33)$$

where m_p is the proton mass, and F_1, F_2 are the *spin independent* nucleon structure functions which are, in general, functions of $Q^2 \equiv -q^2$ and

$$\nu \equiv \frac{P\cdot q}{m_p}, \qquad (1.34)$$

or of Q^2 and

$$x \equiv \frac{Q^2}{2P\cdot q}. \qquad (1.35)$$

$W^A_{\mu\nu}$ is an antisymmetric tensor which arises for the process (1.27) with polarized μ^+ and **p**, and is given by

$$W^A_{\mu\nu} = \varepsilon_{\mu\nu\rho\sigma} q^\rho \left\{ m_p s^\sigma G_1 + \left(\frac{P\cdot q}{m_p} s^\sigma - \frac{q\cdot s}{m_p} P^\sigma\right) G_2 \right\}, \qquad (1.36)$$

where G_1, G_2 are structure functions which also depend, in general, on Q^2 and ν.

In the naive PM, for $\nu, Q^2 \to \infty$ such that $x = Q^2/(2m_p\nu) =$ constant, we expect to obtain structure functions which *scale*[8] (i.e. are functions of x only):

$$\begin{aligned} m_p^2 \nu G_1(Q^2,\nu) &\to g_1(x), \qquad (1.37)\\ m_p \nu^2 G_2(Q^2,\nu) &\to g_2(x), \end{aligned}$$

where g_1 and g_2 are known as the *spin dependent nucleon structure functions*. This limit is called the *Bjorken limit*. As is well known, similar properties hold for the structure functions F_1 and F_2. With the help of (1.37), it can be shown[10] that g_2 does not contribute to longitudinally polarized deep-inelastic scattering in the scaling limit.

Using (1.37), we may now express $W^A_{\mu\nu}$, defined in (1.36), in terms of g_1 and g_2:

$$W^A_{\mu\nu} = \varepsilon_{\mu\nu\rho\sigma}\frac{q^\rho}{P\cdot q}\left\{s^\sigma g_1 + \left(s^\sigma - \frac{q\cdot s}{P\cdot q}P^\sigma\right)g_2\right\}. \tag{1.38}$$

Introduce the differential cross sections

$$\frac{d\sigma(+-)}{dQ^2d\nu}, \quad \frac{d\sigma(++)}{dQ^2d\nu}, \tag{1.39}$$

where $\frac{d\sigma(+\mp)}{dQ^2d\nu}$ is the cross section when the muon-proton spins are antiparallel (parallel). The difference of these two cross sections is given by[11,13,3]

$$\frac{d\sigma(+-)}{dQ^2d\nu} - \frac{d\sigma(++)}{dQ^2d\nu} = \frac{4\pi\alpha^2}{E^2Q^2}[m_p(E+E'\cos\theta)G_1(Q^2,\nu) - Q^2G_2(Q^2,\nu)], \tag{1.40}$$

where θ is the laboratory scattering angle. Since, in this process, the nucleon is longitudinally polarized, G_2 will make a negligible contribution. To obtain g_1 experimentally, rather than using (1.40) directly, the asymmetry

$$A \equiv \frac{\frac{d\sigma(+-)}{dQ^2d\nu} - \frac{d\sigma(++)}{dQ^2d\nu}}{\frac{d\sigma(+-)}{dQ^2d\nu} + \frac{d\sigma(++)}{dQ^2d\nu}}. \tag{1.41}$$

was measured. The asymmetry is useful because it cuts out overall normalization factors, which may be difficult to determine experimentally. We now show how A is related to g_1. Define $\sigma_{1/2(3/2)}$ as the virtual photoabsorption cross section when the net angular momentum of the virtual photon and the nucleon in the direction of the incident lepton is 1/2(3/2) in the γ^*-n c.m.. Introduce the asymmetry

$$A_1 = \frac{\sigma_{1/2} - \sigma_{3/2}}{\sigma_{1/2} + \sigma_{3/2}}. \tag{1.42}$$

One can show[11,14] that

$$A_1(x,Q^2) \simeq \frac{g_1(x,Q^2)}{F_1(x,Q^2)} = 2x(1+R(x,Q^2))\frac{g_1(x,Q^2)}{F_2(x,Q^2)}, \quad A_1 \simeq \frac{A}{D}, \tag{1.43}$$

where R is the ratio of the longitudinal to the transverse photoabsorption cross sections and D is a depolarization factor given by

$$D = \frac{y(2-y)}{y^2 + 2(1-y)(1+R)}, \qquad y \equiv \nu/E. \tag{1.44}$$

In the EMC experiment, the proton structure function, $g_1^p(x, Q^2)$, was determined by measuring A, then using the known values of F_2 and R to compute $g_1^p(x, Q^2)$ from (1.43).

At this point, it is worth mentioning the fundamental *Bjorken sum rule*,[15] based on current algebra,

$$M_1^p - M_1^n \equiv \int_0^1 [g_1^p(x) - g_1^n(x)]dx = \frac{1}{6}\frac{G_A}{G_V} C_{\rm NS} \tag{1.45}$$

where G_A and G_V are the nucleon axial-vector and vector coupling constants from nucleon beta decay, satisfying[1]

$$G_A/G_V = 1.2573 \pm 0.0028 \tag{1.46}$$

and $C_{\rm NS}$ represents the nonsinglet higher order corrections. For three quark flavors,[16]

$$C_{\rm NS} = 1 - \frac{\alpha_s}{\pi} - 3.58\left(\frac{\alpha_s}{\pi}\right)^2 - 20.22\left(\frac{\alpha_s}{\pi}\right)^3 + \cdots, \tag{1.47}$$

where α_s is determined in the $\overline{\rm MS}$ scheme. In the next section, we will discuss the recent experimental findings pertaining to the Bjorken sum rule.

One can derive less rigorous sum rules based on SU(3) symmetry and the assumption of an unpolarized strange sea. These *Ellis-Jaffe sum rules*[17] are

$$\begin{aligned} M_1^p &= \frac{1}{18}[C_{\rm NS}(3F + D) + 2C_{\rm S}(3F - D)] \\ M_1^n &= \frac{1}{9}[-DC_{\rm NS} + C_{\rm S}(3F - D)], \end{aligned} \tag{1.48}$$

where F and D are the weak hyperon decay constants satisfying[18] $F/D = 0.575 \pm 0.016$, $F + D = G_A/G_V$, and $C_{\rm S}$ is the singlet correction coefficient.[19]

1.3 Experimental Developments and Prospects in Spin Physics

The older DIS data on polarized lepton-proton scattering[11,12] covered the x-range $0.01 < x < 0.7$ and were evaluated at an average $< Q^2 >= 10.7$ GeV^2. This did not enable direct testing of the Bjorken sum rule (1.45), as there was no direct information on M_1^n. Now, the Spin Muon Collaboration (SMC)[20] have performed the experiment on a deuteron target in the range $0.006 < x < 0.6$, $< Q^2 >= 4.6$ GeV^2. As well, the E142 collaboration at SLAC[21] have performed the experiment on a neutron target in the range $0.03 < x < 0.6$, $< Q^2 >= 2$ GeV^2. Hence, we may now test directly the Bjorken sum rule. As well, the data are precise enough to check the Ellis-Jaffe sum rules. The extraction of the partonic contributions to the proton spin is outlined in Sect. 2.1.1.

Originally, there was disagreement between the conclusions of the E142 and SMC experiments. This arose from assumptions about the small-x region not covered by the E142 experiment and from the fact that the experiments were performed at different $< Q^2 >$. Evolving to a common $< Q^2 >= 5$ GeV^2, the data were shown to agree.[22]

At $< Q^2 >= 5$ GeV^2, taking into account the higher order corrections, the Bjorken sum rule (1.45) implies

$$M_1^p - M_1^n = 0.185 \pm 0.004, \qquad < Q^2 >= 5 \text{ GeV}^2. \tag{1.49}$$

The error represents the uncertainties in $\alpha_s(Q^2)$ and G_A/G_V, as well as the neglected higher orders and higher twist contributions. Experimentally, it is found that

$$M_1^p - M_1^n = 0.181 \pm 0.032, \qquad < Q^2 >= 5 \text{ GeV}^2, \tag{1.50}$$

in good agreement with the theoretical predictions.

We now compare the Ellis-Jaffe sum rules (1.48) with the experimental measurements. At $< Q^2 >= 5$ GeV^2, they imply

$$M_1^p = 0.169 \pm 0.005, \qquad M_1^n = -0.016 \pm 0.005. \tag{1.51}$$

Experimentally, on the other hand,

$$M_1^p = 0.135 \pm 0.015, \qquad M_1^n = -0.027 \pm 0.014. \tag{1.52}$$

in disagreement with the theoretical predictions.

At present, there is no experimental information for the processes considered in this thesis. But the work of chapters 3 and 4, requiring longitudinally and transversely polarized proton-proton collisions, will be tested experimentally at BNL's RHIC (Relativistic Heavy-Ion Collider). The work of chapter 5, requiring polarized photon-photon collisions, will likely be tested sometime in the not too distant future. We briefly review the experimental status for both types of processes.

The RHIC Spin Collaboration, of which our group are members, was formed recently with the intent of studying polarized p–p collisions at RHIC.[23] It has recently obtained approval and funding for producing polarized protons at RHIC. They will be able to detect large-p_T photons and dimuon pairs, relevant to the work of chapters 3 and 4, respectively. The planned p–p center-of-mass energies are $\sqrt{S} = 100, 200, 500$ GeV, with an expected luminosity of $\mathcal{L} = 2 \times 10^{32}$ cm^{-2}sec^{-1}. Recent tests[24] at BNL's alternating gradient synchotron (AGS) have successfully produced polarized proton beams at 25 GeV (the transfer energy for RHIC) using the Siberian snake technique. Direct photon production and Drell-Yan will be among the first spin physics experiments carried out when RHIC goes on-line (1999 or 2000).

Recently, there has been much interest in producing (polarized) photons of high energy at a high energy photon linear collider (PLC). The generally accepted method of producing such photons is via backscattering of polarized laser light off electrons (positrons) at a linear e^+e^- collider with energies of up to 500 GeV.[25] High degrees of polarization could be achieved and the photons could carry a large fraction of the electron energy. Studies have concluded[26] that luminosities, $\mathcal{L}_{\gamma\gamma} \approx 1.5 \times 10^{33}$ cm^{-2}sec^{-1}, could be reached at TESLA (TeV Energy Superconducting Linear Accelerator (proposal)). It is also argued that it would be simpler to use electrons instead of positrons in the initial design. As well, a high luminosity, $\mathcal{L}_{\gamma\gamma} \approx 10^{34}$ cm^{-2}sec^{-1}, low energy, 2×5 GeV photon collider could be constructed at SLAC with a minor upgrade. Of course, this energy is too low for the applications considered in chapter 5, but is still of theoretical interest.

Chapter 2

General Background

2.1 Estimates of the Polarized Parton Distributions

The only available experimental data for longitudinally polarized high energy nucleon collisions at this point are from deep-inelastic scattering. As we will show, this process is rather insensitive to the nucleon's polarized gluon distribution. For transversely polarized processes, there are no experimental data. Hence, there is absolutely no experimental information on the transversity distributions. For these reasons, we shall investigate the constraints which may be imposed on the polarized parton distributions and detail their construction. We shall also plot the resulting scale dependent distributions, having performed the necessary evolution and parameterization of the distributions in the energy range of interest.

2.1.1 The Longitudinal Distributions

In order to construct the polarized parton distributions, we must identify the various components of the proton. We consider the proton as consisting of a valence up distribution, $\Delta F_{u_v}(x, Q^2)$, and a valence down distribution, $\Delta F_{d_v}(x, Q^2)$; also, of a gluon distribution, $\Delta F_g(x, Q^2)$, as well as a sea quark distribution, $\Delta F_{q_s}(x, Q^2)$,

and a sea antiquark distribution, $\Delta F_{\bar{q}}(x,Q^2)$, which represent the possibility of pair creation within the proton.

The breakdown of the light quark distributions in the proton is then

$$\begin{aligned}
\Delta F_u(x,Q^2) &= \Delta F_{u_v}(x,Q^2) + \Delta F_{u_s}(x,Q^2) \\
\Delta F_d(x,Q^2) &= \Delta F_{d_v}(x,Q^2) + \Delta F_{d_s}(x,Q^2) \\
\Delta F_s(x,Q^2) &= \Delta F_{s_s}(x,Q^2),
\end{aligned} \tag{2.1}$$

and

$$\Delta F_{\bar{q}}(x,Q^2) = \Delta F_{q_s}(x,Q^2). \tag{2.2}$$

We may further define the distribution,

$$\Delta\Sigma(x,Q^2) \equiv \sum_{i=1}^{3}[\Delta f_{q_i}(x,Q^2) + \Delta f_{\bar{q}_i}(x,Q^2)]. \tag{2.3}$$

It is important to determine constraints which limit the allowable sets of parton distributions. Using a specific parameterized form for an unpolarized distribution, $F(x,Q^2)$, we may determine $F^{+/+}$, $F^{-/+}$ from

$$F^{+/+}(x,Q^2) = \frac{1}{2}[F(x,Q^2) + \Delta F(x,Q^2)] \tag{2.4}$$

$$F^{-/+}(x,Q^2) = \frac{1}{2}[F(x,Q^2) - \Delta F(x,Q^2)], \tag{2.5}$$

(see (1.18), (1.21)). This provides a useful check, since $F^{+/+}(x,Q^2)$, $F^{-/+}(x,Q^2)$ must be positive everywhere. Also, by demanding that the sum of the contributions to the proton spin is 1/2, we obtain, for a longitudinally polarized proton with positive helicity, the sum rule

$$\frac{1}{2}\Delta\Sigma + \Delta g + < L_z >= \frac{1}{2}, \tag{2.6}$$

where L_z is the net z-component of the angular momentum carried by the partons, $\Delta\Sigma$ is the first moment of $\Delta\Sigma(x, Q^2)$, defined in (2.3) and Δg is the first moment of $\Delta f_{g/p}(x, Q^2)$, i.e.

$$\Delta g \equiv \int_0^1 dx \Delta f_{g/p}(x, Q^2). \tag{2.7}$$

$< L_z > \neq 0$ in general, due to the small intrinsic transverse momentum of the partons. The contribution of $\Delta\Sigma(Q^2)$ does not change with Q^2 as a result of helicity conservation of massless quarks and the fact that when a gluon splits into a quark and an antiquark, the q and $\bar{q}$ have opposite helicities. Changes to Δg are compensated by changes to $< L_z >$ such that $\Delta g + < L_z >$ is conserved. Hence, large Δg implies equally large, negative $< L_z >$. This is understood because, since Δg increases as a result of collinear radiation by quarks, the total spin of the partons is increasing with Q^2. Hence the orbital angular momentum must change so as to compensate. More specifically, at large Q^2, $\Delta g \sim \ln Q^2$, meaning $< L_z > \sim -\ln Q^2$. At any rate, since $< L_z >$ is unknown, we cannot reasonably constrain Δg in this way.

We now consider the relation between $g_1(x)$ and the quark distributions in the *naive* PM. Assuming we can neglect the intrinsic transverse momentum of the quarks within the hadron, by angular momentum conservation a quark can only absorb a photon with antiparallel spin in the γ^*–p c.m.. So, if the net angular momentum of the photon-nucleon system is 1/2(3/2), the quark must have spin parallel (antiparallel) to the nucleon. Thus

$$A_1 \equiv \frac{\sigma_{1/2} - \sigma_{3/2}}{\sigma_{1/2} + \sigma_{3/2}} = \frac{\sum_i e_i^2 [f_{q_i}^{+/+}(x) - f_{q_i}^{-/+}(x)]}{\sum_i e_i^2 [f_{q_i}^{+/+}(x) + f_{q_i}^{-/+}(x)]}, \tag{2.8}$$

where the index i runs over all flavors of quarks *and* antiquarks. Also in the naive PM,

$$F_1(x) = 1/2 \sum_{i=1}^{2N_f} e_i^2 [f_{q_i}^{+/+}(x) + f_{q_i}^{-/+}(x)], \tag{2.9}$$

where N_f (= 3) is the number of flavors. Substituting (2.8) and (2.9) in (1.43) gives

$$g_1^p(x) = 1/2 \sum_{i=1}^{2N_f} e_i^2 \Delta f_{q_i}(x). \tag{2.10}$$

Note that $\Delta f_{q_i}(x)$ are the polarized *proton* densities, defined in (1.17), for quarks *or* antiquarks of flavor i.

We now define

$$\Delta q_i = \int_0^1 dx[\Delta f_{q_i}(x) + \Delta f_{\bar{q}_i}(x)]. \tag{2.11}$$

Using (2.10) and (2.11) gives for the first moment,

$$M_1^p \equiv \int_0^1 g_1^p(x)dx \tag{2.12}$$

$$= 1/2 \sum_{i=1}^{N_f} e_i^2 \Delta q_i \tag{2.13}$$

$$= 1/2\ [4/9\ \Delta u + 1/9\ \Delta d + 1/9\ \Delta s]. \tag{2.14}$$

For M_1^n, we simply replace $\Delta u \rightarrow \Delta d$. We hence obtain the leading order result

$$M_1^p - M_1^n = \frac{1}{6}(\Delta u - \Delta d). \tag{2.15}$$

One may also make use of less rigorous SU(3) relations which imply

$$\Delta u + \Delta d - 2\Delta s = 3F - D. \tag{2.16}$$

Comparison with experiment[11,20,21] yields

$$\frac{1}{2}\Delta\Sigma \approx 0.25, \qquad \frac{1}{2}\Delta s \approx -0.1, \tag{2.17}$$

(noting that there is appreciable uncertainty in Δs). From (2.6) we see that, as mentioned previously, the net contribution of the quarks to the proton spin is rather small, requiring large gluon polarization and/or large $< L_z >$. It should be noted

Figure 2.1: The gluonic contribution to deep-inelastic scattering at $\mathcal{O}(\alpha_s)$. Dashed line: gluon, wavy: photon, solid: quark.

that the extrapolation to small x remains controversial and could influence these conclusions (especially for Δs, since $\Delta f_{\bar{s}}(x)$ is small and peaked at small x).

So far, there is no contribution from the polarized gluon distribution. Taking into account HOC, there is a gluonic contribution to DIS arising from the graphs of Fig. 2.1. This modifies all the above relations such that we must make the substitution

$$\Delta f_{q_i}(x,Q^2) \rightarrow \Delta f_{q_i'}(x,Q^2) = \Delta f_{q_i}(x,Q^2) - \frac{\alpha_s}{2\pi}\Delta f_g(x,Q^2), \tag{2.18}$$

in the leading order expressions. As well, g_1 must be multiplied by the factor $(1 - \alpha_s/\pi)$. Since $\Delta f_{\bar{s}}(x,Q^2)$ is small, we see that a large Δg could be mistaken for a moderate, negative Δs.

Experimentally, there is a scarcity of data at the very small and very large x values. Hence, it is useful to have some guides as to the behaviour of the longitudinal distributions in these regions.

For $x \rightarrow 0$, one can use Regge theory arguments to show that, in the unpolarized case, the parton momentum distributions have the form

$$F_{a/p}(x,Q_0^2) \sim x^{1-\alpha(0)}, \qquad Q_0^2 \approx \text{a few GeV}^2 \tag{2.19}$$

with $\alpha(0)$ being the intercept of the leading Regge exchange for the process $\gamma^* a \to \gamma^* a$.[13] For a = polarized quark, it is generally believed that the leading exchange is a low-lying trajectory (possibly a_1) with $\alpha(0) \sim 0$. This implies $\Delta F_{q/p}(x, Q_0^2) \sim x$; a finding consistent with the low-x EMC and SMC data.

We stated earlier that the HOC to polarized DIS imply the substitution (2.18). In this sense, the data are consistent with

$$\Delta F_{g/p}(x, Q_0^2) \to 0, \quad x \to 0. \tag{2.20}$$

This is generally accepted as being correct, although the exact small-x behaviour is a matter of debate. Hence, the need for direct experimental information on $\Delta F_{g/p}(x, Q_0^2)$ is quite apparent.

For the large-x region, the theory is not so rigorous. Intuitively, if x is large, then one may expect that the parton, a, determines the spin direction of the proton since it carries almost all its momentum. For a = quark, this means that the *remaining* two quarks would combine with $L_z = 0$. For a = gluon, the remaining three quarks will have $L_z = -1/2$ (of course, this picture is somewhat oversimplified). In other words

$$F_{a/p}^{-/+}(x) \ll F_{a/p}^{+/+}(x) \to \Delta F_{a/p}(x) \approx F_{a/p}(x), \qquad x \to 1. \tag{2.21}$$

All the above implies that $\Delta F_{g/p}(x)$ peaks at small $x \neq 0$, unlike $F_{g/p}(x)$, which peaks at $x = 0$.

It should be stressed that the assumed very small- or large-x behaviour does not have a major impact on the predictions of chapter 3, as these regions do not contribute significantly to the measurable cross sections (especially the large-x region).

Rationale similar to the above was used by Ref. 27 to construct 2 sets of polarized parton distributions, both fitting the EMC data (the only data available at the time

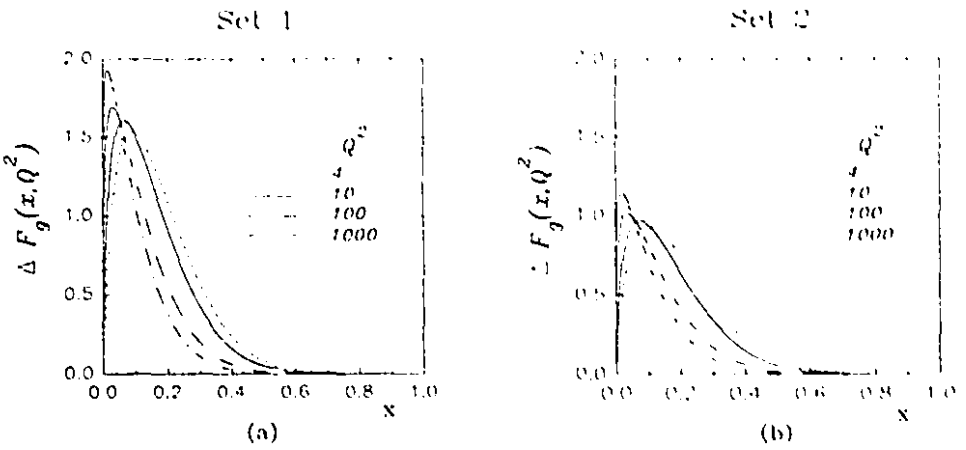

Figure 2.2: The proton's polarized gluon distribution, $\Delta F_g(x, Q^2)$, for Q^2 = 4, 10, 100 and 1000 GeV^2: (a) Set 1; (b) Set 2.

the work of chapter 3 was done). Set 1 assumes a rather large gluon polarization (and zero strange-quark input), satisfying $\Delta g = 5$, $Q_0^2 = 4$ GeV^2. For Set 2 (moderate gluon polarization, negative strange sea), $\Delta g = 3$. Now that new data are available, we have checked that these sets still fit reasonably the data on $g_1^p(x)$, except at small x ($\lesssim 10^{-2}$), where the predictions underestimate the data. Additionally, Set 2 comes rather close to the distributions of Ref. 28, which were obtained by fitting to the recently obtained data on $g_1^p(x)$.

The evolution to all Q^2 (of interest) was performed (numerically) by using directly the evolution equations of Sect. 2.3.2. We do not work in moment space as is commonly done. Then, scale-dependent parameterizations were constructed for both sets. They are given in Appendix A.1.

In Figs. 2.2–2.6, we plot the longitudinal distributions for Set 1 (figures (a)) and Set 2 (figures (b)), for $Q^2 = 4$, 10, 100, 1000 GeV^2.

Fig. 2.2 presents the polarized gluon distribution, $\Delta F_g(x, Q^2)$. We see explicitly the peak at small x. As well, the distributions are rather soft; they decrease rapidly

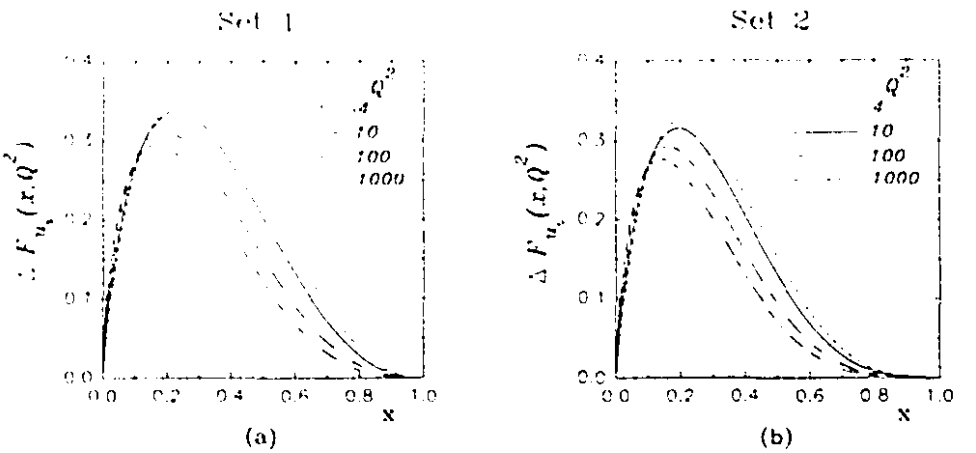

Figure 2.3: The proton's polarized up-valence distribution, $\Delta F_{u_v}(x, Q^2)$, for $Q^2 = 4$, 10, 100 and 1000 GeV^2: (a) Set 1; (b) Set 2.

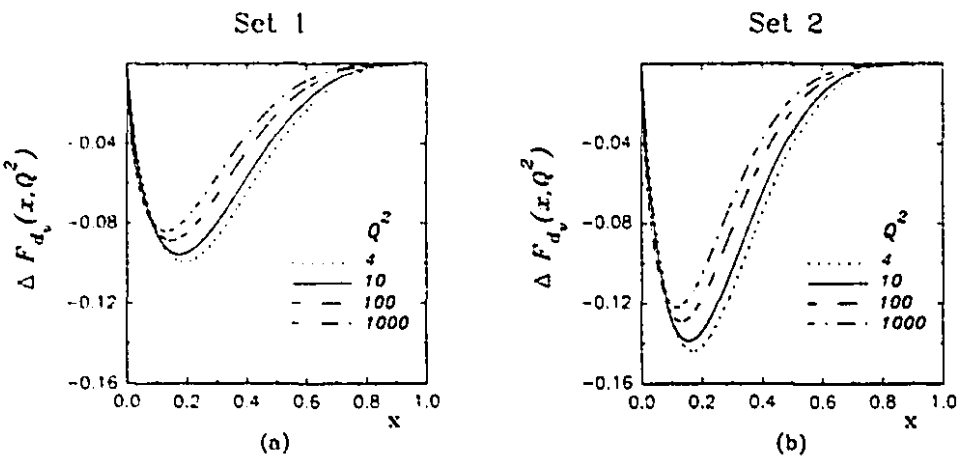

Figure 2.4: The proton's polarized down-valence distribution, $\Delta F_{d_v}(x, Q^2)$, for $Q^2 = 4$, 10, 100 and 1000 GeV^2: (a) Set 1; (b) Set 2.

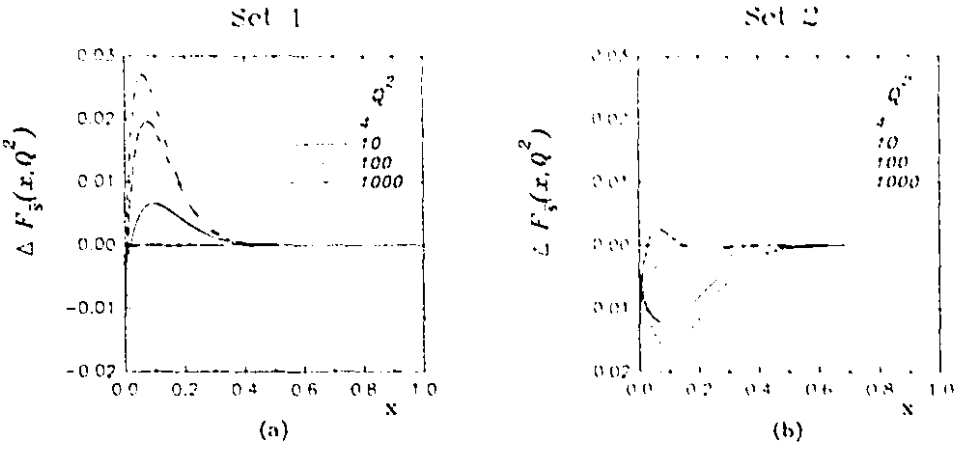

Figure 2.5: The proton's polarized strange-antiquark distribution, $\Delta F_{\bar{s}}(x, Q^2)$, for $Q^2 =$ 4, 10, 100 and 1000 GeV^2: (a) Set 1; (b) Set 2.

with increasing x. This softness increases with increasing Q^2 as a result of gluonic radiation ($g \rightarrow gg, q\bar{q}$).

Fig. 2.3 shows the up-valence distribution, $\Delta F_{u_v}(x, Q^2)$. Compared to the gluon distribution it is rather hard, and softens rather slowly with increasing Q^2. The down-valence distributions, $\Delta F_{d_v}(x, Q^2)$, are shown in Fig. 2.4. They are found to be negative, i.e. more likely to be polarized oppositely to the proton.

Fig. 2.5 shows the strange-antiquark distribution, $\Delta F_{\bar{s}}(x, Q^2)$. It is quite small throughout, and rather soft. For Set 1, it is zero at $Q^2 = 4$ GeV^2, but becomes nonzero at higher energies due to pair creation arising from the gluon distribution. For Set 2, it is negative at $Q^2 = 4$ GeV^2, but the evolution makes it quite a bit smaller for $Q^2 \approx 1000$ GeV^2.

In Fig. 2.6, we plot $\Delta F_{\bar{u}}(x, Q^2) = \Delta F_{\bar{d}}(x, Q^2)$. For Set 1, these are equivalent to $\Delta F_{\bar{s}}(x, Q^2)$. For Set 2, they are zero at input, but become nonzero at higher energies. The resulting curves are somewhat smaller than those in Set 1, since the contribution from the gluon distribution is smaller.

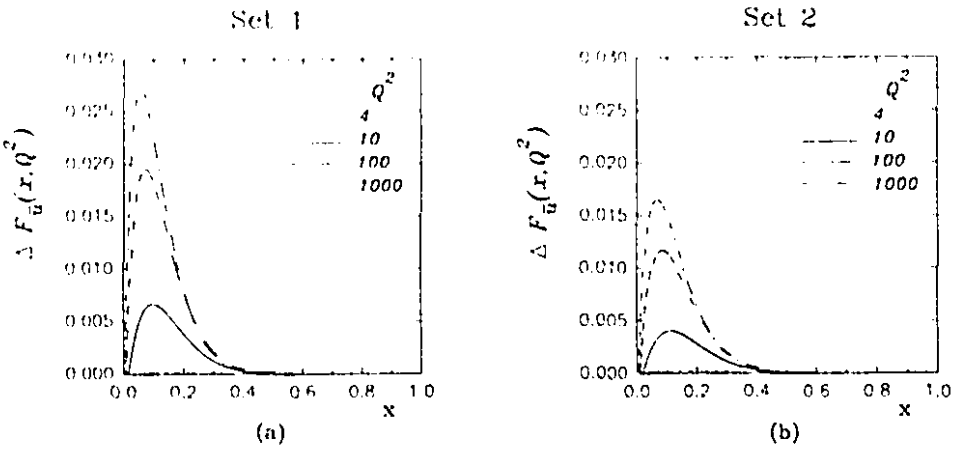

Figure 2.6: The proton's polarized up-antiquark distribution, $\Delta F_{\bar{u}}(x, Q^2)$, for $Q^2 = 4$, 10, 100 and 1000 GeV^2: (a) Set 1; (b) Set 2.

2.1.2 The Transversity Distributions

Unlike the case of the longitudinal distributions, no experimental information is available for the transversity distributions. However, one can make some educated guesses and impose the positivity constraint,

$$|\Delta_T F_q(x, Q^2)| < F_q(x, Q^2) \tag{2.22}$$

for all x, Q^2. Analogously to (2.6) we may write

$$\frac{1}{2}\Delta_T\Sigma + < L_\perp >= \frac{1}{2}, \tag{2.23}$$

with obvious notation. This does not serve as a major constraint, since $< L_\perp >$ is not known. We will consider the valence and sea distributions separately.

Valence Distributions

Let us consider the proton as consisting only of up and down valence quarks, i.e. uud, and no gluons or sea quarks. Furthermore, we ignore the internal motion of the quarks within the proton.

In the proton's rest frame, there is no preferred direction. Hence, the net probability of finding a quark polarized in the direction of the proton's spin, $\hat{y}$, minus the probability of finding it oppositely polarized is simply equal to Δf_{q_v}, the magnitude (first moment) of the longitudinal distribution. Now, boost in the $\hat{z}$ direction, where $\hat{z} \perp \hat{y}$. Conservation of transversity (for both the quarks and the proton) under such boosts implies

$$\Delta_T f_{q_v} = \Delta f_{q_v} \rightarrow \Delta_T F_{q_v} = \Delta F_{q_v}. \tag{2.24}$$

However, this does not give us information about the x-dependence. As well, radiative effects (as well as intrinsic motion effects) change the above picture since, as will be shown in Sect. 2.3.2, the transversity distributions evolve differently with Q^2 than do the longitudinal ones. This evolution comes about from gluonic radiation, which softens the distributions. So we simply assume that at some low energy scale, Q_0^2,

$$\Delta_T F_{q_v}(x, Q_0^2) = \Delta F_{q_v}(x, Q_0^2), \quad Q_0^2 = 4 \text{ GeV}^2, \tag{2.25}$$

where we use Set 1 of Ref. 27. This is in fair agreement with the predictions of the relativistic MIT bag model. We manifestly satisfy (2.22) for all x, Q^2 in this way.

The evolution to all Q^2 is performed using the evolution equations of Sect. 2.3.2. Scale dependent parameterizations for this evolution are presented in Appendix A.2. In Fig. 2.7 we plot the proton's transversity valence distributions for $Q^2 = 1$, 4, 300 and 10^5 GeV^2; going to lower energy scales would be meaningless since the parton model breaks down below $Q \approx 1$ GeV. In particular, Fig. 2.7 (a) presents the up-valence distribution and Fig. 2.7 (b) presents the down-valence distribution.

As for the longitudinal case, we notice a softening of the distributions for larger Q^2; the evolutions are similar. Unlike the longitudinal case, however, $\Delta_T f_q$ is not

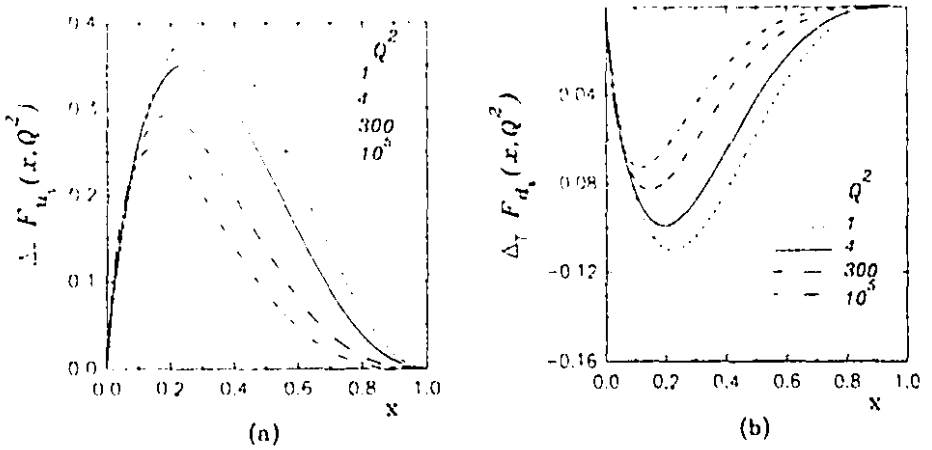

Figure 2.7: The proton's transversity valence distributions for $Q^2 = 1,\ 4,\ 300$ and 10^5 GeV^2: (a) $\Delta_T F_{u_v}(x, Q^2)$; (b) $\Delta_T F_{d_v}(x, Q^2)$.

conserved, since gluonic radiation can change a quark's transversity; the net transversity decreases as Q^2 increases. As a result, we notice that there is not much of an increase in the transversity distributions at small x, as Q^2 is increased.

Sea Distributions

The situation is not so straightforward for the sea quarks. At energy scale Q_0, there will be some innate transversity sea distribution, but it is not known what its magnitude or shape will be. Hence, the only definite constraint is given by (2.22). As well, we assume that the small- and large-x behaviour is similar to the unpolarized distribution, using the unpolarized distributions (set SL) of Ref. 29 as a reference. We take (for $Q_0^2 = 4$ GeV^2)

$$\Delta_T F_{\bar{q}}(x, Q_0^2) = -0.24 x^{0.1}(1-x)^{9.5}, \quad \bar{q} = \bar{u}, \bar{d}, \bar{s}. \tag{2.26}$$

In Fig. 2.8 (a) we plot the proton's transversity up-antiquark distribution ($= \bar{d}, \bar{s}$) at $Q_0^2 = 4$ GeV^2 as well as the corresponding unpolarized distribution. We see that (2.22) is satisfied and that the transversity sea has the same general shape as the unpolarized sea.

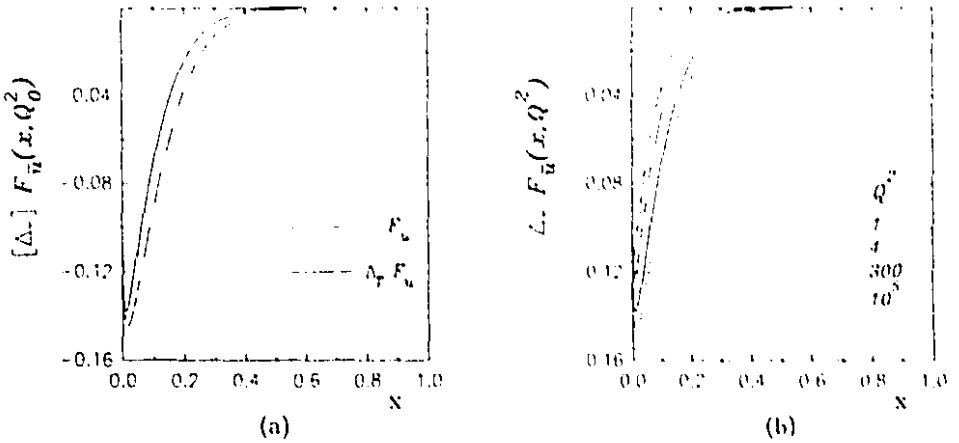

Figure 2.8: The proton's transversity up-antiquark distribution $\Delta_T F_u(x, Q^2)$: (a) input at $Q_0^2 = 4$ GeV^2 (dashed line is minus the corresponding unpolarized); (b) for $Q^2 = 1$, 4, 300 and 10^5 GeV^2.

The evolution was performed and the resulting Q^2-dependent parameterizations are given in Appendix A.2. Fig. 2.8 (b) shows the evolution to $Q^2 = 1$, 4, 300, 10^5 GeV^2. The evolution is much simpler than in the longitudinal or unpolarized cases due to the absence of $g \to q\bar{q}$ effects.

2.2 Regularization Schemes

As soon as one calculates a physical quantity (i.e. a cross section) beyond leading order in perturbative field theory, divergences develop. One can see this on the basis of power counting. In 4 dimensions, the phase space for particles occurring in virtual loops is

$$\int \frac{d^4q}{(2\pi)^4}. \tag{2.27}$$

Hence, if in the Feynman graph, there are terms with the ultraviolet (high energy) behaviour q^m, with $m \geq -4$, a divergence will develop in the ultraviolet region. We call this an ultraviolet (UV) divergence. Similarly, if the behaviour is q^m, with $m \leq -4$ in the infrared (low energy) region, an infrared (IR) divergence will develop.

This type of IR divergence is referred to as a soft divergence. A similar argument shows that soft (but not UV) divergences can arise in bremsstrahlung graphs.

Another type of IR divergence, which we call a mass (or collinear) singularity occurs in real bremsstrahlung graphs where a massless particle splits into two or more massless, collinear particles. Then, an internal propagator develops a pole. For the case $p_1 \to p_2^* + k$, we can write the 4-dimensional phase space as (in a frame with fixed $|\mathbf{p_1}|$, $|\mathbf{k}|$)

$$\sim \int_0^\pi \sin\theta d\theta = \int_{-1}^1 d(\cos\theta), \tag{2.28}$$

where θ denotes the angle between p_1 and k, for instance. So, if we are integrating a function $\sim 1/(p_1.k)^m \sim 1/[|\mathbf{p_1}||\mathbf{k}|(1-\cos\theta)]^m$ with $m \leq 1$, a singularity develops for $\theta = 0$. If p_1, p_2, k weren't all massless, the singularity could not develop.

One also obtains mass singularities in loop diagrams. To see this, we consider a diagram which contains only photons and massive fermions, and has an IR divergence (i.e. the on-shell electron self-energy). Generally, it will contain terms proportional to

$$f(\mu^2/m^2), \tag{2.29}$$

where μ^2 is some mass scale introduced by the regularization method (see below) and f is some function (i.e. ln). For $m \neq 0$, these terms are finite, but for $m \to 0$ an *additional* singularity develops; or, more precisely, the IR singularity structure changes. Hence, diagrams of this type are said to also have mass singularities. This terminology applies to all diagrams with this behaviour, not just fermion-photon diagrams.

The idea behind regularization is that we should consider the usual physical situation as a limit of some unphysical situation. The unphysical situation, referred

to as a *regularization*, should be such that the singularities appear as terms which diverge in the limit where we approach the physical situation, but are finite in the regularization. Then, the divergences will appear as functions of the regularization parameters, which are singular in the physical limit of the parameters.

After regularization, some of the divergences will cancel. For QED-type graphs (having massive fermions) all the IR divergences cancel via the Bloch-Nordsieck mechanism,[30] by which the soft bremsstrahlung singularities cancel with the virtual soft singularities. For non-QED-type graphs, any remaining mass singularities must be removed by renormalization, as described in Sect. 2.3. In general, there are also UV divergences which must be removed by renormalization.

In what follows, we shall review the most commonly used *regularization schemes* and discuss which of them are most appropriate for the calculations performed in this work.

2.2.1 Non-Dimensional Methods

Cut-Off Method

In this method, we regularize the UV divergences by replacing the upper bound of ∞ in the virtual momentum integrations by some cutoff, Λ. Hence, Λ parameterizes the UV divergence. Unfortunately, this violates translation invariance under momentum shifts and can lead to non-unique results.

For the IR divergences, one generally gives the photon/gluon a mass. This violates local gauge invariance of the Lagrangian and hence leads to problems with consistency. In other words, the Feynman rules are only consistent with photons/gluons being massless. Hence non-unique results could arise, depending on the methodology and choice of gauge parameters. For example, if one has massless quarks, one finds

that the final results depend on whether one sets the gluon or quark masses to zero first.[31]

Pauli-Villars Regulators

Suppose one has a UV divergent integral over some momentum, k, involving the propagator $1/(m^2 - k^2)$. One makes the substitution,[32]

$$\frac{1}{m^2 - k^2} \rightarrow \frac{1}{m^2 - k^2} - \frac{1}{M^2 - k^2} = \frac{M^2 - m^2}{(m^2 - k^2)(M^2 - k^2)} \tag{2.30}$$

so that the UV region is regulated by an additional power of $1/k^2$ for finite values of the regularization parameter, M. In the limit $M \rightarrow \infty$, we recover the physical situation. This is equivalent to adding (actually subtracting) a fictitious particle of mass M, having the same couplings as the particle of mass m (= 0 for gluons/photons). This method has been shown to respect all the necessary invariances for QED and QCD. For the electroweak theory, which has massive bosons, gauge invariance has been shown to be violated.[33] As well, no innate IR regularization is provided, similar to the cutoff method. This makes both methods too cumbersome to apply to complex QCD calculations.

Analytic Regularization

For the propagator $1/(m^2 - k^2)$, we make the substitution[34]

$$\frac{1}{m^2 - k^2} \rightarrow \frac{1}{(m^2 - k^2)^a} \tag{2.31}$$

with $a = 1 + \eta$. Then UV and IR divergences show up as poles in $1/\eta$. Since we are again warping the Feynman rules, problems with consistency arise and gauge invariance is known to be violated in QCD using analytic regularization.

2.2.2 Dimensional Methods

We have seen that all of the conventional, non-dimensional regularizations are cumbersome and unsuitable for performing systematic, multiloop (or even one-loop) QCD calculations, in general. It turns out that using *dimensional continuation*, one may regularize all the divergences in a systematic, straightforward manner, while preserving all the necessary invariances.

There are two parts to the dimensional continuation: the continuation of the *momenta*, and the continuation of all other *tensor structures* (i.e. gamma matrices). The continuation of the momenta is unique, but there are various methods for continuing the remaining tensors. The choice of the latter defines which dimensional method is being used.

Continuation of the Momenta

In order to regularize both UV and IR (both soft and collinear) divergences, we continue the momenta from 4 to $n = 4 - 2\varepsilon$ dimensions. This means that the phase space for virtual momentum integrations is generalized to

$$\int \frac{d^4q}{(2\pi)^4} \rightarrow \int \frac{d^nq}{(2\pi)^n}. \tag{2.32}$$

The same applies to bremsstrahlung integrals. To preserve the dimensionality of the Lagrangian, we must introduce an arbitrary mass scale, μ, via

$$g \rightarrow g\mu^\epsilon. \tag{2.33}$$

Since each loop momentum integration is accompanied by a factor g^2, we see that the dimensions of the Feynman amplitude will be preserved, after corrections.

After Wick rotation ($q_0 \rightarrow iQ_0$, $q_i \rightarrow Q_i$) we can generalize the Euclidean phase

space to arbitrary integer dimensions via

$$d^nQ = Q^{n-1}dQd\Omega_n, \quad (Q \equiv \sqrt{Q_0^2 + Q^2}). \tag{2.34}$$

with

$$d\Omega_n = \prod_{m=1}^{n-1} \sin^{n-1-m}\theta_m d\theta_m. \tag{2.35}$$

Before Wick rotation, the integrands are put into a form depending only on q^2. So after Wick rotation, they depend only on Q^2. Hence, the angular integral just gives an overall factor

$$\frac{2\pi^{n/2}}{\Gamma(n/2)} \tag{2.36}$$

and the UV divergences manifest as poles in ε, coming from the integral over dQ, while the IR divergences come from the Feynman parameter integrations.

Having obtained an analytic expression for the angular integral in terms of the dimensional parameter n we continue this to the complex plane. Similarly, all loop integrals can be reduced, using Feynman parameters to the fundamental integral

$$\int \frac{d^nq}{(2\pi)^n} \frac{(q^2)^r}{(q^2 - C)^m} = \frac{i(-1)^{r-m}}{(4\pi)^{n/2}\Gamma(n/2)} C^{r-m+n/2} B(r + n/2, m - r - n/2), \tag{2.37}$$

(see, for example, Ref. 35) with $m > 0$, $r \geq 0$ and B the Euler beta function. This expression may also be continued to the complex plane. This continuation becomes necessary because, in general there are both UV and IR divergences. On the basis of power counting, we need $\varepsilon > 0$ for the UV divergences and $\varepsilon < 0$ for the IR divergences. Yet, we may only work in one dimension at any point in the calculation. Let $\varepsilon, \varepsilon'$ determine the (integer) dimensions in which we initially determine the IR, UV divergent integrals, respectively. Having analytic expressions for these integrals in terms of $\varepsilon, \varepsilon'$ we must continue to real (or complex) $\varepsilon = \varepsilon'$ so that we work in only

one dimension at any point. This continuation is valid since integrals in non-integer dimensions are *defined* as a continuation from integer to non-integer dimensions.

An important example of this analytic continuation occurs for integrals containing both UV and IR divergences. They may always be reduced to the form (2.37) with $C = 0$. The integral must have dimensions of $\text{mass}^{2(r-m+n/2)}$, but since there are no dimensional parameters, it must vanish.

To see how this is related to analytic continuation, we may take two approaches. Working directly with the formula (2.37) implies that we must work consistently in n such that $Re(r - m + n/2) > 0$ in order to have a well defined, analytic expression $(= 0)$. So we obtain zero without ever splitting into $\varepsilon < 0$, $\varepsilon' > 0$. Alternatively, we may simply split the integration into two parts using some intermediate cutoff, Λ, such that, after Wick rotation

$$\int_0^\infty Q^{n-1} dQ \to \int_0^\Lambda Q^{n-1} dQ + \int_\Lambda^\infty Q^{n'-1} dQ, \tag{2.38}$$

where $n > 4$ and $n' < 4$ *initially*. Then we get, after some algebra

$$\int \frac{d^n q}{(2\pi)^n} \frac{1}{(q^2)^{m-r}} = \frac{i(-1)^{m-r}}{(4\pi)^{n/2}\Gamma(n/2)} \left\{ \frac{\Lambda^{n-2(m-r)}}{(n/2-(m-r))} - \frac{\Lambda^{n'-2(m-r)}}{(n'/2-(m-r))} \right\} \tag{2.39}$$

Continuing to $n = n'$ (or $\varepsilon = \varepsilon'$) we obtain zero. This may be viewed as an exact cancellation of the IR and UV divergences. We also notice that the only poles occur at $n = 2(m - r)$, meaning that if $m - r \neq 2$, dimensional continuation gives no $1/\varepsilon$ pole from the UV region, regardless of the value of C in (2.37), since the UV region is independent of C. This observation also follows directly from (2.37).

Concerning the collinear divergences, the angular integral (2.28), over the term $\sim 1/p_1 \cdot k$, is modified to

$$\sim \int_0^\pi \frac{\sin^{1-2\varepsilon}}{1-\cos\theta} d\theta = \int_{-1}^1 d(\cos\theta) \frac{(1-\cos\theta)^{-\epsilon}}{1-\cos\theta} (1+\cos\theta)^{-\epsilon} \tag{2.40}$$

due to the n-dimensional phase space. As for the IR divergent loop integrals, we take $\varepsilon < 0$ initially, rendering the integral finite. Hence, through dimensional continuation, all of the divergences occurring in QCD (or in any field theory integrals) may be regularized!

Continuation of the Tensors

The tradeoff for the convenience in regularization is the inconvenience and/or ambiguity associated with the continuation of the tensors. There are two popular methods for the continuation of the tensor structures: dimensional regularization (DREG) and dimensional reduction (DRED). Within DREG, there are two commonly used approaches to deal with the γ_5-matrix (or the tensor $\varepsilon^{\mu\nu\lambda\rho}$); both are described below.

Dimensional Regularization

In dimensional regularization,[36,37] all the tensors and gamma matrices are continued to n dimensions. More precisely, we continue the relations obeyed by the tensors. This means

$$g_n^{\mu\nu} g_{\mu\nu}^n = n, \qquad \gamma^\mu \gamma^\nu + \gamma^\nu \gamma^\mu = 2 g_n^{\mu\nu}. \tag{2.41}$$

where $g_n^{\mu\nu}$ is the n-dimensional metric tensor such that the indices run from 1 to n, instead of from 1 to 4 (note: we are starting from 1 instead of 0, for clarity). The usual convention is

$$\mathrm{Tr}[I] = 4. \tag{2.42}$$

One could take $\mathrm{Tr}[I] = n$, but this just amounts to a finite renormalization (discussed in Sect. 2.3.2) and hence does not change physical predictions. The cyclicity of the traces is also assumed.

As well, the usual convention is to divide by $2-2\varepsilon$ helicity states for gluons/photons and 2 for fermions, when averaging over initial states. This is related to the continuation of the helicity sum rule

$$\sum_{\lambda} A^{\mu}(p,\lambda)A^{*\nu}(p,\lambda) = -g_n^{\mu\nu} \tag{2.43}$$

which now involves the $n = 4-2\varepsilon$ dimensional metric tensor; since there should be $n-2$ helicity states, we get $2-2\varepsilon$. Here $A^{\mu}(p,\lambda)$ is the gluon/photon polarization vector for gluon/photon momentum p and helicity λ. Again, different conventions simply amount to finite renormalizations.

When the γ_5 matrix, or the Levi-Civita tensor $\varepsilon^{\mu\nu\lambda\rho}$ occurs, the generalization to n dimensions is not so straightforward. Two popular schemes exist within DREG; the HVBM scheme and the anticommuting-γ_5 scheme, which we shall describe below.

Anticommuting-γ_5 Scheme

A general prescription was developed[38] to eliminate γ_5's, $\varepsilon^{\mu\nu\lambda\rho}$'s in n dimensions. We describe this method, using polarized QCD/QED as a motivating example, but it can be applied to various electroweak processes which innately involve the γ_5-matrix.

Polarized quarks introduce a γ_5 through the helicity projection operator

$$\Pi^{\pm} = \frac{1 \pm \gamma_5}{2}. \tag{2.44}$$

We may see explicitly how polarized gluons (or photons) introduce the γ_5 matrix and demonstrate the above mentioned prescription for their elimination. Let $A_1^{\mu}(p_1,\lambda_1)$ be the polarization vector of $\bar{g}$ and $\lambda_1 = \pm 1$ its helicity. In $\Delta|M|^2$ one obtains combinations of Dirac matrices of the form

$$(\not{A}_1 \not{p}_1 \not{p}_2 \cdots \not{p}_n \not{A}_1^*)_{\pm} \equiv \not{A}(p_1,+1)\not{p}_1\not{p}_2\cdots\not{p}_n\not{A}^*(p_1,+1) - \not{A}(p_1,-1)\not{p}_1\not{p}_2\cdots\not{p}_n\not{A}^*(p_1,-1) \tag{2.45}$$

where the b_i are general vectors. We work in a general axial gauge defined by

$$A_1^2 = 0, \quad A_1 \cdot A_1^* = -1, \quad A_1 \cdot p_1 = 0, \quad A_1 \cdot \eta = 0, \quad \eta \cdot p_1 \neq 0, \tag{2.46}$$

where η is the normalization vector. For a subprocess $p_1 + p_2 \rightarrow x$, we take $\eta = p_2$, working the c.m. of p_1, p_2 in what follows.

In calculating the traces, γ_5 is introduced by anticommuting the A_1^* and generalizing the 4-dimensional relation

$$[\not{A}_1 2(b \cdot A_1^*)]_\pm = \gamma_5(\not{p}_2 \not{p}_1 \not{b} - \not{b} \not{p}_1 \not{p}_2)/p_1 \cdot p_2, \tag{2.47}$$

which, in 4 dimensions follows from

$$(A_1^\rho A_1^{*\sigma})_\pm = \frac{-i}{p_1 \cdot p_2} \varepsilon^{\rho\sigma\tau\nu} p_{1\tau} p_{2\nu}. \tag{2.48}$$

Defining

$$(\not{A}_1 \not{b}_1 \not{b}_2 \cdots \not{b}_n \not{A}_1^*)_\pm \equiv \gamma_5 \Pi_n(b_1 b_2 \cdots b_n)/p_1 \cdot p_2, \tag{2.49}$$

we have the recurrence relation

$$\Pi_{n+1}(b_1 b_2 \cdots b_{n+1}) = (\not{p}_2 \not{p}_1 \not{b}_{n+1} - \not{b}_{n+1} \not{p}_1 \not{p}_2) \not{b}_1 \not{b}_2 \cdots \not{b}_n - \Pi_n(b_1 b_2 \cdots b_n) \not{b}_{n+1} \tag{2.50}$$

with a similar relation for $A_2^\mu(p_2, \lambda_2)$. Having now traces containing two γ_5 matrices we may anticommute and eliminate the γ_5's via

$$\gamma_5 \gamma_\mu = -\gamma_\mu \gamma_5, \quad \gamma_5^2 = 1, \tag{2.51}$$

in accord with Ref. 39.

Having first eliminated the γ_5's and $\varepsilon^{\mu\nu\lambda\rho}$'s, the remaining traces may be evaluated as in usual DREG. The major limitation is that this method only works when there are traces involving an even number of γ_5's. This is the general regularization used in our calculation for direct photon production, which will be discussed in Sect. 3.3.

HVBM Scheme

This scheme was originally introduced with dimensional regularization[36] and then later made formal in Ref. 40. It is known to be mathematically consistent. The idea is that we formally take $n > 4$ everywhere, but keep the γ_5 matrix and $\varepsilon^{\mu\nu\lambda\rho}$ in 4 dimensions. More precisely,

$$\{\gamma_5, \gamma_\mu\} = 0; \ \mu \leq 4, \qquad [\gamma_5, \gamma_\mu] = 0; \ \mu > 4, \tag{2.52}$$

which follows from the definition

$$\gamma_5 = \frac{i}{4!}\varepsilon_{\mu_1\mu_2\mu_3\mu_4}\gamma^{\mu_1}\gamma^{\mu_2}\gamma^{\mu_3}\gamma^{\mu_4} \tag{2.53}$$

where

$$\varepsilon_{\mu_1\mu_2\mu_3\mu_4} = 0, \quad \mu_i > 4; \tag{2.54}$$

otherwise, it is the usual Levi-Civita tensor.

This scheme is somewhat cumbersome in that it treats the first four dimensions differently than the remaining $n - 4$. Practical calculations are now possible using Tracer[41]. The other disadvantage of this scheme, in polarized processes, is that it manifestly violates helicity conservation of massless fermions, due to the non-anticommutativity of the γ_5 matrix. This requires special treatment, as will be discussed in Sect. 3.1. We do not use this scheme in this work.

Dimensional Reduction

Dimensional reduction[42] is perhaps the simplest of all the dimensional methods. It was originally introduced because DREG violates the supersymmetric Ward identities. It is also manifestly mathematically consistent. The idea is simple; all γ-matrices and tensors are taken to be 4-dimensional, and formally $n < 4$. This implies that the components of all momenta between n and 4 must vanish. We have

the following contraction identities

$$g^{\mu\nu}g_{\mu\nu} = 4, \quad g_n^{\mu\nu}g_{\mu\nu}^n = g^{\mu\nu}g_{\mu\nu}^n = n \tag{2.55}$$

and the usual 4 dimensional relations like

$$\gamma^\mu\gamma^\nu + \gamma^\nu\gamma^\mu = 2g^{\mu\nu}. \tag{2.56}$$

It is also useful to define

$$\gamma_\varepsilon^\mu \equiv \gamma_\nu(g^{\mu\nu} - g_n^{\mu\nu}). \tag{2.57}$$

This method is particularly simple for the calculation of tree graphs (i.e. graphs not involving loops) since the traces are equal to their 4-dimensional counterparts, implying gauge invariance. One may thus use 4-dimensional helicity amplitude methods, for instance. Then the phase space integrals are carried out in n dimensions, providing an IR regulator. As well, the anticommuting γ_5 implies helicity conservation of massless fermions.

The only subtlety comes from the fact that the virtual momentum integrations generate the tensor $g_n^{\mu\nu}$, which is generally contracted with 4-dimensional γ-matrices. This can lead to a term $\sim \gamma_\varepsilon^\mu$ which must be removed by a counterterm, as discussed in Appendix D. Fortunately, these terms are easy to identify, and once general counterterms have been developed, one can simply do all the traces in 4 dimensions. Then one integrates in n dimensions and adds some simple counterterms to remove the terms arising from the γ_ε^μ terms. Equivalently, we can work at the amplitude level and throw away the γ_ε^μ terms as they appear.

Admittedly, DREG does not have this difficulty for virtual loops not involving the γ_5 matrix: but DRED has no problem when the γ_5 appears. The HVBM scheme is known to generate spurious divergences (at two loops) for loop graphs involving

γ_5. In light of these considerations, we use DRED in the calculation of the transverse Drell-Yan process (Chapter 4) and for heavy-quark production by photons (Chapter 5). As well, we use it for the subset of diagrams in direct photon production (Chapter 3) involving traces with only one γ_5.

Finally, we note that various problems with DRED have been pointed out[43], most of which have been resolved[44] and do not apply to the calculations presented here.

2.3 Renormalization

When we calculate physical quantities, some of the divergences will cancel via the Bloch-Nordseick mechanism or via the KLN theorem[45] which states that the cross section will be free of IR divergences if we sum over initial and final degenerate states. There is no automatic cancellation of UV singularities, or mass singularities in differential cross sections. Also, external lines contain non-cancelling soft divergences, before wave function renormalization. In fact, one can operationally *define* a mass singularity as any non-cancelling IR divergence which is still present after wave function renormalization. Once all the singular terms are removed by renormalization, we set the regularization parameters to their physical values and obtain the physical result.

In order to account for these remaining singularities, we postulate that the physical parameters, which we now call *bare* parameters, i.e. charge, mass, wave functions, parton distributions, etc... are actually infinite (or infinitesimal) in the limit where the regularization parameters return to their physical values. We also postulate that the experimentally observed physical parameters, which we will now call *renormalized* parameters, are multiplicatively related[46] with the bare ones via *renormalization constants*, Z_i. For instance, the bare parameters occurring in the QCD Lagrangian

(1.12) are related with the renormalized ones via

$$G^a_\mu = Z_3^{1/2} G^a_{r\mu}, \quad \eta^a_{1,2} = \tilde{Z}_3^{1/2} \eta^a_{r1,2}, \quad \psi = Z_2^{1/2} \psi_r$$

$$g = Z_g g_r, \quad \xi = Z_3 \xi_r, \quad m = Z_m m_r, \tag{2.58}$$

where the subscript r denotes renormalized.

These constants are determined order by order in the renormalized coupling by demanding that the physical cross section is finite. There is some ambiguity in what finite part to subtract. The schemes for doing this are known as *renormalization schemes*. Renormalization schemes will be discussed in the next section.

In order to systematically determine the renormalization constants, we must rewrite the QCD Lagrangian in terms of the renormalized parameters and determine the Feynman rules for the resulting counterterms. Let $\mathcal{L}_R$ denote $\mathcal{L}$ of (1.12) with all the bare parameters replaced by renormalized ones. Then

$$\mathcal{L} = \mathcal{L}_R + \mathcal{L}_C, \tag{2.59}$$

where $\mathcal{L}_C$ represents effectively the *interaction* terms which give rise to Feynman rules for the counterterms.

Up to a total divergence, we may write[47]

$$\begin{aligned}
\mathcal{L}_C &= (Z_3 - 1)\frac{1}{2} G^{a\mu}_r \delta_{ab} (g_{\mu\nu}\partial^2 - \partial_\mu \partial_\nu) G^{b\nu}_r \\
&+ (\tilde{Z}_3 - 1)\eta^a_{r1} \delta_{ab} (-i\partial^2) \eta^b_{r2} \\
&+ (Z_2 - 1)\overline{\psi}^i_r (i\gamma^\mu \partial_\mu)\psi^i_r - (Z_2 Z_m - 1) m_r \overline{\psi}^i_r \psi^i_r \\
&- (\hat{Z}_1 - 1)\frac{1}{2} g_r f^{abc} (\partial_\mu G^a_{r\nu} - \partial_\nu G^a_{r\mu}) G^{b\mu}_r G^{c\nu}_r \\
&- (Z_4 - 1)\frac{1}{4} g_r^2 f^{abe} f^{cde} G^a_{r\mu} G^b_{r\nu} G^{c\mu}_r G^{d\nu}_r \\
&- (\tilde{Z}_1 - 1) i g_r f^{abc} (\partial^\mu \eta^a_{r1}) \eta^b_{r2} G^c_{r\mu} \\
&+ (Z_{1F} - 1) g_r \bar{\psi}^i_r T^a_{ij} \gamma^\mu \psi^j_r G^a_{r\mu},
\end{aligned} \tag{2.60}$$

where

$$\hat{Z}_1 \equiv Z_g Z_3^{3/2}, \quad Z_4 \equiv Z_g^2 Z_3^2, \quad \tilde{Z}_1 \equiv Z_g \tilde{Z}_3 Z_3^{1/2}$$

$$Z_{1F} \equiv Z_g Z_2 Z_3^{1/2}. \tag{2.61}$$

From (2.60) we obtain the Feynman rules for the counterterms. For instance, for the quark self-energy, the counterterm is

$$i[(Z_2 - 1)\not{p} - (Z_2 Z_m - 1)m_r]\delta_{ij} \tag{2.62}$$

and for the gluon-quark vertex, we have

$$i(Z_{1F} - 1)g_r T^a_{ij}\gamma_\mu. \tag{2.63}$$

From (2.61) we see that there are four different ways to determine Z_g. The equivalence of these methods leads to the *Slavnov-Taylor identity*[48]

$$\frac{\hat{Z}_1}{Z_3} = \frac{\tilde{Z}_1}{\tilde{Z}_3} = \frac{Z_{1F}}{Z_2} = \frac{Z_4}{\hat{Z}_1}. \tag{2.64}$$

This identity is valid in a gauge invariant regularization such as DREG or DRED.

To remove the mass singularities, we must renormalize the structure functions as well. The systematic approach to performing the renormalization is via the operator product expansion. In this approach, the renormalization constants relate the bare and renormalized composite operators via

$$O^{r(j)}_{\mu_1\cdots\mu_n} = O^{(i)}_{\mu_1\cdots\mu_n}(Z_n^{-1})_{ij}. \tag{2.65}$$

This method has been applied successfully to inclusive DIS.

In the parton approach, we renormalize the parton densities directly via

$$f_{i/A}(x) = f^r_{i/A}(x, M_f^2) + c_s \sum_j \frac{\alpha_s}{2\pi}\int_x^1 \frac{dy}{y} f^r_{j/A}(y, M_f^2) P_{ij}(x/y), \tag{2.66}$$

where c_s is some, renormalization scheme dependent, singular coefficient (the meaning of the P_{ij} will be given in Sect. 2.3.2) and M_f^2 denotes the *factorization* (energy) scale, also denoted as Q^2 (especially in DIS). In this way, we see that renormalization schemes which differ by some finite amount at $\mathcal{O}(\alpha_s^n)$ will necessarily lead to P_{ij} which differ at $\mathcal{O}(\alpha_s^{n+1})$ (by some finite amount, since the P_{ij} are finite). This is because, any additional finite subtraction at $\mathcal{O}(\alpha_s^n)$ leads to infinite differences at $\mathcal{O}(\alpha_s^{n+1})$, requiring modification of P_{ij} at $\mathcal{O}(\alpha_s^{n+1})$. We note that the form (2.66) is quite general since, in n dimensions, P_{ij} may have components of $\mathcal{O}(\varepsilon)$, which give rise to a finite subtraction when multiplied by $1/\varepsilon$.

The interpretation is that a parton in a hadron A, may come directly from the hadron or from another parton j in the hadron which emits i collinearly, having momentum fraction x/y. The P_{ij} are determined so as to cancel all mass singularities not cancelled via the Bloch-Nordseick mechanism. The connection between the operator approach and the parton approach will be given in Sect 2.3.2.

Similarly, the fragmentation functions renormalize as

$$\begin{aligned} \mathcal{D}_{A/i}(z) &= \mathcal{D}^r_{A/i}(z, M_f^2) + c_s \sum_j \frac{\alpha_j}{2\pi} \int_z^1 \frac{dy}{y} \mathcal{D}^r_{A/j}(z/y, M_f^2) P_{ji}(y) \\ &= \mathcal{D}^r_{A/i}(z, M_f^2) + c_s \sum_j \frac{\alpha_j}{2\pi} \int_z^1 \frac{dy}{y} \mathcal{D}^r_{A/j}(y, M_f^2) P_{ji}(z/y), \end{aligned} \tag{2.67}$$

where $\alpha_j = \alpha_s$, unless $j = \gamma$, in which case $\alpha_j = \alpha$.

2.3.1 Renormalization Schemes

All renormalization schemes have the common property that the UV divergent part must be subtracted. We now describe four renormalization schemes within the framework of DREG or DRED.

Minimal Subtraction (MS)

In the minimal subtraction scheme,[49] we simply subtract the $1/\varepsilon$ pole which arises from UV divergences. In other words, we choose the renormalization constants Z_i so that only the $1/\varepsilon$ poles are canceled in the Feynman amplitudes.

Modified Minimal Subtraction ($\overline{MS}$)

This scheme was introduced in Ref. 50. It was introduced because the $1/\varepsilon$ pole arising from the UV divergent graphs always occurs in the form

$$\frac{1}{\varepsilon}\frac{\Gamma(1+\varepsilon)}{(4\pi)^{-\varepsilon}} = \frac{1}{\varepsilon} - \gamma_E + \ln 4\pi + \mathcal{O}(\varepsilon). \tag{2.68}$$

where γ_E is Eulers constant. This follows from (2.37) with $m - r = 2$. Hence we subtract $\frac{1}{\varepsilon} - \gamma_E + \ln 4\pi$ everywhere and the resulting expression will be free of the unphysical terms γ_E, $\ln 4\pi$. We use this scheme for all coupling constant renormalizations and for the renormalization of the stucture functions, discussed below. In this work, coupling constant renormalization only occurs in direct photon production.

On-Shell Subtraction

In this scheme, we define the mass and wave function renormalization constants so that the corrections to the self-energies vanish in the on-shell limit. From the form of the wave function renormalization counterterms (i.e. (2.62), (2.63)) one finds that, in the on-shell scheme, at one-loop, the net effect of wave function renormalization, after mass renormalization, is to multiply the self energy insertions on external lines by a factor 1/2. This is due to a cancellation between the wave function renormalization constants occurring in vertex and self-energy counterterms. Or equivalently, the effect is not to include the insertions at all, but multiply the Feynman amplitude by a factor $Z_i^{1/2}$ for each external line with wave function renormalization constant Z_i.

One must adopt this scheme in calculating physical cross sections in order to

cancel the infrared divergence arising from soft gluonic bremsstrahlung. As a result, we renormalize external lines on shell in all cross section calculations. Mass renormalization is only relevant to heavy quarks, and we use the on-shell scheme when considering heavy quark production in Chapter 5.

In the massless case, wave function renormalization is particularly simple, since the self energy insertions on external lines vanish in DREG and DRED. This can be seen on dimensional grounds. The self-energy insertion is proportional to

$$\mu^{2k\epsilon} \int \frac{d^n q_1}{(2\pi)^n} \cdots \int \frac{d^n q_k}{(2\pi)^n} F(p, q_1, \ldots, q_k). \tag{2.69}$$

where p is the momentum of the external particle, F is some function and k denotes the loop-level at which we are working. The integral must have dimensions $(\text{mass})^{-2k\epsilon}$, since the corrections have the same dimensions as the Born term, but since $p^2 = 0$, we cannot form a scalar with dimensions of mass; hence the insertion vanishes.

Since the self energy necessarily has a UV divergence, we may conclude that there has been an exact cancellation between UV and IR divergences resulting from the continuation $\epsilon = \epsilon'$ discussed in Sect. 2.2.2. Alternatively, since we cannot form any scalars with dimensions of mass, all integrals reduce to the form (2.37) with $C = 0$, which was shown to vanish using dimensional continuation.

$\overline{MS}$ (Universal) Subtraction for Parton Distributions and Fragmentation Functions

This is the equivalent of the $\overline{\text{MS}}$ scheme as applied to the renormalization of the parton distributions and fragmentation functions (throughout, unless a distinction is made, by parton distributions we mean both parton distributions and fragmentation functions).

We must define the factor c_s occurring in (2.66), (2.67) to define our subtraction

scheme (as usual, we do not consider any $\mathcal{O}(\varepsilon)$ contributions to P_{ij} as this would not be $\overline{\rm MS}$). The appropriate value is (at one-loop)[51]

$$c_s = \frac{1}{\varepsilon}\left(\frac{4\pi\mu^2}{M_f^2}\right)^{\varepsilon}\frac{\Gamma(1-\varepsilon)}{\Gamma(1-2\varepsilon)} = \left(\frac{\mu^2}{M_f^2}\right)^{\varepsilon}\left(\frac{1}{\varepsilon} - \gamma_{\rm E} + \ln 4\pi\right) + \mathcal{O}(\varepsilon) \tag{2.70}$$

where the terms of $\mathcal{O}(\varepsilon)$ do not contribute in the limit $\varepsilon \to 0$ and are dropped. In addition, there is a factor $(\mu^2/M_f^2)^{\varepsilon}$ which introduces the factorization scale, M_f, in the cross section.

Some explanation of this additional factor is in order. If we do not include the factor $(\mu^2/M_f^2)^{\epsilon}$, then in the cross section, the collinear divergence will appear with a factor $(\mu^2/k^2)^{\epsilon}$ relative to the factorization counterterm, where k^2 is some momentum squared (i.e. s). This is because there is an extra $g^2\mu^{2\epsilon}$ factor in the bremsstrahlung cross section relative to the Born cross section, but the dimensions must be the same. Hence the final finite result will contain the logarithm, $\ln(k^2/\mu^2)$. Since in dimensional methods, we only need to introduce the parameter μ, there is no distinction between energy scales, μ, which are related to UV renormalization and those related to renormalization of the mass singularities. If we now include the factor (μ^2/M_f^2) in c_s, then the finite cross section will contain the logarithm, $\ln(k^2/M_f^2)$, instead. So we simply make a distinction between the UV renormalization scale, μ, and the mass singularity renormalization scale M_f. In our calculations, we always take $\mu = M_f$, hence the result coincides with the usual $\overline{\rm MS}$ result.

When combined with the evolution of the parton distributions (which are functions of M_f), the sensitivity to scale changes in the parton distributions is reduced due to the terms $\sim \ln(k^2/M_f^2)$ in the cross section. A similar statement holds for the coupling, since coupling renormalization introduces terms $\sim \ln(k^2/\mu^2)$. The evolution (renormalization group) equations for the parton distributions and coupling

constant will be given in the next section.

2.3.2 Renormalization Group/Evolution Equations

In the previous section, we saw that different subtraction schemes may be adopted (i.e. MS or $\overline{\text{MS}}$). These will in general lead to different analytical results for the cross section. But physical predictions should be unique to any given order. As a result, there must be some additional scheme dependence of the physical parameters to compensate. First, we discuss the renormalization group equation for the coupling constant, then we examine the evolution of the parton distributions, as well as the choice of scale ambiguity relevant to both.

Coupling Constant Renormalization Group Equation

In order that two renormalization schemes be equivalent, we should be able to get the result of one scheme by making finite renormalizations of the physical parameters (i.e. coupling) in the other. Hence, different regularization schemes (i.e. DRED and DREG) should be equivalent to different subtraction schemes. Thus, working at any order in α_s, at some energy scale, μ^2, one may choose suitable parameters in either scheme so as to reproduce experiment.

As one goes to another energy scale, μ'^2, the physical parameters in each scheme must change in such a way that differences in physical predictions between any two schemes are higher order in α_s.

Before determining the evolution of the coupling with μ^2, we note that since μ is arbitrary, the physical results should not depend on it:

$$\frac{d}{d\mu}\tilde{G}_n^{\text{tc}}(p,g,m)|_{g,m} = 0, \tag{2.71}$$

where $\tilde{G}_n^{\text{tc}}(p,g,m)$ is the unrenormalized truncated, connected, n-point Greens function and p represents the external momenta. In the MS (or $\overline{\text{MS}}$) scheme, this leads to

a renormalization group equation known as the *t'Hooft-Weinberg equation*.[49,52] We also obtain an equation determining $g_r(\mu^2)$ as a function of μ^2/μ_0^2 and $g_r(\mu_0^2)$ (for arbitrary μ, μ_0).

Define

$$\beta \equiv \mu \frac{\partial g_r}{\partial \mu}|_{g,m} \,. \tag{2.72}$$

Then, in the MS ($\overline{\rm MS}$) scheme, we can show that

$$\beta(g) \equiv -\beta_0 g^3 - \beta_1 g^5 - \beta_2 g^7 + \mathcal{O}(g^9) = g^2 \frac{dA_g}{dg}, \tag{2.73}$$

where

$$Z_g = 1 + \frac{A_g}{\varepsilon} + \frac{B_g}{\varepsilon^2} + \cdots, \tag{2.74}$$

noting that terms of $\mathcal{O}(\varepsilon)$ in A_g do not affect $\beta(g)$, since we take $\varepsilon \to 0$ after renormalization. Z_g may be determined using

$$Z_g = \frac{\tilde{Z}_1}{\tilde{Z}_3 Z_3^{1/2}}, \tag{2.75}$$

for instance (see (2.61)). It can be shown that β_0 and β_1 are scheme independent and that

$$\begin{aligned} \beta_0 &= \frac{1}{(4\pi)^2} \frac{11N_c - 2N_f}{3} \\ \beta_1 &= \frac{1}{(4\pi)^4} \left[102 - \frac{38}{3} N_f \right]. \end{aligned} \tag{2.76}$$

The solution of the renormalization group equation for α_s at one-loop is

$$\alpha_s(\mu^2) = \frac{\alpha_s(\mu_0^2)}{1 + 4\pi\beta_0 \alpha_s(\mu_0^2) \ln(\mu^2/\mu_0^2)}, \tag{2.77}$$

which relates $\alpha_s(\mu^2)$ to $\alpha_s(\mu_0^2)$, where μ_0^2 is some arbitrary scale. We see that as $\mu^2 \to \infty$, $\alpha_s \to 0$. This is known as asymptotic freedom and holds for $N_f \leq 16$. We are far below this limit at present energies ($N_f \leq 6$).

We can put (2.77) in a more useful form by noting that there exists μ^2 such that $\alpha_s(\mu^2) = \infty$. Define

$$\Lambda^2 \equiv \mu_0^2 \exp\left[\frac{-1}{4\pi\beta_0\alpha_s(\mu_0^2)}\right], \tag{2.78}$$

then

$$\alpha_s(\mu^2) = \frac{1}{4\pi\beta_0 \ln(\mu^2/\Lambda^2)} \tag{2.79}$$

and we see explicitly that $\alpha_s(\Lambda^2) = \infty$ and perturbative QCD fails for $Q^2 \approx \Lambda^2$. So now, instead of having to define some arbitrary scale, μ_0 at which to determine $\alpha_s(\mu_0^2)$ and then evolving to μ^2 via (2.77), we simply determine, experimentally, the quantity Λ at *any* energy. The assumption being that Λ is independent of μ_0, since μ_0 is arbitrary, while Λ is in some sense a physical observable. By comparing predictions, like the cross section for $e^+e^- \to 3$ jets divided by $e^+e^- \to 2$ jets at some $\mu_0^2 = s$, with experiment, we may determine $\alpha_s(\mu_0^2)$ so as to agree with experiment, then obtain Λ using (2.78).

The actual value of Λ (or α_s) determined will depend on the subtraction (or regularization) scheme since, beyond leading order, predictions carry scheme dependence in general, which is to be reflected in different values of Λ. In addition, the renormalization group equation for α_s changes beyond leading order. Keeping next-to-leading logarithms in the solution of the renormalization group equation leads to

$$\alpha_s(\mu^2) = \frac{1}{4\pi\beta_0 \ln(\mu^2/\Lambda^2)}\left[1 - \frac{\beta_1}{\beta_0^2}\frac{\ln\ln(\mu^2/\Lambda^2)}{\ln(\mu^2/\Lambda^2)}\right], \tag{2.80}$$

where, now

$$\Lambda \equiv \mu_0 e^{-1/(2\beta_0 g^2)}\left(\frac{1+\beta_1 g^2/\beta_0}{\beta_0 g^2}\right)^{\beta_1/(2\beta_0^2)}, \qquad g^2 \equiv g^2(\mu_0). \tag{2.81}$$

Experimentally, using the $\overline{\text{MS}}$ scheme, one finds $\Lambda \simeq 0.2$ GeV, which is in the neighborhood of the lightest hadrons (i.e. pions) masses.

It can be shown that when calculating cross sections at the n-loop level, one must use $n+1$-loop evolution equations to get physical predictions which are scheme independent to n-loop order in α_s; this means that differences in predictions of different schemes are an order higher in α_s.

Evolution of the Parton Distributions

In the parton model, the evolution of the parton distributions is determined via the Altarelli-Parisi splitting functions,[53] $P_{ij}(x)$, related to the probability of parton j splitting into parton i, having a fraction x of parton j's momentum, and an arbitrary set of collinear partons (depending on the order) carrying the remainder of the momentum.

We can make this clearer by considering the $2 \to n$ process (all particles massless)

$$a(p_a) + b(p_b) \to c_1(k_1) + c_2(k_2) + \cdots + c_n(k_n). \tag{2.82}$$

Let the angle between k_1 and p_a be denoted by θ. Then in the limit $\theta \approx 0$, we have (at one-loop)

$$|M|^2_{2\to n}(ab \to c_1 \cdots c_n) \sim \sum_d P_{da}(z)|M|^2_{2\to n-1}(db \to c_2 \cdots c_n), \tag{2.83}$$

where $a \to d + c_1$ and

$$k_1 \approx (1-z)p_a \to p_d \approx zp_a \tag{2.84}$$

with analogous relations for the polarized cases. This is (loosely speaking) the original method used by Altarelli and Parisi to define the split functions. The important point is that whenever P_{ij} arises in this way, either i is real and j is virtual or j is real and i is virtual; there are no processes $a \to b + c$ where all three particles are massless and real.

In the operator product expansion, one determines directly the anomalous dimension matrix

$$\gamma_n^{ij} = \begin{bmatrix} \gamma_n^{qq} & \gamma_n^{qg} \\ \gamma_n^{gq} & \gamma_n^{gg} \end{bmatrix} \tag{2.85}$$

using

$$\gamma_n \equiv \mu \frac{\partial Z_n}{\partial \mu} Z_n^{-1}|_{g=0}, \tag{2.86}$$

where Z_n^{ij} is defined by (2.65). The γ_n^{ij} are related to the P_{ij} via

$$\gamma_n^{ij} = \int_0^1 dx x^{n-1} P_{ij}(x). \tag{2.87}$$

Hence, one could conceivably invert the γ_n^{ij} to determine the P_{ij} via the inverse Mellin transform

$$P_{ij}(x) = \int_{\delta-i\infty}^{\delta+i\infty} \frac{dn}{2i\pi} x^{-n} \gamma_n^{ij}, \tag{2.88}$$

where δ is a conveniently chosen arbitrary constant. The scheme dependence (at two loops) of the P_{ij} arises, in this approach, from the scheme dependence of the anomalous dimensions. Alternatively, one may work directly with the parton model expression (2.66) to determine the P_{ij} to the desired order in α_s by demanding the cancellation of the mass singularities in the cross sections.

At the one-loop level, the longitudinally polarized split functions

$$\Delta P_{ab}(z) \equiv P_{a_+b_+}(z) - P_{a_-b_+}(z), \tag{2.89}$$

with $+,-$ denoting helicities, are given by

$$\begin{aligned}
\Delta P_{qq}(z) &= C_F \left[\frac{1+z^2}{(1-z)_+} + \frac{3}{2}\delta(1-z) \right] = C_F \left[\frac{2}{(1-z)_+} - 1 - z + \frac{3}{2}\delta(1-z) \right], \\
\Delta P_{qg}(z) &= z - 1/2, \\
\Delta P_{gq}(z) &= C_F(2-z), \\
\Delta P_{gg}(z) &= N_c \left[(1+z^4) \left(\frac{1}{z} + \frac{1}{(1-z)_+} \right) - \frac{(1-z)^3}{z} + \left(\frac{11}{6} - \frac{N_f}{3N_c} \right) \delta(1-z) \right]
\end{aligned} \tag{2.90}$$

$$= 2N_c\left[\frac{1}{(1-z)_+} + 1 - 2z\right] + \frac{11N_c - 2N_f}{6}\delta(1-z).$$

The function $1/(1-w)_+$ is defined through

$$\int_{w_1}^1 dw \frac{f(w)}{(1-w)_+} = \int_{w_1}^1 dw \frac{f(w)-f(1)}{(1-w)} + f(1)\ln(1-w_1). \tag{2.91}$$

Here we give the other commonly used "+" function.

$$\int_{w_1}^1 dw f(w)\left(\frac{\ln(1-w)}{(1-w)}\right)_+ = \int_{w_1}^1 dw[f(w)-f(1)]\frac{\ln(1-w)}{(1-w)} + \frac{f(1)}{2}\ln^2(1-w_1). \tag{2.92}$$

for later use. We note that

$$\Delta P_{qg}(z) = -\Delta P_{qg}(1-z) \rightarrow P_{q+g+}(z) = P_{q-g+}(1-z), \tag{2.93}$$

representing the fact that when a gluon splits into a $q\bar{q}$ pair, the q and $\bar{q}$ have opposite helicities. Also, $\Delta P_{gq}(z) > 0$, meaning that polarized quarks tend to produce gluons polarized in the same direction.

Analogously, we may define the transversity splitting function

$$\Delta_T P_{ab}(z) \equiv P_{a^\dagger b^\dagger}(z) - P_{a^\dagger b^\dagger}(z), \tag{2.94}$$

which, at one-loop, is given by[54]

$$\Delta_T P_{qq}(z) = C_F\left[\frac{2}{(1-z)_+} - 2 + \frac{3}{2}\delta(1-z)\right]. \tag{2.95}$$

Noting that $P_{qq}(z) = \Delta P_{qq}(z)$ and that

$$P_{a^\dagger b^\dagger}(z) = \frac{1}{2}[P_{qq}(z) - \Delta_T P_{qq}(z)], \tag{2.96}$$

we see explicitly from (2.90) and (2.95) that

$$P_{a^\dagger b^\dagger}(z) = (1-z)/2, \tag{2.97}$$

meaning that transversity can change as a result of collinear gluon radiation (hard, in particular), unlike $P_{q\,q}(z) = 0$ the longitudinal case. So, in this sense, there is no analogy between transversity and helicity of massless quarks.

Having obtained the split functions, to the desired order (so far only one-loop polarized split functions are known), we evolve the parton densities to any scale, Q^2, using the Gribov-Lipatov-Altarelli-Parisi (GLAP) equations[55,53]

$$\begin{aligned}
\frac{d\Delta f_{q_v}(x,Q^2)}{d(\ln Q^2)} &= \frac{\alpha_s(Q^2)}{2\pi}\int_x^1 \frac{dy}{y}[\Delta P_{qq}(\frac{x}{y})\Delta f_{q_v}(y,Q^2) + \Delta P_{qg}(\frac{x}{y})\Delta f_g(y,Q^2)] \\
\frac{d\Delta f_{q_v}(x,Q^2)}{d(\ln Q^2)} &= \frac{\alpha_s(Q^2)}{2\pi}\int_x^1 \frac{dy}{y}[\Delta P_{qq}(\frac{x}{y})\Delta f_{q_v}(y,Q^2)] \\
\frac{d\Delta f_g(x,Q^2)}{d(\ln Q^2)} &= \frac{\alpha_s(Q^2)}{2\pi}\int_x^1 \frac{dy}{y}[\sum_{i=1}^{2N_f}\Delta P_{gq}(\frac{x}{y})\Delta f_{q_i}(y,Q^2) \\
&+ \Delta P_{gg}(\frac{x}{y})\Delta f_g(y,Q^2)].
\end{aligned} \tag{2.98}$$

Note that since (2.66) and (2.67) have the same form, the evolution equations for the fragmentation functions are the same as those for the parton densities, with $f \to \mathcal{D}$ and $P_{ij} \to P_{ji}$.

For the transversity densities, the evolution is given by

$$\frac{d\Delta_T f_q(x,Q^2)}{d(\ln Q^2)} = \frac{\alpha_s(Q^2)}{2\pi}\int_x^1 \frac{dy}{y}[\Delta_T P_{qq}(\frac{x}{y})\Delta_T f_q(y,Q^2)]. \tag{2.99}$$

In Appendix A, we use the GLAP equations directly to get Q^2-dependent parameterizations for the polarized parton distributions in the proton.

These equations have a simple physical interpretation: (i) a quark may split into a collinear quark or gluon (and an arbitrary number of collinear partons, depending on the order), which contributes to both the evolution of the quark and gluon distributions; (ii) a gluon may split into a collinear gluon, contributing to the evolution of the gluon distribution; (iii) a gluon may split into a quark-antiquark pair, contribut-

ing to the evolution of the sea quark distributions. Note that at the two-loop level, the split function $P_{\bar{q}q}$ appears.

At first sight, it seems like a strictly additive process: the distributions receive contributions from radiation of harder (more energetic) partons, increasing the magnitude of the distributions at small x. Somehow, the distributions should decrease at large x, due to the softening of the partons which radiate. This is taken into account by the terms $\sim 1/(1-x)_+$. From (2.91) we see that these will yield a term $\sim \Delta F(x)\ln(1-x)$. Since $x<1$, the contribution has opposite sign to $\Delta F(x)$, representing a softening of the distribution at x, with increasing energy scale, Q^2.

Choice of Scale Ambiguity

We have explicitly shown the dependence of the physical parameters (coupling and structure functions) on the arbitrary scale μ (or M_f). Presumedly, this dependence should be cancelled by the explicit dependence of the renormalized cross section (or Feynman amplitude) on μ. Working to any finite order though, the choice of μ does indeed affect the predictions, rather sensitively at leading or even next-to-leading order in QCD. Hence, working to finite order, there must be some limitations on the choice of μ.

Implicitly there are limitations. In the previous section, we pointed out that the $\overline{\rm MS}$ (or MS) scheme introduces terms $\sim \ln(k^2/\mu^2)$ (where k^2 is some momentum scale occurring in the cross section) into the cross section. The limitation on μ is the following. From the beginning, in applying perturbation theory to generate the Feynman rules, we assumed a (reasonably) convergent perturbation series. In order to ensure this, we must choose μ^2 of the same order as k^2, i.e. a typical momentum transfer squared, so as not to develop large logarithms which will ruin the perturbation expansion.

The other logarithms which occur are $\sim \ln(\mu^2/\Lambda^2)$ in $\alpha_s(\mu^2)$. Since $\mu^2 \approx |k^2|$ and since α_s becomes large for $\mu^2 \approx \Lambda^2$, we see that the overall constraint on μ^2, k^2

$$\mu \approx \sqrt{|k^2|} \gg \Lambda \tag{2.100}$$

may be applied in order to ensure a (reasonably) reliable perturbation series. We already assumed that

$$M_f \approx \sqrt{|k^2|} \gg \Lambda, \tag{2.101}$$

in order to use the parton model, and hence the Altarelli-Parisi equations. As noted earlier, we always take $\mu = M_f$ in our calculations.

Chapter 3

Large-p_T Direct Photon Production

Direct photon production in unpolarized proton-proton collisions has been a major tool not only in testing perturbative QCD, but in constraining the gluon distribution.[56] This is because processes such as deep inelastic scattering are rather insensitive to the gluon distribution in a direct sense (since it arises only in next-to-leading order), while being rather sensitive to the quark distributions (valence in particular). On the other hand, direct photon production in p-p collisions has approximately linear sensitivity to the gluon distribution at leading order.

The EMC[11] (and now the SMC[20] and E142[21]) experiment has raised questions about the *longitudinal* spin dependence of the parton distributions. The EMC group concluded that, in the naive parton model, the net contribution of the quarks' spin to that of the proton was consistent with zero (with the new data, the quarks contribute more, but still rather little, as discussed in Sect. 2.1.1). This would imply that either a large part of the proton's spin comes from the angular momentum of the partons or that there is a sizable contribution from the gluon spin (or both of these combined). The essential question, therefore, is the size of the polarized gluon distribution, Δg, as determined using the perturbative QCD approach.[57,58]

A number of polarized reactions dominated by subprocesses with gluons in the initial state have been considered:

$$\vec{p}\vec{p} \to \gamma X, ^{59} \qquad \vec{p}\,p \to \vec{l}^{-}\, l^{+} X, ^{60} \qquad \vec{p}\vec{p} \to Q\bar{Q}X, ^{61}$$

$$\vec{\gamma}^{(*)}\vec{p} \to Q\bar{Q}X, ^{62} \qquad \vec{\gamma}\vec{p} \to hX, ^{63} \qquad \vec{p}\,p \to \vec{\gamma} X, ^{64} \quad \ldots$$

where the arrows above the particles indicate longitudinal polarization and X represents an arbitrary set of final state particles. These processes were previously calculated only to leading order. We present the first complete calculation[65] of higher order corrections, to $\mathcal{O}(\alpha\alpha_s^2)$, with analytical results for $\vec{A}\vec{B} \to \gamma X$ and numerical results for $\vec{p}\vec{p} \to \gamma X$ (much of the non-Abelian corrections follow from those in Ref. (38)). Soon after, an independent calculation was published.[66] These represent the first ever *nontrivial* HOC in $\vec{p}\vec{p}$ collisions.

The HOC are important since they are comparable in magnitude to the leading order results. Large corrections of opposite sign would lead to small cross sections and this would differ from the unpolarized case (large, positive HOC).[67,68] This would not be good since a perturbatively stable asymmetry is needed to determine reliably the ratio of the polarized to the unpolarized gluon distributions. Also, HOC reduce the sensitivity to the arbitrary mass scales μ, M_f, discussed in Sect. 2.3.

RHIC is the ideal collider for studying this process and the RHIC Spin Collaboration[23] has been formed with the intent of studying polarized processes there. Direct photon production will be studied in the energy range $100 \leq \sqrt{S} \leq 500$ GeV in the first experiments scheduled for 1999 or 2000. The experimental details are given in Sect. 1.3.

Figure 3.1: Feynman diagrams for the gluon-quark subprocess. (a) $\vec{g}\vec{q} \rightarrow \gamma q$ (b) $\vec{g}\vec{q} \rightarrow \gamma qg$. Dashed lines represent gluons.

3.1 Basic Subprocesses and Squared Amplitudes

We may write the general process as follows

$$A(P_A, \lambda_A) + B(P_B, \lambda_B) \rightarrow \gamma(p_3) + X, \tag{3.1}$$

where λ_A, λ_B indicate the helicities (actually chiralities) of A, B.

In large-p_T direct photon production, the photon is produced at large transverse momentum (p_T) with respect to the beam axis, and it is produced via QCD hard scattering at the subprocess level (i.e. not via secondary decays). Hence, we must determine the squared amplitudes for all the contributing subprocesses.

We group the subprocesses according to the following subsets:

(i) $\vec{g}\vec{q} \rightarrow \gamma q$ (Fig. 3.1a), $\vec{g}\vec{q} \rightarrow \gamma qg$ (Fig. 3.1b). This is the *dominant* subprocess.

(ii) $\vec{q}\bar{\vec{q}} \rightarrow \gamma g$ (Fig. 3.2a), $\vec{q}\bar{\vec{q}} \rightarrow \gamma gg$ (Fig. 3.2b), $\vec{q}\bar{\vec{q}} \rightarrow \gamma q\bar{q}$ (Fig. 3.2c). The $\vec{q}$, $\bar{\vec{q}}$ annihilate in this subset.

(iii) $\vec{g}\vec{g} \rightarrow \gamma q\bar{q}$ (Fig. 3.3a).

(iv) $\vec{q}\vec{q} \rightarrow \gamma qq$ (Fig. 3.3b) (or $\vec{q}\bar{\vec{q}} \rightarrow \gamma q\bar{q}$ with $\vec{q}$, $\bar{\vec{q}}$ not annihilating).

We make the important note that each subset is separately *gauge invariant*. Also, the $\vec{g}\vec{g}$ and $\vec{q}\vec{q}$ subprocesses give little contribution (except in certain kinematic

Figure 3.2: Feynman diagrams for the quark-antiquark subset where the $\vec{q}$, $\bar{\vec{q}}$ annihilate. (a) $\vec{q}\,\bar{\vec{q}} \to \gamma g$. (b) $\vec{q}\,\bar{\vec{q}} \to \gamma gg$. (c) $\vec{q}\,\bar{\vec{q}} \to \gamma q\bar{q}$. Dotted lines represent ghosts.

Figure 3.3: Feynman diagrams for (a) the gluon-gluon subprocess: $\bar{\vec{g}}\,\bar{\vec{g}} \to \gamma q\bar{q}$ (b) the quark-quark subprocess: $\vec{q}\,\bar{\vec{q}} \to \gamma qq$ (or the subset $\vec{q}\,\bar{\vec{q}} \to \gamma q\bar{q}$ with $\vec{q}$, $\bar{\vec{q}}$ not annihilating).

regions where $\bar{\vec{q}}\,\bar{\vec{q}}$ gives some contribution) since they have no loop graphs (and hence no soft divergences) which, together with the related soft and collinear gluon bremsstrahlung contributions, give rise to a dominant part.[68] The $q\bar{q}$ subprocess also contributes little, in $\bar{\vec{p}}\,\bar{\vec{p}}$ collisions, due to the smallness of the polarized antiquark distributions in the proton.

Define

$$\Delta|M|^2 \equiv \frac{1}{2}[|M|^2(++) - |M|^2(+-)], \tag{3.2}$$

where $|M|^2(\lambda_1\lambda_2)$ denotes the squared amplitude for the subprocess where p_1, p_2 have helicities λ_1, λ_2 respectively. We have, as usual, summed over colors and final helicities and averaged over initial colors. This is the quantity of interest for use in the parton model.

The calculation is somewhat simplified by noting that the entire set (ii) follows from the corresponding unpolarized cross sections[67,68] by an overall minus sign. This is because helicity conservation of massless fermions implies

$$M(+,+) = 0 \tag{3.3}$$

for these graphs. The same applies to the interference between graphs ii(c) and (iv) for the quark-antiquark case. The two quark lines in (iv) are connected in the interference so that

$$\Delta|M|^2_{q\bar{q}} = -|M|^2_{q\bar{q}} \tag{3.4}$$

for these sets of graphs. We note here that (3.3) is not satisfied in the HVBM scheme to $\mathcal{O}(\varepsilon)$ (or $\mathcal{O}(1)$ after phase space integrations). Hence the authors of Ref. 66 (who use the HVBM scheme) were forced to introduce a new subtraction scheme, which they call $\overline{\text{MS}}_p$, in order to satisfy (3.3) and in order to agree with various results from the operator product expansion, relevant to deep-inelastic scattering.

In 4 dimensions, the squared matrix elements of the $2 \to 3$ particle subprocesses can be written in a compact product form[69,70] involving only 2 factors. In the limit where one of the outgoing photons or gluons is soft, we obtain an expression proportional to the remaining $2 \to 2$ squared amplitude.

For $\bar{q}\,(p_1)\;\bar{q}\,(p_2) \to \gamma(p_3)q(p_4)g(p_5)$ (subset i(b)), we find (with $(ij) \equiv p_i \cdot p_j$)

$$\begin{aligned}
\Delta|M|^2 \;=\; & \frac{e_q^2 e^2 g^4}{2^5}\frac{C_F}{N_c}\{3[(12)-(25)]^2(15)(24) - 3[(45)-(14)]^2(15)(24) \\
& - 2[(12)-(25)]^3(24) + 2[(45)-(14)]^3(24) \\
& - 2[(45)-(14)](24)^3 + 2[(12)-(25)](24)^3 + (12)(14)^3 - (12)^3(14) \\
& + (45)(25)^3 - (45)^3(25) \\
& + [(45)-(14)]^3[(12)-(25)] - [(45)-(14)][(12)-(25)]^3\}\frac{1}{(12)(45)(14)(25)}
\end{aligned}$$

$$\times \left\{ \frac{(24)}{(23)(43)} - N_c^2 \frac{(12)(45)+(14)(25)}{(15)(24)} \frac{(24)}{(23)(43)} \right\}. \tag{3.5}$$

for $\vec{g}\ (p_1)\ \vec{g}\ (p_2) \to \gamma(p_3)q(p_4)\bar{q}(p_5)$ (subset (iii)),

$$\begin{aligned}
\Delta|M|^2 &= \frac{e_q^2 e^2 g^4}{2^8} C_F \{(12)^3(45)+(12)(45)^3+(14)^3(15)+(14)(15)^3+(24)^3(25) \\
&+ (24)(25)^3-[(14)+(24)]^3[(15)+(25)]-[(15)+(25)]^3[(14)+(24)]\} \\
&\times \left\{ \frac{(45)}{(43)(53)} - N_c^2 \frac{(14)(25)+(15)(24)}{(12)(45)} \frac{(45)}{(43)(53)} \right\} /(14)(15)(24)(25),
\end{aligned} \tag{3.6}$$

and for $\vec{q}_\alpha\ (p_1)\ \vec{q}_\beta\ (p_2) \to \gamma(p_3)q_\alpha(p_4)q_\beta(p_5)$ (subset (iv)),

$$\begin{aligned}
\Delta|M|^2 &= \frac{e^2 g^4}{2^4} \frac{C_F}{N_c} \left\{ \frac{(12)^2+(45)^2-(15)^2-(24)^2}{(14)(25)} \right. \\
&+ \delta_{\alpha\beta} \left[\frac{(12)^2+(45)^2-(14)^2-(25)^2}{(15)(24)} + \frac{1}{3} \frac{(14)(25)+(15)(24)-(12)(45)}{(14)(25)(15)(24)} \right. \\
&\times \left. [(12)^2+(45)^2] \right] \left\} \left\{ e_\alpha^2 \frac{(14)}{(13)(43)} + e_\beta^2 \frac{(25)}{(23)(53)} \right. \right. \\
&- \left. \left. e_\alpha e_\beta \left[\frac{(12)}{(13)(23)} + \frac{(45)}{(43)(53)} - \frac{(15)}{(13)(53)} - \frac{(24)}{(23)(43)} \right] \right\}.
\end{aligned} \tag{3.7}$$

This form is quite compact and useful in Monte Carlo calculations, for instance. As well, it serves as a good check of the squared amplitudes.

3.2 General Formalism and Kinematics

Firstly, we define the observables

$$S = (P_A + P_B)^2, \quad \eta = \ln(\cot\frac{\theta_3}{2}), \quad p_T = p_{3,\perp}, \quad x_T = \frac{2p_T}{\sqrt{S}} \tag{3.8}$$

where θ_3 is the angle between p_3 and P_A in the P_A, P_B c.m..

For a general subprocess (with respect to the intial particles) contribution

$$\vec{a}\ (p_1) + \vec{b}\ (p_2) \to c(p_3') + x' \to \gamma(p_3) + x; \quad p_3 = zp_3' \tag{3.9}$$

we may define the invariants

$$s = (p_1 + p_2)^2, \quad t = (p_1 - p_3)^2, \quad u = (p_2 - p_3)^2, \quad s_2 = (p_1 + p_2 - p_3)^2, \quad (3.10)$$

$$v = 1 + \frac{t}{s}, \quad w = -\frac{u}{s+t} \quad \rightarrow \quad t = -s(1-v), \quad u = -svw, \quad s_2 = sv(1-w).$$

Also note

$$p_1 = x_a P_A, \quad p_2 = x_b P_B \quad \rightarrow \quad s = x_a x_b S. \quad (3.11)$$

For the general process $\bar{A} + \bar{B} \rightarrow \gamma + X$, we are interested in the inclusive cross section

$$E\Delta\frac{d\sigma}{d^3p}(S, p_T, \eta) = \frac{1}{2}\left\{E\frac{d\sigma}{d^3p}(A(+)B(+) \rightarrow \gamma X) - E\frac{d\sigma}{d^3p}(A(+)B(-) \rightarrow \gamma X)\right\}, \quad (3.12)$$

where the + and − denote helicities, and $p \equiv p_3$, $E \equiv E_3$. For $A = B$ (i.e. pp collisions), $\sigma(\eta) = \sigma(-\eta)$ due to symmetry.

Since E/d^3p is a Lorentz invariant, the contribution of (3.9) is, according to (1.16),

$$\begin{aligned} E\Delta\frac{d\sigma}{d^3p} &= \sum_{abc}\int_0^1 \frac{dx_a}{x_a}\frac{dx_b}{x_b}\frac{dz}{z^2}\Delta F_{a/A}(x_a, M_f^2)\Delta F_{b/B}(x_b, M_f^2)\mathcal{D}_{\gamma/c}(z, M_f^2) \\ &\times E\Delta\frac{d\hat{\sigma}_{abc}}{d^3p}\theta(s+t+u) + (1-\delta_{ab})(A \leftrightarrow B, \eta \leftrightarrow -\eta). \end{aligned} \quad (3.13)$$

The $\theta(s+t+u)$ and $(\eta \leftrightarrow -\eta)$ arise since we are now fixing p_3.

We do not consider any finite fragmentation contributions, $\mathcal{D}_{\gamma/k}(z)$, other than from

$$\mathcal{D}_{\gamma/\gamma}(z) = \delta(1-z). \quad (3.14)$$

Since the fragmentation function $\mathcal{D}_{\gamma/q}(z)$ is $\mathcal{O}(\alpha)$ and is convoluted with Born cross sections of $\mathcal{O}(\alpha_s^2)$, the fragmentation contribution can be viewed as a higher order effect ($\mathcal{O}(\alpha_s^2\alpha)$). Since these fragmentation functions are not well known at this time, we reserve their inclusion for a future work. The $\mathcal{D}_{\gamma/q}$ are found to depend radically

on the choice of factorization scheme beyond leading order,[71] and there are unknown hadronic components. Also, at large x_T values, the contributions will be small, due to the softness of the $\mathcal{D}_{\gamma/q}(z)$.

Hence (3.13) reduces to

$$E\Delta\frac{d\sigma}{d^3p} = \sum_{ab}\int_0^1\frac{dx_a}{x_a}\int_0^1\frac{dx_b}{x_b}\Delta F_{a/A}(x_a,M_f^2)\Delta F_{b/B}(x_b,M_f^2) \times E\Delta\frac{d\hat{\sigma}_{ab}}{d^3p}\theta(s+t+u)+(1-\delta_{ab})(A\leftrightarrow B,\eta\leftrightarrow-\eta). \tag{3.15}$$

Using the relation, for an arbitrary function G,

$$\int_0^1\frac{dx_a}{x_a}\int_0^1\frac{dx_b}{x_b}\frac{G(x_a,x_b)}{s^2v}\theta(s+t+u)=\frac{1}{p_T^4}\int_{v_1}^{v_2}dv\,v(1-v)\int_{w_1}^1 dw\,w\,G(v,w). \tag{3.16}$$

we obtain

$$E\Delta\frac{d\sigma}{d^3p} = \sum_{ab}\frac{1}{p_T^4}\int_{v_1}^{v_2}dv\,v(1-v)\int_{w_1}^1 dw\,w\Delta F_{a/A}(x_a,M_f^2)\Delta F_{b/B}(x_b,M_f^2) \times\left(s^2vE\Delta\frac{d\hat{\sigma}_{ab}}{d^3p}\right)+(1-\delta_{ab})(A\leftrightarrow B,\eta\leftrightarrow-\eta). \tag{3.17}$$

with

$$x_a=\frac{x_T}{2}\frac{e^\eta}{vw},\ x_b=\frac{x_T}{2}\frac{e^{-\eta}}{1-v},\ w_1=\frac{x_T}{2}\frac{e^\eta}{v},\ v_1=\frac{x_T}{2}e^\eta,\ v_2=1-\frac{x_T}{2}e^{-\eta}. \tag{3.18}$$

Momentum conservation leads to the constraints

$$x_{T,\max}=\frac{1}{\cosh\eta},\qquad \eta_{\max}=\cosh^{-1}\left(\frac{1}{x_T}\right)=\ln\left(\frac{1}{x_T}+\sqrt{\frac{1}{x_T^2}-1}\right), \tag{3.19}$$

for fixed η, x_T respectively.

The subprocess cross section is given by

$$E\Delta\frac{d\hat{\sigma}_{ab}}{d^3p}=E\Delta\frac{d\hat{\sigma}_{ab}^{\mathrm{B}}}{d^3p}+E\Delta\frac{d\hat{\sigma}_{ab}^{\mathrm{HO}}}{d^3p} \tag{3.20}$$

where $\hat{\sigma}_{ab}^{\rm B}$ is the Born term and $\hat{\sigma}_{ab}^{\rm HO}$ is the renormalized higher order correction, given by (in n dimensions)

$$E\Delta\frac{d\hat{\sigma}_{ab}^{\rm HO}}{d^{n-1}p} = E\Delta\frac{d\hat{\sigma}_{ab}^{0}}{d^{n-1}p} + E\Delta\frac{d\hat{\sigma}_{ab}^{\rm fact}}{d^{n-1}p} + E\Delta\frac{d\hat{\sigma}_{ab}^{\rm UV}}{d^{n-1}p} \tag{3.21}$$

where $\hat{\sigma}_{ab}^{\rm fact}$ is the factorization counterterm arising from the renormalization of the appropriate structure functions, $\hat{\sigma}_{ab}^{\rm UV}$ is the counterterm arising from coupling constant renormalization, and $\hat{\sigma}_{ab}^{0}$ is the unrenormalized higher order correction, which is the sum of the bremsstrahlung and virtual (if present) contributions

$$E\Delta\frac{d\hat{\sigma}_{ab}^{0}}{d^{n-1}p} = E\Delta\frac{d\hat{\sigma}_{ab}^{\rm V}}{d^{n-1}p} + E\Delta\frac{d\hat{\sigma}_{ab}^{\rm Br}}{d^{n-1}p}. \tag{3.22}$$

For $\hat{\sigma}_{ab}^{\rm B}$ and $\hat{\sigma}_{ab}^{\rm V}$, we may use the $2 \to 2$ particle phase-space given by Eq. B.18. For $\hat{\sigma}_{ab}^{\rm Br}$, we use the $2 \to 3$ particle phase-space (B.17), which is explicitly derived in Appendix B.1.

In order to carry out the various bremsstrahlung integrals encountered, we must reduce the complicated ratios of products of dot-products arising from the traces into a minimal form, suitable for integration. Basically, one needs to express the dot-products in the numerators in terms of those occurring in the denominators (i.e. propagators). This is made systematically possible by the complete set of reduction formulas given in Appendix B.3 in the form of a theorem. When combined with standard partial fractioning, we may reduce all terms arising from the traces into an integrable form, which we then use to obtain $\hat{\sigma}_{ab}^{\rm Br}$.

The evaluation of the loop integrals is straightforward, involving well known massless tensor integrals only. Having obtained $\hat{\sigma}_{ab}^{\rm V}$ and $\hat{\sigma}_{ab}^{\rm Br}$, using the regularization procedures described in the next section, there are still non-cancelling UV and mass singularities in the sum (3.22). The renormalization procedure required to remove these singularities is described in the next section as well.

3.3 Regularization and Renormalization Procedures

In this section, we describe our regularization and renormalization procedures. In particular, we show the origin of $\hat{\sigma}_{ab}^{\rm fact}$ and $\hat{\sigma}_{ab}^{\rm UV}$ occuring in (3.21). We also show how gauge invariance was checked explicitly.

We use dimensional regularization with an anticommuting γ_5 (Sect. 2.2.2), in general, with $\overline{\rm MS}$ subtraction. For subsets (i), (ii) and (iii) the traces contain two γ_5 matrices. For $\overline{q}\overline{q}\to\gamma qq$ (or, more generally, the subset (iv)), some traces involve only one γ_5 since they contain only one helicity projection operator. Hence, we use dimensional reduction (DRED) for this subset of graphs.

There are two types of renormalization counterterms that must be added. We must add both coupling constant and structure function renormalization counterterms (the on-shell wave function renormalizations are trivial as discussed in Sect. 2.3.1, due to masslessness of all the particles).

Firstly, let us consider the coupling constant renormalization. The counterterms arise from expressing the unrenormalized strong coupling g, appearing in the bare Born term, $\hat{\sigma}_{ab}^{\rm B,0}$, in terms of the renormalized coupling g_r. They are related via (see also Eq. 2.58)

$$g = Z_g g_r, \tag{3.23}$$

where Z_g is the coupling renormalization constant determined in the $\overline{\rm MS}$ scheme. It is given by

$$\begin{aligned} Z_g &= 1 - \frac{g_r^2}{(4\pi)^{2-\varepsilon}} \frac{\Gamma(1+\varepsilon)}{\varepsilon} \frac{(33-2N_f)}{6} \\ &= 1 - \frac{g_r^2}{(4\pi)^2} \left(\frac{1}{\varepsilon} - \gamma_E + \ln 4\pi \right) \frac{(33-2N_f)}{6} + \mathcal{O}(\varepsilon) \end{aligned} \tag{3.24}$$

where the $\mathcal{O}(\varepsilon)$ terms are dropped, as they do not contribute. This renormalization generates $\hat{\sigma}_{ab}^{\rm UV}$, which does indeed cancel all the UV divergences.

There are two types of structure functions which require renormalization: the parton distributions and the fragmentation functions, $\mathcal{D}_{\gamma/k}$. The renormalization of the parton distributions is performed by expressing the unrenormalized parton distributions occurring in the Born term of (3.13) in terms of the renormalized ones. Using (2.66), with the $\overline{\rm MS}$ definition for c_q given by (2.70), we generate all the counterterms necessary to cancel the mass singularities arising from configurations where an unobserved final state parton (p_4 or p_5) is collinear with p_1 or p_2 and is connected to the same propagator. The origin of such singularities is discussed in Sect. 2.2.

In order to cancel the mass singularities arising from states where one of the outgoing partons is collinear with the photon (connected to the same propagator) we must consider the renormalization of the fragmentation functions, $\mathcal{D}_{\gamma/q}$. The only additional split-function we need is

$$P_{\gamma q}(x) = \frac{1+(1-x)^2}{x}, \tag{3.25}$$

since, to the order at which we are working, the only contribution comes from the term in (2.67) proportional to $\mathcal{D}^r_{\gamma/\gamma}(z/y)P_{\gamma q}(y) = P_{\gamma q}(z)$. Substituting (2.67) in (3.13) generates the remaining contribution to $\hat{\sigma}_{ab}^{\rm fact}$.

The remaining soft (and possibly collinear as well) bremsstrahlung singularities manifest as terms proportional to

$$(1-w)^{-1-2\varepsilon} = -\frac{1}{2\varepsilon}\delta(1-w) + \frac{1}{(1-w)_+} - 2\varepsilon\left(\frac{\ln(1-w)}{1-w}\right)_+ + \mathcal{O}(\varepsilon^2), \tag{3.26}$$

which lead to $1/\varepsilon^2$ poles if multiplied by $1/\varepsilon$ collinear divergences. All such terms cancel in the sum (3.21), (3.22) via the KLN theorem[45], according to which all IR

divergences cancel if we sum over all degenerate states. Here, there is a degeneracy between collinear configurations and contributions arising from the renormalization of the structure functions. There is also a degeneracy between soft gluonic radiation and gluon loops. As always in field theory, degenerate states must be added, order by order, to render a finite result. Having done so, all IR divergences will cancel according to the KLN theorem. This is why, even though there are collinear divergences in a process such as $e^+e^- \to$ jets, no factorization counterterms are necessary: we sum over all final states.

All the above cancellations were checked explicitly, leading to a finite, gauge invariant $\hat{\sigma}_{ab}^{\rm NLO}$, for all a, b. Gauge invariance was checked as follows. Making the substitutions

$$A^\mu(p) \to A^\mu(p) + p^\mu \tag{3.27}$$

in the polarization vectors and

$$g_{\mu\nu} \to g_{\mu\nu} - \frac{\alpha q_\mu q_\nu}{q^2}, \qquad \alpha \text{ arbitrary} \tag{3.28}$$

in the gluon propagators both leave the results unchanged. The results were also found to be independent of the normalization vector chosen for the axial gauge.

3.4 Analytical Results and Scheme Dependences

We may write the Born term in n dimensions as

$$s^2 v E \Delta \frac{d\hat{\sigma}_{ab}^{\rm B}}{d^{n-1}p} \equiv \Phi_{ab} \Delta B_{ab}(v,\varepsilon)\delta(1-w), \tag{3.29}$$

or in 4 dimensions,

$$s^2 v E \Delta \frac{d\hat{\sigma}_{ab}^{\rm B}}{d^3 p} = \Phi_{ab} \Delta B_{ab}(v)\delta(1-w), \tag{3.30}$$

with $\Delta B_{ab}(v) \equiv \Delta B_{ab}(v,0)$.

The renormalized higher order correction has the form (returning to $n = 4$)

$$s^2 v E \Delta \frac{d\hat{\sigma}_{ab}^{\rm HO}}{d^3p} \equiv \frac{\alpha_s}{2\pi} \Phi_{ab} \Delta f(v, w) \tag{3.31}$$

with

$$\begin{aligned}
\Delta f(v,w) &= a_1 \delta(1-w) + b_1 \frac{1}{(1-w)_+} + c \left(\frac{\ln(1-w)}{(1-w)} \right)_+ \\
&+ \left\{ a_2 \delta(1-w) + b_2 \frac{1}{(1-w)_+} + d \right\} \ln \frac{s}{M_f^2} + e \ln v + f \ln(1-vw) \\
&+ g \ln(1-v+vw) + h \ln(1-v) + i \ln w + j \ln(1-w) + k \\
&+ l \frac{\ln(1-v+vw)}{1-w} + m \frac{\ln w}{1-w} + n \frac{\ln\left(\frac{1-vw}{1-v}\right)}{1-w} \qquad (3.32) \\
&\equiv \Delta f_S + \Delta f_H. \qquad (3.33)
\end{aligned}$$

where Δf_S is the soft part arising from soft, virtual and collinear gluons, given by the terms with coefficients a_1–b_2 (see (2.91), (2.92)); Δf_H is the hard part arising from the remaining terms. The coefficients a_1–b_2 are functions of v only, while d–n are functions of both v and w. Here, M_f is introduced through the renormalizations (2.66), (2.67). Also, the coefficient a_1 contains the logarithm, $\ln(s/\mu^2)$, arising from the difference in overall factors in $\hat{\sigma}_{ab}^0$ and in $\hat{\sigma}_{ab}^{\rm UV}$.

The coefficients and Born terms for the subsets (i), (iii) and (iv) are listed in Appendix B.2. For the subset of diagrams (ii) (and the interference with (iv)), the result is simply minus the corresponding unpolarized result, as discussed in Sect. 3.1.

Let us now examine the origin of the coefficients a_1–n in (3.32) and comment on their scheme (in)dependence, taking first the $\overline{q}\overline{q}$ subprocess as an example. We will present arguments valid for any n-dimensional scheme, noting that all differences arise from the continuation of the tensors (i.e. traces) and are $\mathcal{O}(\varepsilon)$. The finite differences arise only after multiplication by the $1/\varepsilon$ poles coming from the phase space integrations.

First we consider the coefficients a_1, b_1 and c. The coefficients b_1, c and part of a_1 arise from soft and collinear gluon bremsstrahlung: the remaining part of a_1 arises from loop graphs. The parts $\sim N_c$ originate from terms $\sim 1/(p_1 \cdot p_5)(p_2 \cdot p_5)$, coming from initial state gluon radiation,[68b] which after phase space integration yield a contribution (Eq. 3.3 of Ref. 68b)

$$\Delta\tilde{f} = \frac{-2}{\varepsilon} N_c \left(\frac{v}{1-v}\right)^{-\varepsilon} (1-w)^{-1-2\varepsilon} (1+\varepsilon^2 \frac{\pi^2}{6}) \Delta B(v,\varepsilon). \tag{3.34}$$

There is a factor $v^{-\varepsilon}(1-w)^{-\varepsilon}$ coming from the $2 \to 3$ phase space and an additional factor $[(1-w)^{-1-\varepsilon}/(1-v)^{-\varepsilon}]/\varepsilon$ coming from the angular integrations in the soft limit. As well, there is a factor $(1+\varepsilon^2\pi^2/6)$ relative to the loop graphs. The scheme dependence is contained in the Born term, $\Delta B(v,\varepsilon)$ (scheme dependent to $\mathcal{O}(\varepsilon)$) which was extracted in a manner independent of the continuation of the tensors.

Using (3.26) and

$$\left(\frac{v}{1-v}\right)^{-\varepsilon} = 1 - \varepsilon \ln \frac{v}{1-v} + \frac{\varepsilon^2}{2} \ln^2 \frac{v}{1-v} \tag{3.35}$$

we get the contribution

$$\begin{aligned} \Delta\tilde{f} \;=\; & N_c \{ \frac{1}{\varepsilon^2}\delta(1-w) - \frac{2}{\varepsilon}\frac{1}{(1-w)_+} - \frac{1}{\varepsilon}\ln\frac{v}{1-v}\delta(1-w) \\ & + 4\left(\frac{\ln(1-w)}{1-w}\right)_+ + \frac{2}{(1-w)_+}\ln\frac{v}{1-v} + \frac{1}{2}\delta(1-w)\ln^2\left(\frac{v}{1-v}\right) \\ & + \frac{\pi^2}{6}\delta(1-w)\} \Delta B(v,\varepsilon) \end{aligned} \tag{3.36}$$

The term $\sim 1/\varepsilon^2$ cancels with a term coming from the loops, also $\sim \Delta B(v,\varepsilon)$. Similarly, the terms $\sim 1/\varepsilon$ are cancelled by a factorization counterterm again $\sim \Delta B(v,\varepsilon)$, since the factorization counterterm comes from the renormalization of the parton distributions in the Born term. From these terms, all the scheme dependence is in $\Delta B(v,\varepsilon)$ as well.

We hence extract

$$b_{1,N_c} = 2\Delta B(v) \ln \frac{v}{1-v}, \quad c_{N_c} = 4\Delta B(v) \tag{3.37}$$

in a scheme independent manner. The same extraction holds for the unpolarized case with $\Delta B(v) \to B(v)$. Similar argumentation may be used for the parts $\sim C_F$, which arise from terms $\sim 1/p_4 \cdot p_5$.

Let us now consider the coefficients a_2, b_2 and d. They arise from factorization counterterms. Since the only difference in factorization counterterms in going from one scheme to another is the difference in the Born term and since the part $\sim \ln(s/M_f^2)$ arises from the product (for some x, y)

$$\sim \frac{1}{\varepsilon}\left(\frac{s}{M_f^2}\right)^{\varepsilon} \Delta B(x,\varepsilon)\Delta P_{ij}(y) \tag{3.38}$$

in the factorization counterterm, we see that $\mathcal{O}(\varepsilon)$ differences in $\Delta B(x,\varepsilon)$ will not affect a_2, b_2 and d. However, they will have an effect on k. Also, a_2 and b_2 are required to follow from the unpolarized case by the replacement $B(v) \to \Delta B(v)$ since the parts $\sim 1/(1-w)_+$ and $\sim \delta(1-w)$ of $\Delta P_{ij}(w)$ and $P_{ij}(w)$ are the same. This was checked explicitly.

Up to this point we have demonstrated explicitly the scheme independence of the coefficients b_1, c, a_2, b_2 and d for all dimensional schemes. We have also shown that b_1, c, a_2 and b_2 follow from the corresponding unpolarized coefficients by $B(v) \to \Delta B(v)$ and this has been used as a partial check of the results. Arguments analogous to those above can be used for the $\bar{q}\bar{q}$ subprocess and for the coefficient d in the $\bar{g}\bar{g}$ and $\bar{q}\bar{q}$ subprocesses.

Let us now examine the origin of the terms $e-j$, l, m, n. We have shown that the terms $\sim 1/(p_1 \cdot p_5)(p_2 \cdot p_5)$ and $\sim 1/(p_4 \cdot p_5)$ contribute to a_1, b_1 and c, but not to $e-j$, l, m, n.

Let $j, j' = 1, 2, 3$ and $f, f' = 4, 5$. Then the remaining terms may be classified in the following manner, depending on their denominators: (1) terms $\sim 1/p_j \cdot p_f$: (2) terms $\sim 1/(p_j \cdot p_f)(p_{j'} \cdot p_{f'})$: (3) terms with no p_f's in the denominator.

The contribution of such terms to Δf may be written as

$$\Delta f_i \sim PS \cdot D_i \cdot \mathrm{Tr}_i(\varepsilon), \tag{3.39}$$

where D_i is the angular integral over a term of the type $i = 1, 2, 3$. $\mathrm{Tr}_i(\varepsilon)$ is a trace factor which is scheme *dependent* to $\mathcal{O}(\varepsilon)$, and PS is an overall phase space factor. For $i = 1$, $D_i \sim 1/\varepsilon$ and therefore the only scheme dependent, finite contribution Δf_1 gives is to k; the $1/\varepsilon$ part being removed via factorization counterterms discussed previously. For $i = 3$, D_i is $\mathcal{O}(1)$, hence the scheme dependent $\mathcal{O}(\varepsilon)$ parts do not contribute in the limit $\varepsilon \to 0$. The remaining terms ($i = 2$) are of the type

$$D_2 \sim \frac{1}{\varepsilon} g^{-\varepsilon}(v, w), \tag{3.40}$$

with, for example, $g(v, w) = (1 - v)(1 - w)/(1 - v + vw)$. As before, the $1/\varepsilon$ pole is removed by the factorization counterterm, the scheme dependent part of which again affects only k. Expanding

$$g^{-\epsilon}(v, w) = 1 - \varepsilon \ln g + \cdots \tag{3.41}$$

shows that only the $\mathcal{O}(1)$ part of $\mathrm{Tr}_2(\varepsilon)$ in (3.39) will contribute to the coefficients of the logarithms: $e - j$, l, m, n. Hence they are scheme independent, within the dimensional methods.

In summary, we have shown that, in n dimensions, the only scheme dependent coefficients in the expansion (3.32) for Δf are a_1 and k. All the same argumentation applies to the unpolarized case, where γ_5 does not occur explicitly. Hence, the two

available regularizations, DREG and DRED will give f which only differ in a_1 and k. Of course, in the polarized case, DREG offers both the anticommuting-γ_5 scheme and the HVBM scheme and perhaps other prescriptions are available. Indeed, the authors of Ref. 66, who use the HVBM scheme, compared their $\vec{g}\vec{q}$ results with ours and found that only the coefficients a_1 and k differed.[72]

3.5 Numerical Results

We take $M_f = \mu = p_T$ and use $\Lambda = 0.2\,\text{GeV}$ (Eq. 2.81) and $N_f = 4$ in the two-loop expressions, (2.80) and (2.76), for $\alpha_s(\mu^2)$. Polarized cross sections are computed using the parameterizations for the longitudinally polarized parton distributions given in Appendix A.1, which correspond to the inputs of Ref. 27 evolved using the one-loop GLAP equations (Sect. 2.3.2) since, at this point, two-loop polarized split functions have not been determined. Except when stated, we assume a large gluon distribution (i.e. Set 1 of Ref. 27). For the unpolarized cross sections, we use the unpolarized distributions (fit S–$\overline{\text{MS}}$) of Ref. 29. We present results, in general, for $\sqrt{S} = 38$, 100, 500 GeV. The latter two energies being representative of RHIC and the first being a typical fixed target energy.

The following factors, which we call K-factors, versus x_T are presented in Fig. 3.4 for energies $\sqrt{S} = 38$, 100, 500 GeV at pseudorapidities $\eta = 0$, 1, 1.6:

$$K_{gq} = \frac{\sigma_{\text{B}}(gq) + \sigma_{\text{HO}}(gq)}{\sigma_{\text{B}}(gq)}, \quad K_{gg} = \frac{\sigma(gg)}{\sigma_{\text{B}}(gq)}, \quad K_{qq} = \frac{\sigma(qq)}{\sigma_{\text{B}}(gq)}, \tag{3.42}$$

and

$$K = \frac{\sigma_{\text{NLO}}(gq) + \sigma_{\text{NLO}}(q\bar{q}) + \sigma(gg) + \sigma(qq)}{\sigma_{\text{B}}(gq) + \sigma_{\text{B}}(q\bar{q})} = \frac{\sigma_{\text{B}} + \sigma_{\text{HO}}}{\sigma_{\text{B}}}, \tag{3.43}$$

where $\sigma(ab) \equiv E\Delta d\sigma_{ab}/d^3p$.

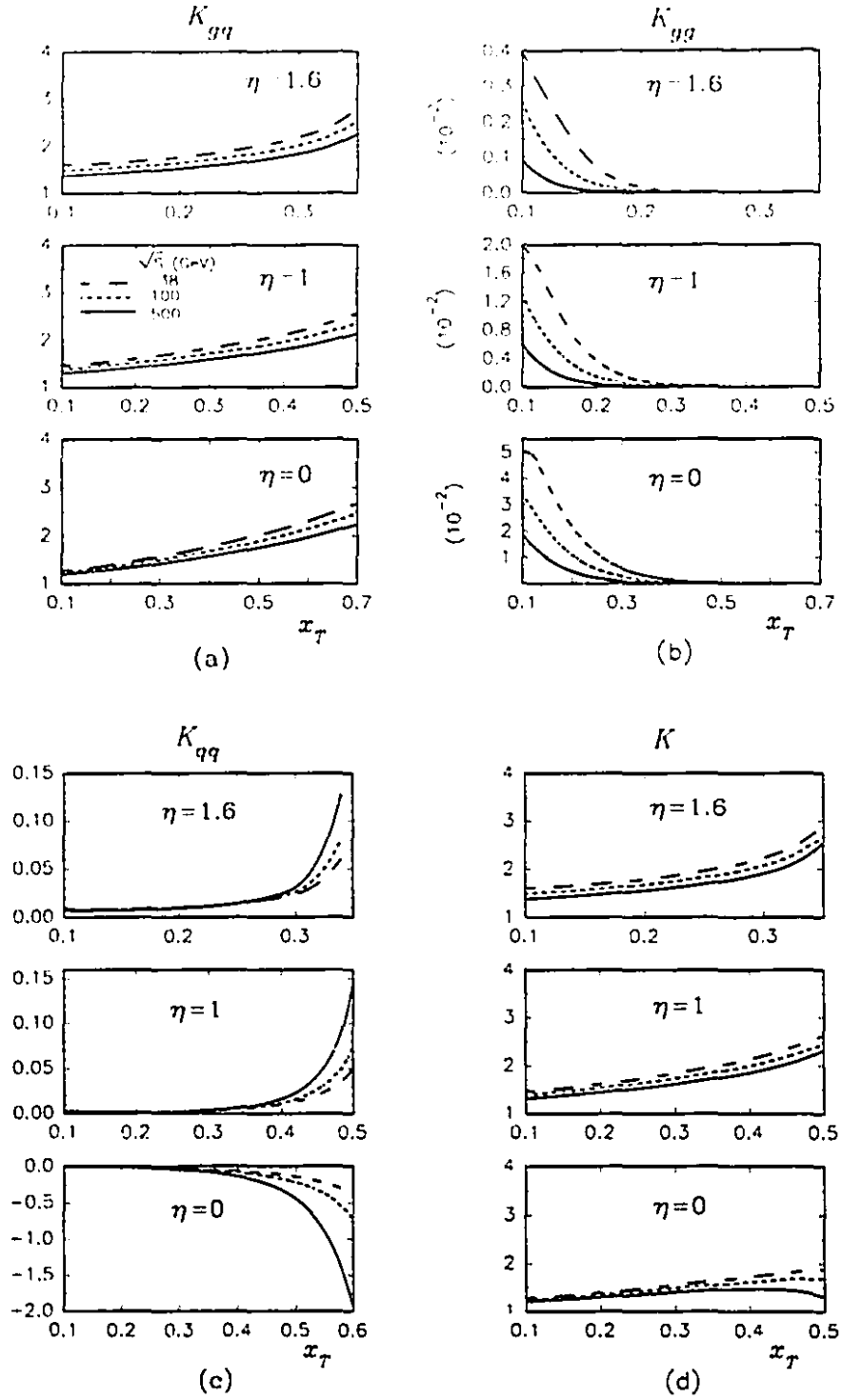

Figure 3.4: The various K-factors versus x_T for $\eta = 1.6, 1, 0$: **(a)** K_{gq}; **(b)** K_{gg}; **(c)** K_{qq}; **(d)** K. The long-dashed, short-dashed, and solid lines represent $\sqrt{S} = 38$, 100 and 500 GeV, respectively.

We see that $K_{gq} > 1$ everywhere and is fairly large, ranging from $1.25 \sim 2.5$ in general, and increasing towards the kinematic maximum. The K-factor is seen to decrease here with increasing energy, at fixed x_T, due to the diminishing of the strong coupling.

We observe that K_{gg} is roughly a factor of 100 smaller than K_{gq} on average. This is to be expected since, even though the gluon distributions are large, at small x in particular, the $2 \rightarrow 3$ kinematics are quite suppressed relative to the $2 \rightarrow 2$ kinematics. Basically, the integration region for $2 \rightarrow 3$ kinematics is such that we integrate over regions where the parton distributions (gluon in particular) give small contributions (i.e. large x); this waters down the cross section quite a bit. One understands this as follows: since there are 3 particles in the final state, for fixed p_T there are many possible configurations which satisfy momentum conservation and require larger energy (i.e. larger x) than for $2 \rightarrow 2$ kinematics. As one increases x_T or η, this effect becomes more pronounced since we require greater energy.

As for K_{gg}, K_{qq} is seen to be negligible throughout most of the domain, except at large x_T and $\eta = 0$ where the K-factor is sizable and negative. This effect is due to the relative hardness of the valence quark distributions as compared to the gluon distribution (i.e. the valence distributions are dominant at large x). We see again that for fixed x_T, the $2 \rightarrow 3$ kinematics are suppressed for larger η; except not as much as for the $\bar{g}\bar{g}$ subprocess, due to the relative hardness of the valence distributions. Unlike the other K-factors, $|K_{qq}|$ increases with $\sqrt{S}$. This is due to the slow evolution of the valence distributions relative to the gluon distribution. $K_{q\bar{q}}$ was found to be small throughout due to the smallness of the polarized antiquark distributions.

We see that the total K-factor, K, is almost indistinguishable from K_{gq} except

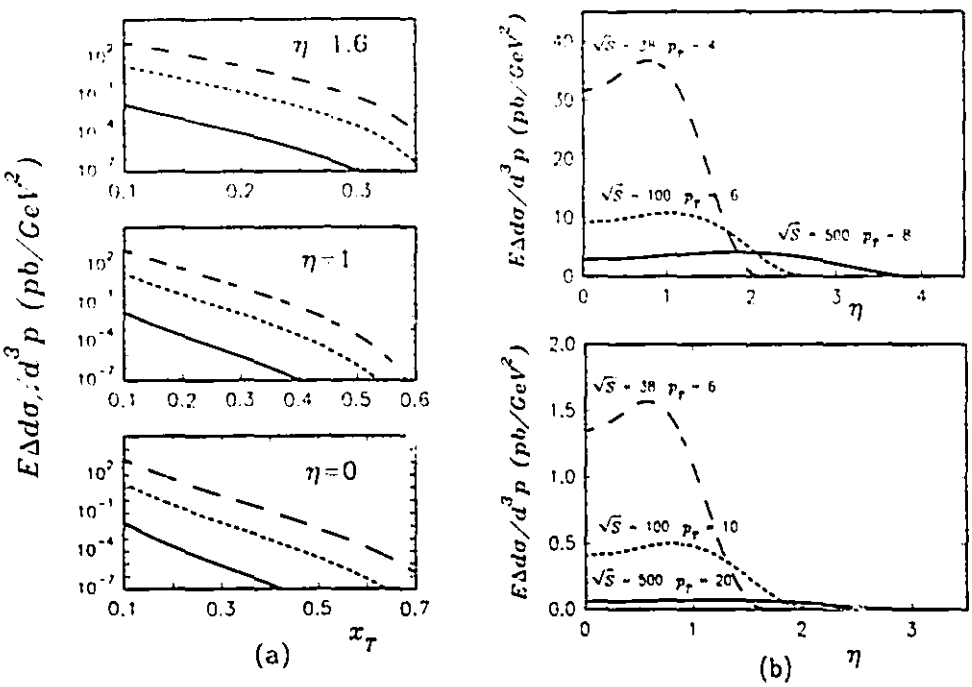

Figure 3.5: The cross section $E\Delta d\sigma/d^3p$ (a) versus x_T for the same energies and rapidities as in Fig. 3.4; (b) versus η for various $\sqrt{S}$ and p_T.

at rather large x_T (and, in particular at $\eta = 0$) where the $\overline{q}\,\overline{q}$ subprocess contributes (negatively). However, at those larger x_T, the cross sections are quite small, as we shall see below. Also, we shall see that $1 \lesssim \eta \lesssim 1.6$ is the interesting region, not $\eta \approx 0$.

Fig. 3.5(a) shows the cross section, $E\Delta d\sigma/d^3p$ versus x_T for the same values of $\sqrt{S}$ and η as in Fig. 3.4. The cross sections are sizable, reaching the nanobarn range for small x_T, at $\sqrt{S} = 38$ GeV, and are roughly a factor of 100 smaller for $\sqrt{S} = 100$ GeV; certainly large enough for reliable measurements at RHIC. We see explicitly that the cross sections are quite suppressed as x_T approaches the kinematic maximum, partly due to the vanishing of all parton distributions for $x \to 1$. As well, for fixed x_T but increasing $\sqrt{S}$ (i.e. p_T), the cross sections drop off quickly. This is due to the $1/p_T^4$ dependence in (3.17).

Fig. 3.5(b) presents the cross section plotted versus η for various values of $\sqrt{S}$

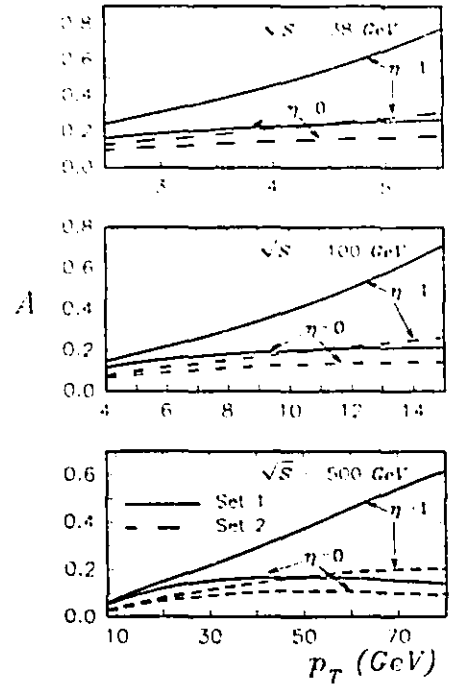

Figure 3.6: The asymmetry $A = (E\Delta d\sigma_{\rm NLO}/d^3p)/(Ed\sigma_{\rm NLO}/d^3p)$ versus p_T at $\sqrt{S} = 38$, 100, 500 GeV for $\eta = 1, 0$. Solid line: large polarized gluon solution (Set 1), dashed line: moderate gluon solution (Set 2).

and p_T. We notice a peak generally around $\eta \approx 1$, not $\eta = 0$ as in the unpolarized case. We can understand this by examining the behaviour of the Born term. The form of the $\bar{q}\bar{q} \rightarrow \gamma q$ cross section is such that it gives dominant contributions from integration regions where it increases with $|\eta|$. At the same time, the cross section is multiplied by parton distributions, decreasing at large $|\eta|$ (i.e. large x) - hence the peak at $\eta \neq 0$. Since the HOC simply amount to a slowly varying K-factor, this feature is preserved in next-to-leading order (actually it is enhanced since K increases with η).

Fig. 3.6 presents the asymmetry,

$$A = \frac{E\Delta d\sigma_{\rm NLO}/d^3p}{Ed\sigma_{\rm NLO}/d^3p}, \tag{3.44}$$

for $\sqrt{S}$ = 38, 100, 500 GeV, versus p_T with both a large and a moderate polarized gluon distribution (Sets 1 and 2 of Ref. 27) for $\eta = 0$ and $\eta = 1$. We see that A is quite large, in particular at large p_T values and for $\eta = 1$. This is because at large-x_T (i.e. large x, Q^2), the softening of the gluon distribution makes the dominant contributions come from regions where the polarized gq cross section is increasing with η relative to the unpolarized one. Hence, the combination of large p_T, η maximizes the asymmetry (although the cross section drops off with p_T). For $\eta = 1$ there is a large difference between the moderate and large polarized gluon solutions meaning that experiment should be well able to distinguish between the two cases. An interesting byproduct of the softness of the gluon distribution is that, for fixed p_T, the asymmetry is more sensitive to η for the Set 1 (softer) than it is for Set 2. From the parameterizations given in Appendix A.1, we can see that Set 1 drops off more quickly at large x than Set 2.

We may clarify the above observations somewhat by looking at the polarized and unpolarized cross sections separately, for some fixed $\sqrt{S}$, p_T and plotted versus η. This is done in Fig. 3.7, for $\sqrt{S}$ = 100 GeV, p_T = 6 GeV. In Fig 3.7 (a), we see explicitly the peaking of the Born level cross section at $\eta \approx 1$ and the enhancement of this effect, in next-to-leading order, due to the fact that K increases with η at fixed $\sqrt{S}$, p_T. In Fig. 3.7 (b), we see explicitly the drop-off of the unpolarized cross section with increasing η.

With K-factors $\gtrsim 1.5$, the question of perturbative stability naturally arises. In fact, we are most interested in the ratio of the polarized to the unpolarized gluon distribution, which can be inferred from the asymmetry by choosing suitable polarized parton distributions so as to agree with the experimentally measured A, using some set of well-known unpolarized parton distributions. It is well known that over-

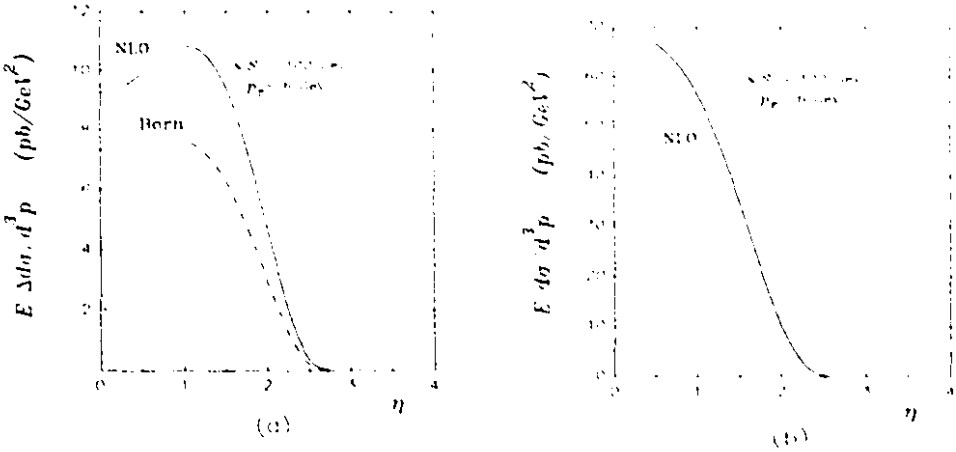

Figure 3.7: The cross section $E\Delta d\sigma/d^3p$ vs. η for $\sqrt{S}$ = 100 GeV, p_T = 6 GeV: (a) polarized (dashed line is Born term); (b) unpolarized.

all normalization factors are difficult to predict accurately in QCD. It would not be good if the ratio of the polarized gluon distribution to the unpolarized one were to vary radically in going from a leading order to a next-to-leading order analysis. This would imply perturbative instability.

Fig. 3.8 presents the Born level and next-to-leading order asymmetry, versus p_T, for $\eta = 1$. Fig. 3.8 (a) presents A for $\sqrt{S} = 100$ GeV, and Fig. 3.8 (b) presents A for $\sqrt{S} = 500$ GeV. For $\sqrt{S} = 100$ GeV, we see that the HOC increase A by $< 10\%$. For $\sqrt{S} = 500$ GeV, the HOC increase A by $< 20\%$. This covers the energy range of interest for RHIC. So, as an overall statement, one could say that the asymmetry is corrected by $\lesssim +15\%$ under HOC for energies and p_T of interest at RHIC. This is a clear indication of perturbative stability. Basically, the corrections to the polarized and unpolarized cross sections are quite similar as discussed in Sect. 3.4, since we can often extract the Born term in a manner independent of the polarizations (especially in the loop graphs and soft bremsstrahlung), leading to large cancellations in the asymmetry.

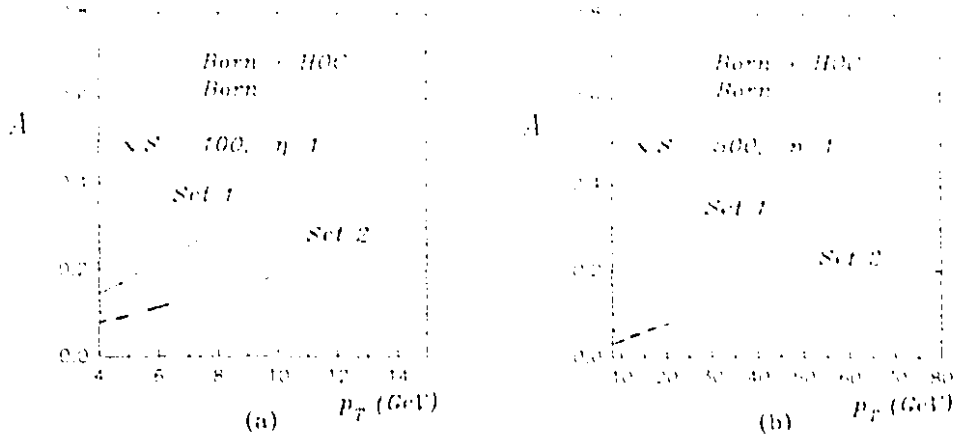

Figure 3.8: The Born level and next-to-leading order asymmetry, versus p_T, for $\eta = 1$ and (a) $\sqrt{S} = 100$ GeV; (b) $\sqrt{S} = 500$ GeV.

Let σ_H, σ_S represent the contributions to σ from Δf_H, Δf_S in (3.33) respectively, for the $\vec{g}\vec{q}$ subprocess. Fig. 3.9 (a) presents the ratio, $-\sigma_H/\sigma_S$, of the hard to the soft cross section versus x_T, for the same $\sqrt{S}$ and η as in Fig. 3.4. We see that, in particular at large η values, the soft cross section is rather dominant. As x_T approaches the kinematic maximum, the soft cross section becomes completely dominant for all η. This trend was first noticed in the corresponding unpolarized case[68] where the soft cross section is even more dominant. The effect arises from the differing behaviour of Δf in the hard and soft parts; the soft cross section picks up substantial contributions from integration regions where the parton distributions are comparatively large. This is because the "+" distributions and $\delta(1-w)$ are peaked at $w = 1$, and hence σ_S obeys approximately $2 \to 2$ kinematics. As discussed regarding K_{gg}, the contribution for $2 \to 3$ kinematics (i.e. σ_H) gets watered down as x_T, η increase. The softness of the gluon distribution for $x \to 1$ makes this effect even more pronounced.

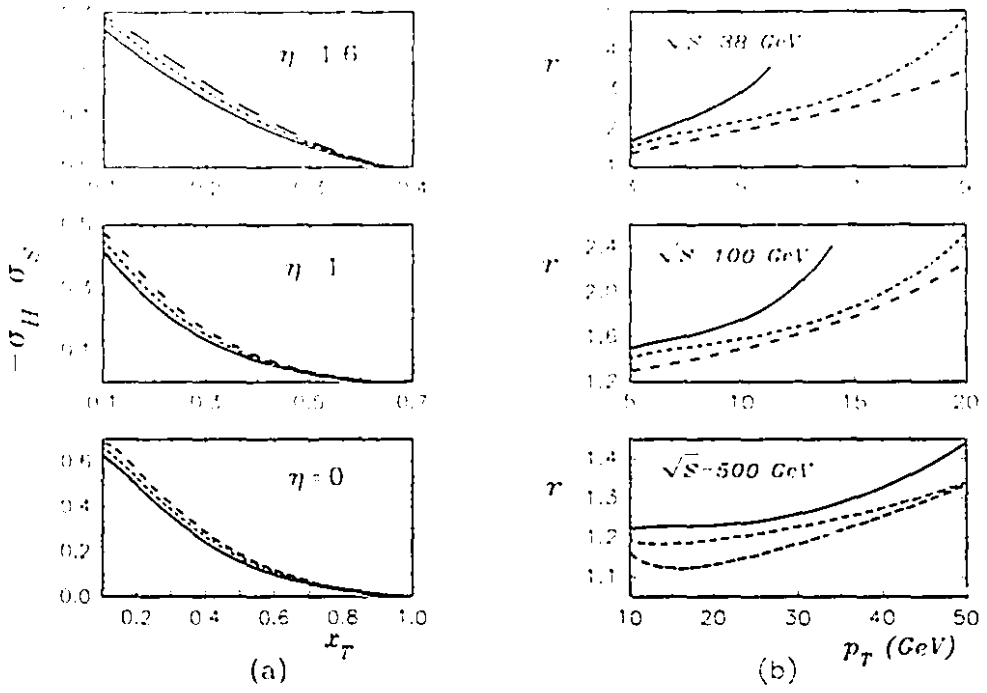

Figure 3.9: The ratios (a) $-\sigma_H/\sigma_S$ versus x_T for the same values of η and $\sqrt{S}$ as in Fig. 3.4; (b) $r = \sigma_{\rm NLO}(M = \mu = p_T/2)/\sigma_{\rm NLO}(M = \mu = 2p_T)$ versus p_T, solid line: $\eta = 1.6$, short-dashed: $\eta = 1$, long-dashed: $\eta = 0$.

Fig 3.9 (b) presents the ratio

$$r = \frac{\sigma_{\rm NLO}(M_f = \mu = p_T/2)}{\sigma_{\rm NLO}(M_f = \mu = 2p_T)} \tag{3.45}$$

versus p_T for $\sqrt{S} = 38, 100, 500$ GeV and $\eta = 0, 1, 1.6$. We see that, in particular for smaller $\sqrt{S}$ and larger p_T, where the K-factors are large, r is rather big. For the larger $\sqrt{S}$ and moderate p_T, the situation is better. This is one reason why perturbative QCD has trouble predicting overall normalization factors. Taking $M_f = \mu = p_T/2$ makes α_s larger and the gluon distribution harder, making $\sigma_{\rm NLO}$ larger, conversely for $M_f = \mu = 2p_T$. These evolution effects are somewhat balanced by the terms $\sim \ln(s/\mu^2)$, $\ln(s/M_f^2)$ occuring in the cross sections. One expects that evolution via two-loop polarized split functions (and including $\mathcal{D}_{\gamma/q}$ effects), once available,

will stabilize $\sigma_{\rm NLO}$. Then, A should be quite stable under such variations, since the evolutions for the polarized and unpolarized parton distributions will be more consistent.

The results agree qualitatively with those of Ref. 66, as can be expected from the similarities in the HOC to the $\vec{g}\vec{q}$ subprocess mentioned in the previous section. Nonetheless, precision agreement will not be possible until detailed parton distributions and two-loop polarized split functions are determined for DRED, the anticommuting-γ_5 scheme and the HVBM scheme.

3.6 Conclusions

We have determined complete next-to-leading order corrections for large-p_T direct photon production in longitudinally polarized hadronic collisions and presented the analytical and numerical results. For $\vec{p}\vec{p}\to\gamma X$ we have shown that they are dominated by the one-loop corrections to $\vec{g}\vec{q}\to\gamma q$, are positive throughout and, in certain kinematic domains, fairly large ($\gtrsim$ 50% of the Born term). The resulting cross sections were sufficiently large for successful experiments; this also holds for the larger p_T values and for $\sqrt{S} = 500\,\text{GeV}$, if the expected large RHIC luminosity is taken into account.

Calculating the corresponding unpolarized cross sections to the same order, we have found substantial asymmetries; and we have shown that experiment can well distinguish between a large and a moderate polarized gluon distribution. Unlike the unpolarized cross sections, which peak at $\eta = 0$, the polarized cross sections peak at around $\eta \approx 1$–1.6, where the asymmetries are also large. Hence, this is the region to look.

Finally, the asymmetry was found to be perturbatively stable. The HOC were

found to make the asymmetry $\lesssim 15\%$ larger on average, for $\sqrt{S}$ and p_T relevant to RHIC. We may conclude that the inclusion of HOC significantly supports the proposed experiments on $\vec{p}\vec{p} \to \gamma X$.

Chapter 4

Drell-Yan Process with Transversely Polarized Hadrons

The interaction of massless quarks with vector bosons (g, γ, $W^{\pm}$, Z) does not change a quark's chirality. But the transversity distribution $\Delta_T f_q(x, Q^2)$ (or formally, the structure function $h_1^q(x, Q^2)$ to which it is related) is chiral odd, i.e. measures the interference between an amplitude containing a left-handed quark and one containing a right-handed quark.[73] Thus $\Delta_T f_q$ does not appear in unitarity graphs (hence in cross sections) in which the quark line goes continuously through a hard subprocess and returns to the parent nucleon (e.g. a left-handed quark, L, Fig. 4.1(a), remains left-handed). As a result, inclusive DIS is not appropriate to measure $\Delta_T f_q$.

To change its chirality, the quark must propagate through some soft QCD process that breaks chiral symmetry spontaneously. This happens when the emitted quark is annihilated by an antiquark from another initial state hadron (Fig. 4.1(b) when the quark on the right is right-handed, R). The best example is the Drell-Yan process for lepton-pair production,[73] $A_\uparrow B_\uparrow \to l^- l^+ + X$, where the up-arrows indicate transverse polarization (transverse Drell-Yan). The above observations also follow from the parton model, where we see explicitly that inclusive DIS gives vanishing transversely polarized cross sections.

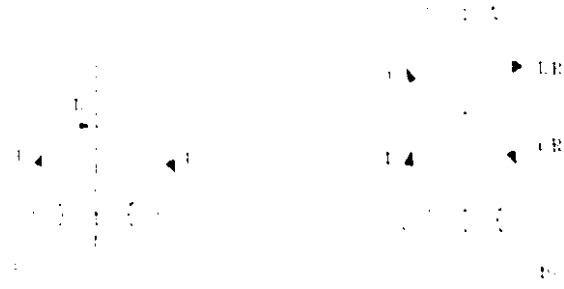

Figure 4.1: (a) A chirality conserving process; (b) chirality non-conserving.

The HOC to transverse Drell-Yan are quite important,[74,75] as in direct photon production, since they are expected to be large and could change some of the features of the Born term. The stability of the asymmetry is also of primary importance.

Let S_A, S_B denote the spin 4-vectors of the hadrons A, B when in the "up-up" configuration. Then the transversely polarized cross section is defined as

$$\Delta_T\sigma \equiv \frac{1}{2}[\sigma(S_A, S_B) - \sigma(S_A, -S_B)]. \tag{4.1}$$

In general, we have the subprocess

$$q(p_1, s_1) + \bar{q}(p_2, s_2) \rightarrow V^*(q) + [g(k)] \rightarrow l^-(p_3) + l^+(p_4) + [g(k)], \tag{4.2}$$

where the p_i are 4-momenta and the the s_i are spin 4-vectors as indicated in Fig 4.2. Here $V = \gamma, Z$ and $l = e, \mu$.

Analogously to (4.1), we may define the polarized subprocess cross section as

$$\Delta_T\hat{\sigma} \equiv \frac{1}{2}[\hat{\sigma}(s_1, s_2) - \hat{\sigma}(s_1, -s_2)]. \tag{4.3}$$

Then we can use the parton model expression (1.16) with the unpolarized quantities replaced by the corresponding transverse ones.

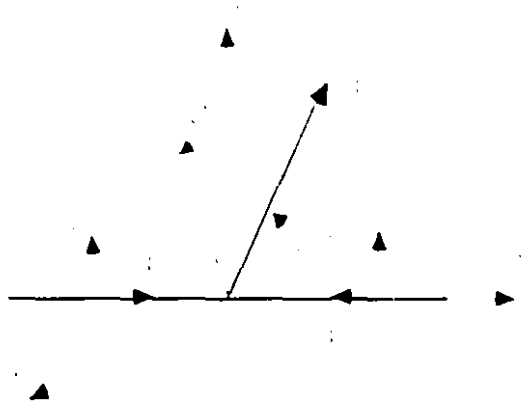

Figure 4.2: Subprocess momenta and spin directions relevant to transverse Drell-Yan.

As pointed out in Sect. 2.1.2, the major uncertainty is in the transversity antiquark distributions, $\Delta_T F_{\bar{q}/p}(x, Q^2)$, of the proton. Hence proton-proton collisions serve as the ideal probe, and experiments are planned at RHIC[23] for this purpose (of course proton-antiproton collisions are ideal for probing the transversity valence distributions).

In what follows, we give the Born terms and HOC for $A_\uparrow B_\uparrow \to l^- l^+ + X$, taking into account production by both γ and Z. As well, we give the corresponding unpolarized cross sections for production by γ. Numerical results are then presented for proton-proton collisions at RHIC's planned energies of $\sqrt{S} = 100, 200, 500$ GeV.

4.1 Born Terms

Throughout, we will assume that the direction (but not the energy) of the outgoing lepton is fixed. It is necessary to fix the azimuthal angle ϕ_3 in order to obtain nonvanishing cross sections. This will be seen explicitly below. Firstly, we define the

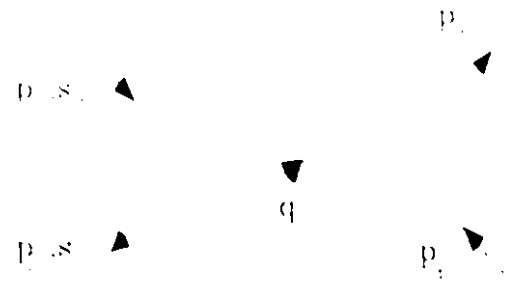

Figure 4.3: Born contribution to transverse Drell-Yan.

observables

$$S = (P_A + P_B)^2, \quad M^2 = (p_3 + p_4)^2, \quad \eta_3 = \ln(\cot\frac{\theta_3}{2}), \quad \tau = \frac{M^2}{S}, \tag{4.4}$$

where P_A, P_B are the momenta of hadrons A, B and θ_3 is the angle p_3 makes with respect to P_A in the P_A, P_B c.m..

Since

$$p_1 = x_a P_A, \qquad p_2 = x_b P_B, \tag{4.5}$$

we have the subprocess invariants,

$$s = (p_1 + p_2)^2 = x_a x_b S, \quad \hat{\tau} = \frac{M^2}{s} = \frac{M^2}{S x_a x_b} = \frac{\tau}{x_a x_b}. \tag{4.6}$$

Furthermore, it is convenient to evaluate the subprocess cross section in the c.m. of p_1, p_2. Hence, we define $\hat{\theta}_3$ as being the angle p_3 makes with respect to p_1 in this frame, and $d\hat{\Omega}_3$ the corresponding solid angle.

For differential cross sections, it is of interest to determine the quantity $\Delta_T d\hat{\sigma}/dM^2 d\hat{\Omega}_3$ (formally $d^2\hat{\Omega}_3$). When we take into account the HOC, it will be necessary to work in n dimensions. Hence, we use the n-dimensional $2 \to 2$ particle phase-space which,

for the kinematics considered here, turns out to be

$$\frac{\Delta_T d\hat{\sigma}_{2\to 2}}{dM^2 d^{n-2}\hat{\Omega}_3} = \left(\frac{2^4}{2M^2}\right)\frac{M^{2\epsilon}}{(2\pi)^{2-2\epsilon}}\frac{\delta(1-\hat{\tau})}{2^{2-2\epsilon}(8M^2)}\Delta_T|M|^2_{2\to 2}. \tag{4.7}$$

The Born contribution is shown in Fig. 4.3. Since we will evaluate the HOC using DRED, we must also evaluate the Born term using DRED. The result is *exactly*

$$\frac{\Delta_T d\hat{\sigma}_{\rm Born}}{dM^2 d^{n-2}\hat{\Omega}_3} = \setminus_B(\varepsilon, y)\delta(1-w); \quad \setminus_B(\varepsilon, y) \equiv \frac{\alpha^2}{N_c}\frac{F_q(M)\mu^{4\epsilon}\pi^{2\epsilon}}{2^{-4\epsilon}M^{4+2\epsilon}}y(1-y)\cos(\tilde{\phi}_1+\tilde{\phi}_2) \tag{4.8}$$

(noting (2.33)) where

$$w \equiv \hat{\tau}, \quad y \equiv \frac{1}{2}(1+\cos\hat{\theta}_3), \quad \tilde{\phi}_{1,2} \equiv \phi_{1,2} - \phi_3 \tag{4.9}$$

and

$$\begin{aligned} F_q(M) &= e_q^2 + (\alpha_l^2+\beta_l^2)(\alpha_q^2-\beta_q^2)\frac{M^4}{(M^2-M_Z^2)^2+(M^2\Gamma_Z/M_Z)^2} \\ &- 2e_q\alpha_l\alpha_q\frac{M^2(M^2-M_Z^2)}{(M^2-M_Z^2)^2+(M^2\Gamma_Z/M_Z)^2}. \end{aligned} \tag{4.10}$$

The constants α_f are defined through the Z-fermion vertex factor

$$-ie\gamma_\mu(\alpha_f - \beta_f\gamma_5). \tag{4.11}$$

The first term in (4.10) arises from photon exchange, the second from Z-exchange and the third from Z-γ interference.

4.2 Virtual Graphs and Gluonic Bremsstrahlung

Firstly, we evaluate the loop graphs of Fig. 4.4. These contain both IR and, at intermediate stages, UV divergences. To regularize them, we work in n dimensions. The transverse polarization introduces explicitly the γ_5 matrix in $\Delta_T|M|^2_{\rm Loops}$ (as well as in $\Delta_T|M|^2_{2\to 3}$). Hence, it is most convenient to use DRED. The only subtlety is

Figure 4.4: Loop contributions: (a) vertex; (b),(c) self-energy.

that we have to add a vertex counterterm to Fig. 4.4 (a) so that the vertex has the correct Lorentz structure. This counterterm is given explicitly in Chapter 5 and is derived in Appendix D, where the Ward identity of QED[76] is explicitly shown to be satisfied after adding the counterterm.

Renormalizing the external quark lines on-shell as in direct photon production, and multiplying by the $2 \to 2$ particle phase-space (4.7), we obtain

$$\frac{\Delta_T d\hat{\sigma}_{\rm Loops}}{dM^2 d^{n-2}\hat{\Omega}_3} = \setminus_B(\varepsilon, y)\delta(1-w)C_F\frac{\alpha_s}{2\pi}\left[-\frac{2}{\varepsilon^2}-\frac{3}{\varepsilon}-7+\frac{2\pi^2}{3}\right]\left(\frac{4\pi\mu^2}{M^2}\right)^{\epsilon}\frac{\Gamma(1-\varepsilon)}{\Gamma(1-2\varepsilon)}. \tag{4.12}$$

In (4.12) and throughout, the $1/\varepsilon$, $1/\varepsilon^2$ poles represent IR divergences.

We now give the bremsstrahlung contributions. Firstly, we must obtain the factorization counterterm, arising from the renormalization of the transversity distributions. For the transverse Drell-Yan process, the procedure is somewhat complicated by the fixing of the azimuthal angle ϕ_3. Nonetheless, we find that the form (2.66) with $P_{qq} \to \Delta_T P_{qq}$, and $\Delta_T P_{qq}$ given by (2.95), holds for the transversity distributions as well. More precisely, using (2.66) with the $\overline{\rm MS}$ definition of c_s (2.70) in the Born term expressions (4.8) and (4.42) for $\Delta_T d\sigma/dM^2 d\eta_3 \phi_3$ leads to a factorization

counterterm which cancels all the collinear divergences:

$$\frac{\Delta_T d\hat{\sigma}_{Fact}}{dM^2 d^{n-2}\hat{\Omega}_3} = \frac{1}{\varepsilon}\lambda_B(\varepsilon,y)\frac{\Gamma(1-\varepsilon)}{\Gamma(1-2\varepsilon)}\left(\frac{4\pi\mu^2}{M^2}\right)^{\varepsilon}\frac{\alpha_s}{2\pi}w^3\Delta_T P_{qq}(w)\left[\frac{1}{[1-y(1-w)]^{1-2\varepsilon}}\right.$$
$$\left. + \frac{1}{[y+w(1-y)]^{1-2\varepsilon}}\right]\left(\frac{s}{M_f^2}\right)^{\varepsilon} \tag{4.13}$$

where M_f^2 is the factorization scale appearing in the parton distributions and (2.70). To our knowledge, this is the first time this procedure has been applied to transversely polarized processes.

To calculate the gluonic bremsstrahlung contribution, we need the $2 \to 3$ phase space. We work in the c.m. of p_1, p_2. It is convenient to work in a frame where $\phi_3 = 0$. So we work in terms of the rotational invariants $\tilde{\phi}_{1,2}$ defined in (4.9). The momentum parameterizations are then (see Eq. 4.2)

$$p_3 = |\mathbf{p_3}|(1;\, 0,\cdots,\sin\hat{\theta}_3,\cos\hat{\theta}_3), \tag{4.14}$$

$$k = |\mathbf{k}|(1;\,\cdots,\sin\theta\cos\phi,\cos\theta), \tag{4.15}$$

$$p_{1,2} = \frac{\sqrt{s}}{2}(1;\,0,\cdots,0,\pm 1), \tag{4.16}$$

$$s_{1,2} = (0;\,\cdots,\sin\tilde{\phi}_{1,2},\cos\tilde{\phi}_{1,2},0) \tag{4.17}$$

where

$$|\mathbf{k}| = \frac{s-M^2}{2\sqrt{s}}, \quad |\mathbf{p_3}| = \frac{M^2/2}{[q_0+|\mathbf{k}|(\sin\hat{\theta}_3\sin\theta\cos\phi+\cos\hat{\theta}_3\cos\theta)]}, \quad q_0 = \frac{s+M^2}{2\sqrt{s}}. \tag{4.18}$$

In this frame the $2 \to 3$ particle phase space is

$$\frac{\Delta_T d\hat{\sigma}_{Br}}{dM^2 d^{n-2}\hat{\Omega}_3} = \left(\frac{2^4}{2s}\right)\frac{1}{(2\pi)^{5-4\varepsilon}}\frac{M^{2-4\varepsilon}}{2^{5-2\varepsilon}}\frac{|\mathbf{k}|^{1-2\varepsilon}}{\sqrt{s}}\frac{2^{1-2\varepsilon}}{\pi^{\varepsilon}}\frac{\Gamma(1-\varepsilon)}{\Gamma(1-2\varepsilon)}$$
$$\times \int d\Omega \frac{\Delta_T|M|^2_{2\to 3}}{[q_0+|\mathbf{k}|(\sin\hat{\theta}_3\sin\theta\cos\phi+\cos\hat{\theta}_3\cos\theta)]^{2-2\varepsilon}}, \tag{4.19}$$

where

$$\int d\Omega = \int_0^{\pi} d\theta \sin^{1-2\varepsilon}\theta \int_0^{\pi} d\phi \sin^{-2\varepsilon}\phi\ . \tag{4.20}$$

Figure 4.5: Gluon bremsstrahlung contributions.

The relevant Feynman diagrams are shown in Fig. 4.5. Evaluating $\Delta_T|M|^2_{2\to 3}$ and performing the phase space integrations yields,

$$\frac{\Delta_T d\hat{\sigma}_{Br}}{dM^2 d^{n-2}\hat{\Omega}_3} = \setminus_B(\varepsilon, y) C_F \frac{\alpha_s}{2\pi}\left(\frac{4\pi\mu^2}{M^2}\right)^{\varepsilon}\frac{\Gamma(1-\varepsilon)}{\Gamma(1-2\varepsilon)}\left\{\frac{w(1-w)}{y(1-y)} - w(1-w)\right.$$

$$\left[\frac{1+w^2}{w+y(1-y)(1-w)^2} + \frac{(1+w)^2 w}{[w+y(1-y)(1-w)^2]^2}\right] - \frac{w^2\ln\left[1+\frac{y(1-y)}{w}(1-w)^2\right]}{y^2(1-y)^2(1-w)}$$

$$+\left[\left(wF(y,w) + \frac{2w^4\ln\left[\frac{(1-y(1-w))^2}{w}\right]}{(1-w)[1-y(1-w)]^4}\right) + (y\to 1-y)\right] + 2w^3\left[\frac{1}{[1-y(1-w)]^{4-2\varepsilon}}\right.$$

$$\left.+\frac{1}{[y+w(1-y)]^{4-2\varepsilon}}\right]\left(-2\ln(1-w) + 2\left(\frac{\ln(1-w)}{1-w}\right)_+ + \frac{1}{\varepsilon}\left[1-\frac{1}{(1-w)_+}\right]\right)$$

$$\left.+\frac{1}{\varepsilon^2}\delta(1-w)\right\} \tag{4.21}$$

where

$$F(y,w) = \frac{1}{3}\left\{\frac{2+5w+11w^2}{1-y(1-w)} + \frac{3yw(1+4w-17w^2)}{[1-y(1-w)]^2} + \frac{6y^2w^2(1-11w+10w^2)}{[1-y(1-w)]^3}\right.$$
$$\left. - \frac{22y^3w^3(1-w)^2}{[1-y(1-w)]^4}\right\} \tag{4.22}$$

$$= \frac{2}{3}\frac{w^3}{(1-w)}\left\{\frac{-11}{[1-y(1-w)]^4}+\frac{3}{w}\frac{1+w}{[1-y(1-w)]^3}+\frac{3}{2w^2}\frac{1+w^2}{[1-y(1-w)]^2}\right.$$
$$\left.+\frac{1}{w^3}\frac{1+w^3}{[1-y(1-w)]}\right\}. \qquad (4.23)$$

Note:

$$\frac{1}{[w+y(1-y)(1-w)^2]} = \frac{1}{1+w}\left(\frac{1}{1-y(1-w)}+\frac{1}{y+w(1-y)}\right). \qquad (4.24)$$

4.3 Unpolarized Contributions

In order to calculate asymmetries, we need to calculate the unpolarized cross sections corresponding to those calculated for the polarized case. To be consistent, we should calculate the unpolarized cross sections in DRED as well, in order to ensure the perturbative stability of the asymmetry. Unfortunately, it is rather complicated to take into account the Z-exchange and $Z-\gamma$ interference. This is because we do not simply get an overall factor like $F_q(M)$ in the unpolarized case. So, for asymmetries, we will restrict to γ-exchange for now and, for simplicity, we will consider the cross section $d\sigma/dM^2d\phi_3$ only.

For the unpolarized case, we calculate $d\hat{\sigma}/dM^2d\phi_3$ directly. We do not first calculate $d\hat{\sigma}/dM^2d\hat{\Omega}_3$, then integrate over $\hat{\theta}_3$ after cancelling the divergences, as we do in the polarized case. Rather, we integrate over $\hat{\theta}_3$ from the beginning, then we integrate over k. We then add the factorization counterterm to $d\hat{\sigma}/dM^2d\phi_3$ directly.

First we need the $2\to 2$ and $2\to 3$ phase spaces. The $2\to 2$ phase space, in the p_1,p_2 c.m. (here equivalent to the rest frame of q), is given by

$$\frac{d\hat{\sigma}_{2\to 2}}{dM^2} = \left(\frac{2^4}{2M^2}\right)\frac{M^{-2-2\varepsilon}}{2^{4-2\varepsilon}}\frac{\delta(1-w)}{\pi^{2-\epsilon}}\frac{\Gamma(1-\varepsilon)}{\Gamma(1-2\varepsilon)}\int d\hat{\Omega}_3|M|^2_{2\to 2}, \qquad (4.25)$$

where $\int d\hat{\Omega}_3$ is defined analogously to (4.20). Since $d\hat{\sigma}/dM^2d\phi_3$ is independent of ϕ_3

in the unpolarized case, we may obtain it via

$$\frac{d\hat{\sigma}}{dM^2 d\phi_3} = \frac{1}{2\pi}\frac{d\hat{\sigma}}{dM^2} \tag{4.26}$$

The $2 \to 3$ particle phase space is given by,

$$\frac{d\hat{\sigma}_{2\to 3}}{dM^2} = \left(\frac{2^4}{2s}\right)\frac{M^{4\varepsilon}}{2^{9-4\varepsilon}}\frac{1}{\pi^{5-2\varepsilon}}\frac{\Gamma^2(1-\varepsilon)}{\Gamma^2(1-2\varepsilon)}w^{\varepsilon}(1-w)^{1-2\varepsilon}\int_{p_1,p_2} d\Omega_k \int_{\mathbf{q}=0} d\hat{\Omega}_3 |M|^2_{2\to 3}. \tag{4.27}$$

where the integral over $\hat{\Omega}_3$ is performed first, in the rest frame of q, then the integral over Ω_k is performed in the c.m. of p_1, p_2.

At the Born level there is only the $q\bar{q} \to l^- l^+$ process. We find that the cross section for this subprocess is given exactly (in DRED) by

$$\frac{d\hat{\sigma}_{\rm Born}}{dM^2 d\phi_3} = \bar{\gamma}_{\rm B}(\varepsilon)\delta(1-w): \quad \bar{\gamma}_{\rm B}(\varepsilon) \equiv \frac{1}{2\pi}\frac{\alpha^2}{N_c}\frac{2e_q^2\mu^{4\varepsilon}\pi^{1+\varepsilon}}{2^{-2\varepsilon}M^{4+2\varepsilon}}\frac{(2-\varepsilon)}{(3-2\varepsilon)(1-2\varepsilon)}\frac{\Gamma(1-\varepsilon)}{\Gamma(1-2\varepsilon)}. \tag{4.28}$$

The *virtual* corrections to this subprocess are found to be

$$\frac{d\hat{\sigma}_{\rm Loops}}{dM^2 d\phi_3} = \bar{\gamma}_{\rm B}(\varepsilon)\delta(1-w)C_F\frac{\alpha_s}{2\pi}\left[-\frac{2}{\varepsilon^2}-\frac{3}{\varepsilon}-\bar{7}+\frac{2\pi^2}{3}\right]\left(\frac{4\pi\mu^2}{M^2}\right)^{\varepsilon}\frac{\Gamma(1-\varepsilon)}{\Gamma(1-2\varepsilon)}. \tag{4.29}$$

The factorization counterterm, obtained in the usual manner, is given by

$$\frac{d\hat{\sigma}_{\rm Fact}}{dM^2 d\phi_3} = \frac{1}{\varepsilon}\bar{\gamma}_{\rm B}(\varepsilon)\frac{\alpha_s}{2\pi}w^{1+\varepsilon}\cdot 2P_{qq}(w)\left(\frac{4\pi\mu^2}{M^2}\right)^{\varepsilon}\frac{\Gamma(1-\varepsilon)}{\Gamma(1-2\varepsilon)}\left(\frac{s}{M_f^2}\right)^{\varepsilon}, \tag{4.30}$$

where the unpolarized quark-quark splitting function is given by

$$P_{qq}(w) = \Delta P_{qq}(w) = C_F\left[\frac{2}{(1-w)_+} - w - 1 + \frac{3}{2}\delta(1-w)\right]. \tag{4.31}$$

This is to be added to the cross section arising from gluonic bremsstrahlung,

$$\begin{aligned}\frac{d\hat{\sigma}_{\rm Br}}{dM^2 d\phi_3} &= \bar{\gamma}_{\rm B}(\varepsilon)\frac{\alpha_s}{2\pi}w^{1+\varepsilon}C_F\left[\frac{2}{\varepsilon^2}\delta(1-w)-\frac{2}{\varepsilon}\left(\frac{2}{(1-w)_+}-w-1\right)\right. \\ &+ \left. 8\left(\frac{\ln(1-w)}{1-w}\right)_+ - 4(1+w)\ln(1-w) - 2(1-w)\right]\left(\frac{4\pi\mu^2}{M^2}\right)^{\varepsilon}\frac{\Gamma(1-\varepsilon)}{\Gamma(1-2\varepsilon)}.\end{aligned} \tag{4.32}$$

In addition, for the unpolarized process, in next-to-leading order, there is a contribution from the subprocess $qg \to l^+ l^- q$ and $(q \to q)$. The factorization counterterm for this subprocess is

$$\frac{d\hat{\sigma}_{\rm Fact}}{dM^2 d\hat{\Omega}_3} = \frac{1}{\varepsilon}\Upsilon_{\rm B}(\varepsilon)\frac{\alpha_s}{2\pi}w^{1+\varepsilon}P_{qg}(w)\left(\frac{4\pi\mu^2}{M^2}\right)^{\varepsilon}\frac{\Gamma(1-\varepsilon)}{\Gamma(1-2\varepsilon)}\left(\frac{s}{M_f^2}\right)^{\varepsilon}, \tag{4.33}$$

where

$$P_{qg}(w) = \frac{1}{2}(1-2w+2w^2) \tag{4.34}$$

and the bremsstrahlung cross section is found to be

$$\begin{aligned}\frac{d\hat{\sigma}_{\rm Br}}{dM^2 d\hat{\Omega}_3} &= \frac{1}{4}\Upsilon_{\rm B}(\varepsilon)\frac{\alpha_s}{2\pi}w^{1+\varepsilon}\left[-\frac{4}{\varepsilon}P_{qg}(w) + 8P_{qg}(w)\ln(1-w)\right.\\ &+ \left.\frac{(1-w)}{2}(2+6w)\right]\left(\frac{4\pi\mu^2}{M^2}\right)^{\varepsilon}\frac{\Gamma(1-\varepsilon)}{\Gamma(1-2\varepsilon)}.\end{aligned} \tag{4.35}$$

4.4 Observable Cross Sections

We now make the connection between the various subprocess contributions given in the previous sections and the observable cross sections. The next-to-leading order subprocess polarized differential cross section is obtained in the sum

$$\frac{\Delta_{\rm T} d\hat{\sigma}}{dM^2 d^{n-2}\hat{\Omega}_3} = \frac{\Delta_{\rm T} d\hat{\sigma}_{\rm Born}}{dM^2 d^{n-2}\hat{\Omega}_3} + \frac{\Delta_{\rm T} d\hat{\sigma}_{\rm Loops}}{dM^2 d^{n-2}\hat{\Omega}_3} + \frac{\Delta_{\rm T} d\hat{\sigma}_{\rm Fact}}{dM^2 d^{n-2}\hat{\Omega}_3} + \frac{\Delta_{\rm T} d\hat{\sigma}_{\rm Br}}{dM^2 d^{n-2}\hat{\Omega}_3}. \tag{4.36}$$

Adding (4.8), (4.12), (4.13) and (4.21) we observe the cancellation of the IR divergences. Taking the limit $n \to 4$ (i.e. $\varepsilon \to 0$) we obtain

$$\begin{aligned}\frac{\Delta_{\rm T} d\hat{\sigma}}{dM^2 d\hat{\Omega}_3} &= \chi_{\rm B}(0,y)\left(\delta(1-w) + C_F\frac{\alpha_s}{2\pi}\left\{\left[-7+\frac{2\pi^2}{3}\right]\delta(1-w)\right.\right.\\ &+ c\left(\frac{\ln(1-w)}{1-w}\right)_+ + \left[3\delta(1-w) + \frac{c}{2}\frac{1}{(1-w)_+} - \frac{c}{2}\right]\ln\frac{s}{M_f^2}\\ &- c\ln(1-w) - \frac{w^2\ln\left[1+\frac{y(1-y)(1-w)^2}{w}\right]}{y^2(1-y)^2(1-w)} + \left.\left(\frac{2w^4\ln\left[\frac{(1-y(1-w))^2}{w}\right]}{(1-w)[1-y(1-w)]^4} + (y\leftrightarrow 1-y)\right)\right.\end{aligned}$$

$$+ \quad \frac{w(1-w)}{y(1-y)} - w(1-w)\left[\frac{1+w^2}{w+y(1-y)(1-w)^2} + \frac{(1+w)^2 w}{[w+y(1-y)(1-w)^2]^2}\right]$$
$$+ \quad [wF(y,w) + (y \to 1-y)]\}). \tag{4.37}$$

where

$$c \equiv 4w^3\left[\frac{1}{[1-y(1-w)]^4} + \frac{1}{[y+w(1-y)]^4}\right].$$

Integrating (4.37) over $\hat{\theta}_3$ (i.e. y) gives

$$\frac{\Delta_T d\hat{\sigma}}{dM^2 d\phi_3} = K_B\left(\delta(1-w) + \frac{\alpha_s}{2\pi}C_F\left\{\left[-\bar{7} + \frac{2\pi^2}{3}\right]\delta(1-w) + \tilde{c}\left(\frac{\ln(1-w)}{1-w}\right)_+\right.\right. \tag{4.38}$$
$$\left.\left. + \quad \left[3\delta(1-w) + \frac{\tilde{c}}{2}\frac{1}{(1-w)_+} - \frac{\tilde{c}}{2}\right]\ln\frac{s}{M_f^2} - \tilde{c}\ln(1-w) - 6\frac{\ln^2 w}{1-w} + 4\frac{1-w}{w}\right\}\right).$$

where

$$K_B = \cos(\tilde{\phi}_1 + \tilde{\phi}_2)\frac{\alpha^2}{3N_c}\frac{F_q(M)}{s^2}, \qquad \tilde{c} = \frac{8}{w}. \tag{4.39}$$

Similarly, adding (4.28), (4.29), (4.30) and (4.32), we obtain for the unpolarized $q\bar{q}$ cross section

$$\frac{d\hat{\sigma}_{q\bar{q}}}{dM^2 d\phi_3} = \Upsilon_B(0)\left(\delta(1-w) + C_F\frac{\alpha_s}{2\pi}\left\{\left[-\bar{7} + \frac{2\pi^2}{3}\right]\delta(1-w) + 8w\left(\frac{\ln(1-w)}{1-w}\right)_+\right.\right.$$
$$\left.\left. +2w\frac{P_{qq}(w)}{C_F}\ln\frac{s}{M_f^2} - 4w(1+w)\ln(1-w) - 2w(1-w)\right\}\right). \tag{4.40}$$

The unpolarized qg cross section is obtained by adding (4.33) and (4.35). The result is

$$\frac{d\hat{\sigma}_{qg}}{dM^2 d\phi_3} = \Upsilon_B(0)\frac{\alpha_s}{2\pi}\left\{wP_{qg}(w)\left[\ln\frac{s}{M_f^2} + 2\ln(1-w)\right] + \frac{(1-w)}{4}(1+3w)w\right\}. \tag{4.41}$$

We comment briefly here on the form of the polarized subprocess cross sections in next-to-leading order. Certain features persist even after inclusion of the HOC. The azimuthal dependence is the same, i.e. proportional to $\cos(2\phi_3 - \phi_1 - \phi_2)$ (or

simply $\cos(2\phi_3)$ if $\phi_1 = \phi_2 \equiv 0$). This is easy to check experimentally. As well, the sign (or zeros) of the corrected subprocess cross section is determined by the sign of $F_q(M)$, as in the Born term. To the extent that the up-quark dominates, which is fairly well, this holds for the process-level cross section as well (keeping in mind that we must sum over the quark flavors u, d, s in the parton model expression).

We now have all the necessary, finite, subprocess cross sections: (4.37), (4.38), (4.40) and (4.41). Hence, we are in a position to determine the observable polarized cross sections using the parton model expression (1.16), with the unpolarized quantities replaced by the corresponding polarized ones.

After performing the appropriate changes of variable, we obtain the contribution of $\Delta_T d\hat{\sigma}/dM^2 d\hat{\Omega}_3$ to the differential physical cross section

$$\frac{\Delta_T d\sigma_{q\bar{q}}}{dM^2 d\eta_3 d\phi_3} = 4\tau \sum_{\substack{i=q,\bar{q}, \\ j=\bar{q},q}} \int_\tau^1 \frac{dx_a}{x_a} \int_{w_1}^1 \frac{dw}{w^2} \Delta_T F_{i/A}(x_a, M_f^2) \Delta_T F_{j/B}(x_b, M_f^2) \frac{\Delta_T d\hat{\sigma}_{ij}/dM^2 d\hat{\Omega}_3}{[x_b e^{\eta_3} + x_a e^{-\eta_3}]^2} \tag{4.42}$$

where

$$w_1 = \tau/x_a, \qquad x_b = w_1/w. \tag{4.43}$$

Note that in the subprocess cross section we have

$$s_1 = S_A, \qquad s_2 = S_B \tag{4.44}$$

according to the definition of $\Delta_T F_q$. Analogously to ϕ_1 and ϕ_2, we may define ϕ_A and ϕ_B as being the azimuthal angles corresponding to S_A and S_B.

For the integrated $q\bar{q}$ cross sections, we have

$$\frac{[\Delta_T] d\sigma_{q\bar{q}}}{dM^2 d\phi_3} = \sum_{\substack{i=q,\bar{q}, \\ j=\bar{q},q}} \int_\tau^1 \frac{dx_a}{x_a} \int_{w_1}^1 \frac{dw}{w} [\Delta_T] F_{i/A}(x_a, M_f^2) [\Delta_T] F_{j/B}(x_b, M_f^2) \frac{[\Delta_T] d\hat{\sigma}_{ij}}{dM^2 d\phi_3}. \tag{4.45}$$

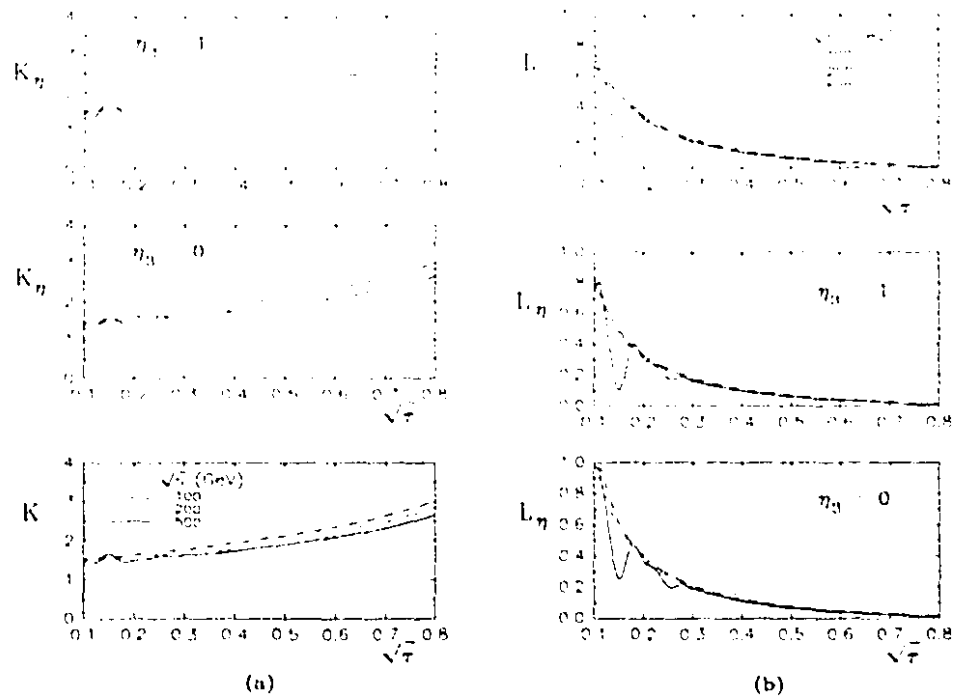

Figure 4.6: **(a)** K-factors; **(b)** L-factors versus $\sqrt{\tau}$ at $\sqrt{S} = 100, 200, 500$ GeV.

Analogously, for the integrated unpolarized qg cross section

$$\frac{d\sigma_{qg}}{dM^2 d\phi_3} = \sum_{\substack{i=q,\bar{q} \\ j=g,q}} \int_\tau^1 \frac{dx_a}{x_a} \int_{w_1}^1 \frac{dw}{w} F_{i/A}(x_a, M_f^2) F_{j/B}(x_b, M_f^2) \frac{d\hat{\sigma}_{ij}}{dM^2 d\phi_3}. \tag{4.46}$$

Since $d\hat{\sigma}_{ij}/dM^2 d\phi_3$ is a function of s, M^2 only, it is $p_1 \leftrightarrow p_2$ symmetric. Hence, if $A = B$ we have only half the terms and a factor of 2.

4.5 Numerical Results

Here we present the numerical results for the production of lepton-pairs in transversely polarized proton-proton collisions. Results will be presented, in general, for energies $\sqrt{S} = 100, 200, 500$ GeV; RHIC's planned energies.[23] For the polarized cross sections, we use the parameterizations of the transversity distributions given in Appendix A.2. For the unpolarized cross sections, relevant to the asymmetries, we

use the set S-$\overline{\rm MS}$ of Ref. 29. In all cases, we take $2\phi_3 - \phi_A - \phi_B = 0$, which maximizes the polarized cross sections, as can be seen from (4.8), (4.37), (4.38) and (4.44). In $\alpha_s(\mu^2)$, we take $\mu = M_f = M$, $N_f = 4$, $\Lambda = 0.2$ GeV. Except where stated, we take into account production by both γ and Z as well as γ-Z interference.

It is convenient to define

$$\sigma \equiv \frac{\Delta_T d\sigma}{dM^2 d\phi_3}, \qquad \sigma_\eta \equiv \frac{\Delta_T d\sigma}{dM^2 d\eta_3 d\phi_3}. \tag{4.47}$$

In terms of these cross sections, Fig. 4.6 (a) presents the ratios

$$K \equiv \frac{\sigma_{\rm Born} + \sigma_{\rm HOC}}{\sigma_{\rm Born}}, \qquad K_\eta \equiv \frac{\sigma_{\eta,{\rm Born}} + \sigma_{\eta,{\rm HOC}}}{\sigma_{\eta,{\rm Born}}}, \tag{4.48}$$

for $\sqrt{S} = 100,\ 200,\ 500$ and $0.1 \leq \sqrt{\tau} \leq 0.8$. Firstly, we notice that all K, K_η are greater than 1 (i.e. *enhance* the Born term); starting at around 1.5 and increasing towards the kinematic endpoint. This feature is quite analogous to that observed in direct photon production. As well, for fixed $\sqrt{\tau}$, the K-factors decrease with increasing $\sqrt{S}$ (and hence M) due to the diminishing of α_s.

For $\sqrt{S} = 200,\ 500$ GeV, we notice peaks and dips before and after the Z-peak. This is because we are taking the ratio of two quantities which vanish at slightly different points. Due to the overall factor $F_q(M)$, defined in (4.10), which multiplies the contribution from each quark flavor, the cross section vanishes before and after the Z-peak, where it becomes positive (i.e. it changes sign). Since we are summing over all quark contributions, the HOC and the Born term vanish at slightly different points, leading to the peaks and dips in the vicinity of the zeros.

Let σ_H, σ_S be defined analogously to the direct photon case. Again σ_S represents the contribution coming from soft, collinear and virtual gluons, and we may ask to

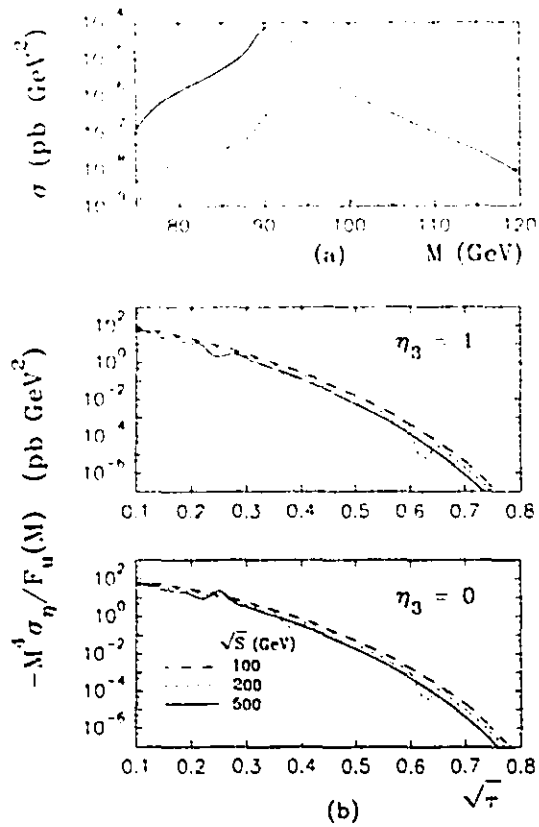

Figure 4.7: Cross sections (a) integrated versus M; (b) differential versus $\sqrt{\tau}$, at $\sqrt{S} =$ (100), 200, 500 GeV.

what extent σ_S dominates the cross section. Fig. 4.6 (b) presents the ratios

$$L = \frac{\sigma_H}{\sigma_S}, \qquad L_\eta = \frac{\sigma_{\eta,H}}{\sigma_{\eta,S}} \tag{4.49}$$

versus $\sqrt{\tau}$, for the same $\sqrt{S}$, η as in Fig. 4.6 (a). As in the direct photon case, the L-factors decrease quickly as we approach the kinematic maximum (for the same reasons), and for $\sqrt{\tau} \gtrsim 0.25$, σ_S dominates. It is therefore σ_S which is responsible for the increase in the K-factors as $\sqrt{\tau} \to 1$. Hence, one might use σ_S to get a first approximation to an $\mathcal{O}(\alpha_S^2)$ contribution (i.e. 2 gluon radiation) for $\sqrt{\tau} \gtrsim 0.25$, and then try to extrapolate to lower $\sqrt{\tau}$ values.

Fig. 4.7 presents various polarized cross sections. Fig. 4.7 (a) presents the integrated polarized cross section σ, versus M, near the Z-peak (where the cross section becomes positive) for $\sqrt{S} = 200$ and 500 GeV. Since we do not present asymmetries

here, it is of interest to see how many events we can expect, or more precisely, the number of events when the protons are polarized in the same direction *minus* the number of events when they are oppositely polarized. RHIC is expected to have a luminosity of $\mathcal{L} \simeq 2 \times 10^{32}$ cm^{-2}sec^{-1}. Taking into account realistic estimates of running time (100 days, 50% efficiency), an integrated luminosity of $L = 800$ pb^{-1} is anticipated. Integrating the cross section, $\Delta_T d\sigma/dM d\phi_3 \cdot L$, between $M = 80$ and $M = 100$ GeV gives a difference of roughly 200 $l^+ + l^-$ events/radian (of ϕ_3), taking both $l = e$ and $l = \mu$, for $\sqrt{S} = 500$ GeV. Negligible rates occur for $\sqrt{S} = 200$ GeV at the Z-peak, due to the suppression of the transversity sea for large x.

Fig. 4.7 (b) shows the quantity $-M^4\sigma_\eta/F_u(M)$ versus $\sqrt{\tau}$ for $\sqrt{S} = 100, 200, 500$ GeV. The purpose of dividing by $F_u(M)$ is to somewhat smoothen the cross sections so that they are similar to the photon exchange contribution (i.e. $\sqrt{S} = 100$ GeV). This works since, to a large extent, the up-quark dominates.

We notice a high degree of scaling, meaning that the plotted quantity varies with $\sqrt{\tau}$ almost independently of $\sqrt{S}$. Changes in $\sqrt{S}$ amount to a shift up or down by an almost constant factor of $1.5 \sim 2$ in the smooth regions (i.e. away from the cross section zeros). This gives us a good measure of the sensitivity of the cross section to changes in μ, M_f occurring in $\alpha_s(\mu^2)$, $\Delta_T F_q(x, M_f^2)$ respectively. This is because the only dependence on $\sqrt{S}$, for fixed $\sqrt{\tau}$, is in α_s and $\Delta_T F_q$ (to the extent that dividing by $F_u(M)$ cancels the mass dependence). Hence the differences in the 3 curves arise solely from differences in $\alpha_s(\mu^2)$ and $\Delta_T F_q(x, M_f^2)$, in these regions. Varying M_f as well, in the term $\sim \ln(s/M_f^2)$, would increase the stability.

Lastly, we consider the asymmetry

$$A \equiv \frac{\Delta_T d\sigma/dM^2 d\phi_3}{d\sigma/dM^2 d\phi_3} \tag{4.50}$$

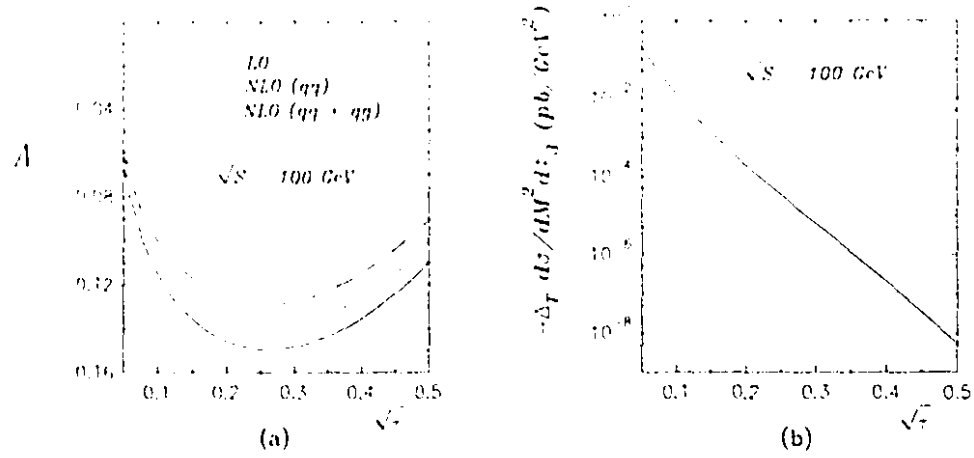

Figure 4.8: (a) Asymmetries at the Born level and in next-to-leading order; (b) corresponding next-to-leading order polarized cross section, versus $\sqrt{\tau}$ at $\sqrt{S} = 100$ GeV.

for transverse Drell-Yan, in the γ-exchange region. Asymmetries are important since they give a measure of the ratio of the transversity distributions to the unpolarized parton distributions, *independent* of the overall normalization factors. Hence large or small measured asymmetries can be used to distinguish reliably between a relatively large or small transversity antiquark distribution, working at any order in α_s. As well, we saw in direct photon production that the asymmetry was perturbatively stable. If this feature holds for transverse Drell-Yan as well, we can extract from the experiment rather precise information about the transversity distributions, without the usual problems associated with convergence in perturbative QCD.

Fig. 4.8 (a) gives the asymmetry for $\sqrt{S} = 100$ GeV and $0.05 \leq \sqrt{\tau} \leq 0.5$ in leading and next-to-leading order. We see that the $q\bar{q}$ contribution is quite stable under HOC, decreasing by $\lesssim 10\%$ throughout. When we include the qg subprocess in the unpolarized cross section, the asymmetry becomes slightly more negative, decreasing by another $\sim 10\%$ throughout. This is because the qg subprocess contributes negatively, in agreement with the finding of Ref. 77. So, the net effect of the HOC is to

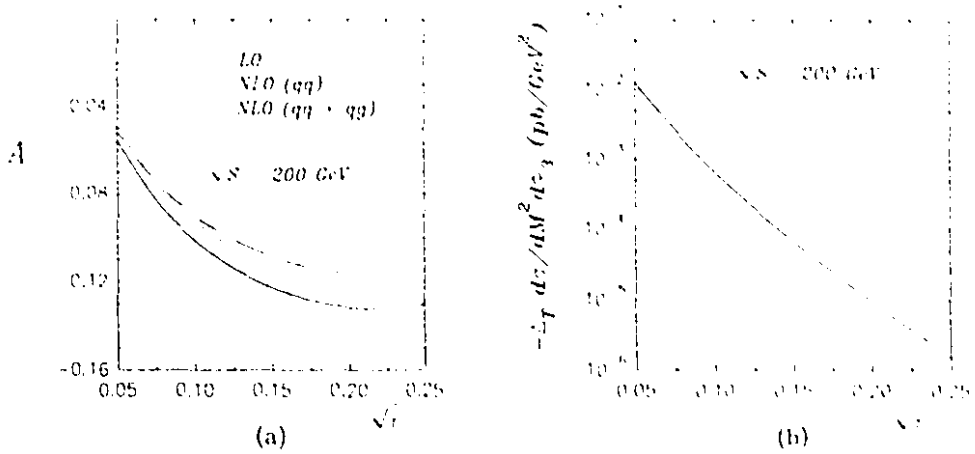

Figure 4.9: (a) Asymmetries at the Born level and in next-to-leading order; (b) corresponding next-to-leading order polarized cross section, versus $\sqrt{\tau}$ at $\sqrt{S} = 200$ GeV.

make the asymmetry $\lesssim 20\%$ more negative.

The stability of the asymmetry can be understood by examining the polarized and unpolarized HOC for $q\bar{q}$ and observing the close similarities. This is particularly true in the dominant region, $w \to 1$ (note $\Delta_T P_{qq}(w) \overset{w\to 1}{\to} P_{qq}(w)$). Hence, the corrections tend to cancel in the asymmetry. This same feature was observed in direct photon production.

Fig. 4.8 (b) shows the polarized cross section in the same region. We see that the smaller $\sqrt{\tau}$ region is ideal here for maximizing the cross section. In the region where the cross sections are sizable, $\sqrt{\tau} \lesssim 0.2$, the asymmetry varies between $0.08 \lesssim -A \lesssim 0.15$. Of course, the measured asymmetry will depend on the size of the $\Delta_T F_q$ and $\Delta_T F_{\bar{q}}$ in particular. Hence, from experiment, a larger or smaller asymmetry would tell us that $\Delta_T F_{\bar{q}}$ was larger or smaller than our guess. Unfortunately, a much smaller $\Delta_T F_{\bar{q}}$ could lead to difficult-to-measure asymmetries.

In Fig. 4.9, the same quantities as in Fig. 4.8 are plotted, but for $\sqrt{S} = 200$ GeV and $0.05 \lesssim \sqrt{\tau} \lesssim 0.25$. Similar conclusions hold for the asymmetry (which is a bit

smaller now), as can be expected from the scaling behaviour of the K-factor (see Fig. 4.6 (a)). The cross sections are somewhat smaller though, due to the $\sim 1/M^4$ factor in γ_H (Eq. 4.8), which amounts to $\sim 2/M^3$ in $\Delta_T d\sigma/dMd\phi_3$. Since the cross section (4.45) receives dominant contributions from $w \approx 1$ (as in direct photon production) and $x_a \approx x_b$, we are sampling the parton distributions near $x \approx \sqrt{\tau}$. This helps to understand the sharp drop-off of the cross section with increasing $\sqrt{\tau}$.

We note that the HOC to transverse Drell-Yan have also been studied in Ref. 74 which only takes into account production by γ and employs a different regularization scheme: giving the gluon a mass. Of course, when two-loop transversity split functions become available, they will most likely be determined using dimensional methods (as in the unpolarized case). Hence, it will not be possible to make use of their result. Yet, the results of Ref. 74 have the same features as ours, except that they work at a fixed $M = 7$ GeV and use two different sets of transversity distributions. Our asymmetry lies in between the ones corresponding to their two sets. As well, they agree on the perturbative stability of the asymmetry. If we extrapolate our K-factors to their mass region, we find fair agreement. Even with all this agreement, there are several differences in the analytical results for the subprocess cross section, $\Delta_T d\hat{\sigma}/dM^2 d\phi_3$, which we determine in common. For instance, they are missing the term $\sim \pi^2 \delta(1-w)$, typical of the corresponding unpolarized and longitudinally polarized cases.[77,57] If both calculations were done consistently, then according to theory, differences in the analytical results are compensated by differences in α_s and $\Delta_T F_q$, as determined in each regularization scheme via comparison with experiment. At this point though, there is no experimental information on $\Delta_T F_q$.*

*After this work was published, a paper came out[78] proposing an upper bound on the absolute value of the transversity distributions. The bound was derived using a leading order (naive parton model) approximation to QCD. Basically, Ref. 78 generalizes constraints from nucleon-nucleon

4.6 Conclusions

To conclude, we have determined complete analytical results for the one-loop HOC to $A_i B_i \to l^- l^+ + X$. For proton-proton collisions, the HOC enhance the Born term by 50 – 100%. Near the Z-peak and in the low-mass region, well measurable cross sections are obtained. HOC are found to make the asymmetries $\lesssim 20\%$ more negative, indicating perturbative stability. For a reasonable choice of transversity distributions, and considering production by γ only, asymmetries between -0.08 and -0.15 are found in the well measurable regions (i.e. $\sqrt{S} = 100$ GeV, $\sqrt{\tau} \lesssim 0.2$). Hence, our work lends good support to the planned experiments at RHIC.

scattering to quark-nucleon scattering. Therefore QCD radiative corrections are absent, and these may significantly modify the bound.[79] Anyway, our u- and d-quark distributions satisfy this bound for most x of interest. The antiquark distributions, on the other hand, are a bit large. Hence, imposition of the bound would somewhat decrease the overall *magnitude* of the cross sections and asymmetries presented here, but not the shape. These points aside, our analysis and conclusions remain unaffected.

Chapter 5

Heavy Quark Production by Polarized and Unpolarized Photons

Higher order corrections for heavy quark ($Q\overline{Q}$) production in unpolarized particle collisions have been determined in detail.[80-82] For polarized particle collisions, however, analytical results were still absent. Even for the unpolarized case, only virtual + soft corrections have been presented analytically.[81] Apart from general reasons, well-known from unpolarized reactions, knowledge of HOC for Q, $\overline{Q}$ production in polarized processes is important for several special reasons.

Beginning with polarized $\gamma\gamma$ collisions, which is the subject of the present work,[83] one reason of special interest is the following. A $\gamma\gamma$ collider becomes particularly important for searches of the standard model Higgs boson when its mass is below the W^+W^- threshold. Then, the predominant decay is $H \to b\bar{b}$ and the background comes from $\gamma\gamma \to b\bar{b}$ with direct or resolved photons. Leaving aside the latter, for the moment, use of polarized photons of equal helicity (when the angular momentum has $J_z = 0$) suppresses this background by a factor m_b^2/s.[84,85] This holds, however, only for the lowest order of α_s. HOC necessarily involve the subprocess $\gamma\gamma \to b\bar{b}g$,

and gluon emission permits the $b\bar{b}$ system to have $J \neq 0$ without suppression; this may result in a sizable background. Of course, another reason the $J_z = 0$ channel is important is that the Higgs signal comes entirely from it. Thus, we maximize the Higgs to background ratio in two different ways.

Furthermore, at higher energies, it will be possible to produce top-quarks in photon-photon collisions. This, when combined with other data on top-quark production from e^+e^- and $p\bar{p}$ collisions, should certainly improve our knowledge of the top-quark parameters. The HOC could have a significant effect on the threshold behaviour. It is also interesting to examine the spin dependence of the HOC in this region. Of course, the analytical results presented here will likely find several other applications. The experimental possibilities for producing γ's via backscattering are discussed in Sect. 1.3.

In this chapter, we present complete analytical results for heavy quark production by both polarized and unpolarized photons. Numerical results are presented for 2-, 3- and 2+3-jet cross sections for the cases where the initial photons have total spin $J_z = 0$ and $J_z = \pm 2$. For b-quark production, this is analyzed as a background to Higgs production. We also consider t-quark production for energies not too far above threshold.

The analytical results presented here are also useful in determining the production of heavy quarks in polarized photon-proton (proton-proton) collisions. This is because the process $\gamma\gamma \to Q\overline{Q}(g)$ is the Abelian (QED) part of the subprocess $\gamma g \to Q\overline{Q}(g)$ ($gg \to Q\overline{Q}(g)$), which is by far the dominant subprocess in γ-p (p-p) collisions.[80,81] The non-Abelian part of $\vec{\gamma}\vec{g} \to Q\overline{Q}(g)$ ($\vec{g}\vec{g} \to Q\overline{Q}(g)$) remains to be calculated.

Figure 5.1: Lowest order contributions to $\gamma\gamma \to Q\overline{Q}$.

5.1 Leading Order Cross Sections

The contributing graphs are shown in Fig. 5.1. We introduce the variables (momenta as in figure)

$$s \equiv (p_1+p_2)^2, \quad t \equiv T-m^2 \equiv (p_1-p_3)^2-m^2, \quad u \equiv U-m^2 \equiv (p_2-p_3)^2-m^2 \quad (5.1)$$

and

$$s_2 \equiv S_2 - m^2 \equiv (p_1+p_2-p_3)^2 - m^2 = s+t+u. \quad (5.2)$$

where m is the heavy-quark mass. Defining

$$v \equiv 1+\frac{t}{s}, \quad w \equiv \frac{-u}{s+t} \quad (5.3)$$

we may express

$$t = -s(1-v), \quad u = -svw, \quad s_2 = sv(1-w). \quad (5.4)$$

The polarized and unpolarized squared amplitudes are defined, respectively, as

$$\Delta|M|^2 \equiv \frac{1}{2}(|M(+,+)|^2-|M(+,-)|^2), \quad |M|^2 \equiv \frac{1}{2}(|M(+,+)|^2+|M(+,-)|^2), \quad (5.5)$$

where $M(\lambda_1,\lambda_2)$ denotes the Feynman amplitude with photons p_1, p_2 having helicity λ_1, λ_2 respectively. The same holds for the cross sections.

For the examples considered in this paper, it is of interest to calculate (numerically) the cross sections for a specific helicity state, $\sigma(\lambda_1,\lambda_2)$. We present analytical

results for the polarized and unpolarized cross sections $\Delta\sigma$, σ. From (5.5) we can obtain the desired cross sections via

$$\sigma(+,+) = \sigma + \Delta\sigma, \qquad \sigma(+,-) = \sigma - \Delta\sigma, \tag{5.6}$$

Defining

$$K(\varepsilon) \equiv \frac{m^{-2\varepsilon}}{s} \frac{\pi(4\pi)^{-2+\varepsilon}}{\Gamma(1-\varepsilon)} \left(\frac{tu - sm^2}{sm^2}\right)^{-\varepsilon} \tag{5.7}$$

we may express the n $(= 4 - 2\varepsilon)$-dimensional 2-body phase space as

$$[\Delta]\frac{d\sigma_{2\to 2}}{dvdw} = K(\varepsilon)\left[(2m)^2[\Delta]|M|^2_{2\to 2}\right]\delta(1-w). \tag{5.8}$$

It will become necessary to work in n dimensions when we determine the HOC (see next section for details).

The resulting leading-order (LO) cross sections are, in DRED (noting (2.33)),

$$\begin{aligned}
\Delta\frac{d\sigma_{\rm LO}}{dvdw} &= 32\pi^2 K(\varepsilon)\delta(1-w)N_c\alpha^2 c_Q^4\mu^{4\varepsilon}\left\{-\frac{t^2+u^2}{tu} + 2\frac{sm^2}{tu}\left(\frac{s^2}{tu} - 2\right)\right\} \\
\frac{d\sigma_{\rm LO}}{dvdw} &= 32\pi^2 K(\varepsilon)\delta(1-w)N_c\alpha^2 c_Q^4\mu^{4\varepsilon}\left\{\frac{t^2+u^2}{tu} + 4\frac{sm^2}{tu} - 4\left(\frac{sm^2}{tu}\right)^2\right\}
\end{aligned} \tag{5.9}$$

where N_c (=3) is the number of quark colors and c_Q is the fractional charge of the heavy-quark. Making use of (5.4), (5.6) we see explicity that $d\sigma_{\rm LO}(+,+)/dvdw$ is suppressed by order m^2/s.

5.2 Loop Contributions

The loop contributions arise from the diagrams of Fig. 5.2 and their $p_1 \leftrightarrow p_2$ interchange. These diagrams contain both ultraviolet and infrared singularities. To regularize them, we use dimensional reduction, which was described in Sect. 2.2.2. This facilitates the handling of the Levi-Civita tensor $\varepsilon^{\mu\nu\lambda\rho}$. As we will show below,

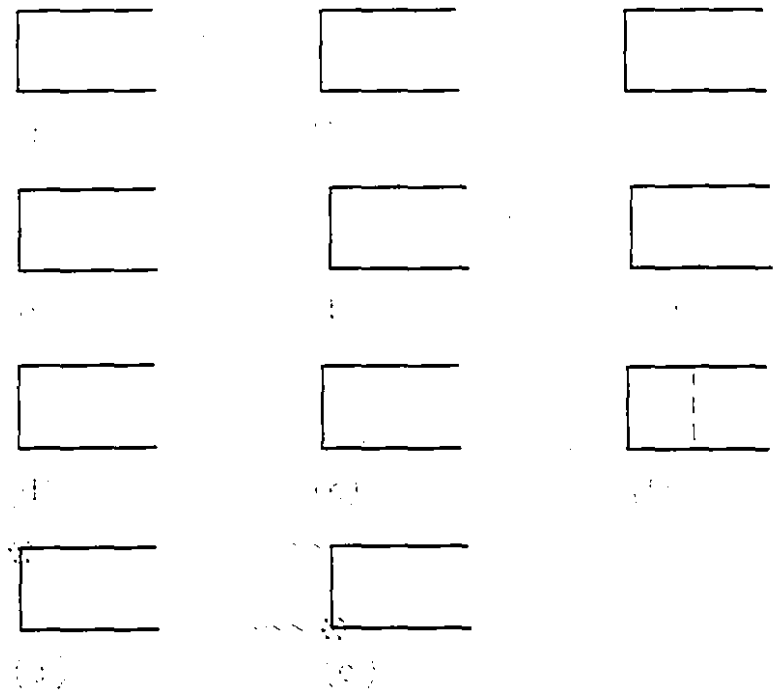

Figure 5.2: Loop graphs for $\gamma\gamma \to Q\overline{Q}$. (a)-(c) self-energy diagrams; (a')-(c') mass counterterm diagrams corresponding to the graphs (a)-(c); (d),(e) vertex diagrams; (d'),(e') dimensional reduction counterterm diagrams corresponding to graphs (d),(e); (f) box diagram.

the analytical expressions for the cross sections are *regularization scheme independent* once all the contributions (including the gluonic bremsstrahlung) are added. Throughout, we work in the Feynman gauge.

The heavy-quark mass and wave function renormalizations are performed on-shell. The self energy graphs are shown in Figs. 5.2 (a)-(c) and the corresponding mass counterterm diagrams in Figs. 5.2 (a')-(c'). The factor 1/2 multiplying (b)-(c') comes from wave function renormalization. The bare mass and wave function are determined in terms of the renormalized ones via

$$m = Z_m m_r, \qquad \psi = Z_2^{1/2}\psi_r, \tag{5.10}$$

(see also (2.58)) where Z_m and Z_2 are the mass and wave function renormalization constants determined in the on-shell scheme. We define

$$C_\varepsilon \equiv \frac{\Gamma(1+\varepsilon)}{(4\pi)^2}\left(\frac{4\pi\mu^2}{m^2}\right)^\varepsilon . \tag{5.11}$$

In dimensional reduction we find, to order g^2,

$$Z_m = 1 - 3g^2 C_\varepsilon C_F\left(\frac{1}{\varepsilon'}+\frac{5}{3}\right), \quad Z_2 = 1 - g^2 C_\varepsilon C_F\left(\frac{1}{\varepsilon'}+5+\frac{2}{\varepsilon}\right) \tag{5.12}$$

with $C_F = 4/3$. We use $1/\varepsilon'$ to indicate which terms are of ultraviolet origin.

In dimensional reduction, we must add to the vertex diagrams of Figs. 5.2 (d), (e) appropriate counterterms (d'), (e') in order to satisfy the Ward identity[76]

$$Z_1 = Z_2 \tag{5.13}$$

between vertex and self-energy graphs, with Z_1 denoting the vertex renormalization constant (see (D.24), (D.25)). The Feynman rule for this vertex counterterm is found to be (in n dimensions)

$$\gamma^\mu \to \frac{-g^2}{(4\pi)^2} C_F \gamma_\varepsilon^\mu \frac{1}{\varepsilon'}, \tag{5.14}$$

where γ_ε^μ is given by (2.57). The derivation of this counterterm and the check of the Ward identity are given in Appendix D.

When all the contributions to the physical cross section (including gluonic bremsstrahlung) are added, the result is free of infrared divergences as there are no mass singularities here. Thus the only scheme dependent part might come from the vertex and self-energy graphs. Having satisfied the Ward identity (5.13) though, means that the scheme dependent part of the corrections cancels between vertex and self-energy graphs. This was explicitly verified by calculating the vertex and self-energy graphs in dimensional regularization. We also checked explicitly that there are no differences between reduction and regularization arising from any other contributions.

More specifically, to obtain the dimensional regularization result for any particular contribution given here, simply replace the LO term by the corresponding LO term from dimensional regularization. When all the contributions are added, the scheme dependent part of the LO term cancels along with the $1/\varepsilon$ infrared divergence multiplying it. Hence, the absence of mass singularities and vacuum polarization graphs leads to scheme independence.

As was stated in Refs. 75 and 86, a counterterm like (5.14) was used to remove an unphysical term. General one-loop counterterms have been developed[87] to convert unpolarized dimensional reduction results into the corresponding dimensional regularization results for the purely massless case. Also, certain equivalences[44] and correspondences[88] between dimensional reduction and dimensional regularization have been noted. In the present case however, satisfaction of (5.13) is sufficient to ensure scheme independence.

Adding the contributions of Figs. 5.2 (a)–(e′) (and the $t \leftrightarrow u$ interchange) resulted in the ultraviolet finite vertex plus self-energy cross section

$$\frac{d\sigma_{\rm vse}}{dvdw} = -\frac{16}{\varepsilon}\pi\alpha_s C_F C_\varepsilon \frac{d\sigma_{\rm LO}}{dvdw} + \delta(1-w)\frac{CK(0)}{(4\pi)^2}\{2A_1[4(\xi(2) - {\rm Li}_2(\frac{T}{m^2}))(1+3\frac{m^2}{t}) \qquad (5.15)$$
$$- \ln(-\frac{t}{m^2})(8 - 6\frac{t}{T} - \frac{t^2}{T^2}) - 2 - \frac{t}{T}] + A_2\ln(-\frac{t}{m^2}) + A_3({\rm Li}_2(\frac{T}{m^2}) - \xi(2)) + A_4 + (t \leftrightarrow u)\}$$

where

$$C \equiv (4\pi)^3 C_F N_c \alpha_s \alpha^2 e_Q^4 \mu^{6\varepsilon}. \qquad (5.16)$$

The corresponding polarized cross section, $\Delta d\sigma_{\rm vse}/dvdw$, can be obtained by replacing the A_i and $d\sigma_{\rm LO}/dvdw$ in (5.15) by ΔA_i and $\Delta d\sigma_{\rm LO}/dvdw$, respectively. The $[\Delta]A_i$ are given in Appendix C.2. We will use this notation throughout. We note the term $\sim 1/\varepsilon$ in (5.15) representing an infrared divergence. Also, note that $[\Delta]A_1$

is proportional to the LO squared amplitude without the $t \leftrightarrow u$ interchange (see Appendix C.2, Eq. C.5).

Since $[\Delta]d\sigma_{\rm LO}/dvdw$ is in general regularization scheme dependent to $\mathcal{O}(\varepsilon)$ (working in n dimensions), we see explicitly that truly scheme independent cross sections will result only when all contributions are added and all infrared divergences are cancelled.

In order to evaluate the box graph of Fig. 5.2 (f), we must reduce the resulting tensor integrals to scalar ones (conveniently listed in Ref. 81) using projective tensor techniques.[89] The tensor integrals have the general form

$$D^{0,\mu,\mu\nu,\mu\nu\lambda}(k_1,k_2,k_3,m_1,m_2,m_3,m_4) \equiv \tag{5.17}$$
$$\mu^{2\varepsilon}\int\frac{d^nq}{(2\pi)^n}\frac{1,q^\mu,q^\mu q^\nu,q^\mu q^\nu q^\lambda}{(q-m_1)^2[(q+k_1)^2-m_2^2][(q+k_1+k_2)^2-m_3^2][(q+k_1+k_2+k_3)^2-m_4^2]}$$

where the k_i are general momenta. As an example, the vector box integral we encounter has the decomposition

$$D^\mu(p_4,-p_2,-p_1,0,m,m,m) = p_4^\mu D_{11} - p_2^\mu D_{12} - p_1^\mu D_{13}. \tag{5.18}$$

In general, the scalar coefficients D_{ij} are not independent. This simplifies the calculation somewhat. Noting that

$$D^\mu(p_4,-p_2,-p_1,0,m,m,m) = -D^\mu(p_3,-p_1,-p_2,0,m,m,m), \tag{5.19}$$

we obtain

$$D_{12} = D_{11} - D_{13}, \tag{5.20}$$

since the D_{ij} in both integrals are the same, due to the fact that they are scalars. Using the same approach, we reduce the number of independent D_{ij} from seven to five in $D^{\mu\nu}$ and from thirteen to eight in $D^{\mu\nu\lambda}$. This method was quite helpful in keeping the very large intermediate expressions as short as possible.

Figure 5.3: Gluonic Bremsstrahlung graphs for $\gamma\gamma \to Q\overline{Q}g$.

Adding the contribution of Fig. 5.2 (f) and the $t \leftrightarrow u$ interchange gives the virtual box cross section

$$\begin{aligned}
\frac{d\sigma_{\rm box}}{dvdw} &= 16\pi\alpha_s C_F C_\varepsilon \frac{d\sigma_{\rm LO}}{dvdw}\frac{2m^2-s}{s\beta}\{2\ln(x)[\frac{1}{2\varepsilon}-\ln(\beta)]+2{\rm Li}_2(-x)-2{\rm Li}_2(x)-3\xi(2)\} \\
&+ \delta(1-w)\frac{CK(0)}{(4\pi)^2}\{-8B_1\frac{2m^2-s}{s\beta}\ln(x)\ln(-t/m^2)+2\frac{B_2}{\beta}[\ln(x)(4\ln(1+x)-\ln(x) \\
&- 4\ln(-t/m^2))+4{\rm Li}_2(-x)+2\xi(2)]+2B_3\ln^2(x)+4\frac{B_4}{\beta}\ln(x)+4B_5\ln(-t/m^2) \\
&+ 8B_6{\rm Li}_2(T/m^2)+4B_7\xi(2)+4B_8+(t\leftrightarrow u)\} \qquad (5.21)
\end{aligned}$$

where

$$\xi(2)=\frac{\pi^2}{6}, \qquad \beta\equiv\sqrt{1-4m^2/s}, \qquad x\equiv\frac{1-\beta}{1+\beta}. \qquad (5.22)$$

The $[\Delta]B_i$ are given in Appendix C.2. We see again the infrared divergence $\sim 1/\varepsilon$.

Independent calculations were performed using FORM[90] and REDUCE[91]. The latter proved useful in factoring the expressions and cancelling powers in the denominators.

5.3 Gluonic Bremsstrahlung Contributions

The bremsstrahlung diagrams are shown in Fig. 5.3. Squaring these diagrams (plus their $p_1 \leftrightarrow p_2$ interchange), we obtain the $2 \to 3$ particle squared amplitude

$$(2m)^2|M|^2_{2\to 3} = \qquad (5.23)$$

$$C[\frac{\tilde{c}_1}{s_2^2} + c_2\, p_2\cdot k + \frac{c_3}{p_2\cdot p_4} + \frac{c_4}{p_2\cdot p_4^2} + c_5\frac{p_2\cdot k}{p_1\cdot p_4^2} + \frac{\tilde{c}_6}{s_2\; p_3\cdot k} + \frac{\tilde{c}_7}{p_3\cdot k^2}$$
$$+ \frac{c_8}{p_1\cdot p_4\; p_2\cdot p_4} + c_9\frac{p_2\cdot k^2}{p_1\cdot p_4} + c_{10}\frac{p_2\cdot k}{p_1\cdot p_4} + \frac{\tilde{c}_{11}/s_2}{p_2\cdot p_4\; p_3\cdot k} + \frac{\tilde{c}_{12}}{p_2\cdot p_4\; p_3\cdot k^2}$$
$$+ \frac{c_{13}}{p_2\cdot p_4^2\; p_3\cdot k} + \frac{\tilde{c}_{14}}{p_2\cdot p_4^2\; p_3\cdot k^2} + c_{15}\frac{p_2\cdot k^2}{p_3\cdot k} + c_{16}\frac{p_2\cdot k}{p_3\cdot k}] + (p_1\rightarrow p_2, t\rightarrow u).$$

As before, we may obtain $\Delta|M|^2_{2\to 3}$ by replacing the c_i in (5.23) by Δc_i. The $[\Delta]c_i$ are given in Appendix C.2. Again, independent calculations were performed using FORM and REDUCE. The former proved useful in partial fractioning and other reductions of the dot-products analogous to those in Appendix B.3, for nonvanishing $q^2 = p_3^2$, $r^2 = p_4^2$.

To obtain the total bremsstrahlung contribution to $[\Delta]d\sigma/dvdw$, we perform the phase-space integrals in the frame where p_4 and k are back-to-back. We find (in agreement with Ref. 81) for the $2\to 3$ phase space

$$[\Delta]\frac{d\sigma_{\rm Br}}{dvdw} = K(\varepsilon)\frac{C_\epsilon}{\mu^{2\epsilon}}\tilde{f}(\varepsilon)\int d\Omega(2m)^2[\Delta]|M|^2_{2\to 3} \tag{5.24}$$

where

$$\tilde{f}(\varepsilon) \equiv \frac{(m^2)^{1-\epsilon}}{S_2^{1-\epsilon}}\frac{sv}{2\pi}\left(\frac{sv}{m^2}\right)^{1-2\epsilon}(1-w)^{1-2\epsilon}\underbrace{\frac{\Gamma(1-\varepsilon)}{\Gamma(1+\varepsilon)\Gamma(1-2\varepsilon)}}_{1-\varepsilon^2\pi^2/3+\cdots} \tag{5.25}$$

and

$$\int d\Omega \equiv \int_0^\pi d\theta_1 \sin^{1-2\epsilon}\theta_1 \int_0^\pi d\theta_2 \sin^{-2\epsilon}\theta_2. \tag{5.26}$$

The gluon angles θ_1 and θ_2 are defined in Appendix C.1 along with all the momenta.

We first evaluate all the phase space integrals in four dimensions since, for $w \neq 1$, all the integrals are finite. For $w = 1$, the terms in (5.23) with coefficients $\tilde{c}_i$ are singular through the relation (3.26), where the "+" distributions are defined in (2.91), (2.92). This means that, for these terms, the integrals must also be evaluated in n

dimensions in the limit $w \to 1$, keeping their $O(\varepsilon)$ part. The resulting integrals are straightforward.

The final result is, with $\bar{y} \equiv \sqrt{(t+u)^2 - 4m^2 s}$,

$$\begin{aligned}
\frac{d\sigma_{\rm Br}}{dvdw} = & \\
& \frac{CK(0)}{(4\pi)^2} 2\pi \tilde{f}(0) \{ \frac{s_2(s+u)}{4S_2} c_2 + \frac{2S_2}{s_2(s+u)} \ln\frac{S_2}{m^2}\, c_3 + \frac{4S_2}{m^2(s+u)^2} c_4 \\
+ \;& c_5 I_5 + c_8 I_8 + c_9 I_9 + c_{10} I_{10} + c_{13} I_{13} + c_{15} I_{15} + c_{16} I_{16} + (t \leftrightarrow u)\} \\
+ \;& \frac{1}{(1-w)_+} \frac{CK(0)}{(4\pi)^2} \frac{1}{S_2} \{ \tilde{c}_1 + \frac{2S_2}{\bar{y}} \ln\frac{T+U-\bar{y}}{T+U+\bar{y}}\, \tilde{c}_6 + 4\frac{S_2}{m^2}\tilde{c}_7 + s_2 I_{11}\tilde{c}_{11} \\
+ \;& s_2^2 I_{12}\tilde{c}_{12} + s_2^2 I_{14}\tilde{c}_{14} + (t \leftrightarrow u)\} + 8\pi\alpha_s C_F C_\varepsilon \frac{d\sigma_{\rm LO}}{dvdw} \frac{1}{s\beta} \{ (2m^2 - s) \qquad (5.27) \\
\times \;& \left[2\ln x (2\ln\frac{sv}{m^2} - \frac{1}{\varepsilon}) - 1 - 2\left({\rm Li}_2\left(\frac{-4\beta}{(1-\beta)^2} \right) + \ln^2 x \right) \right] + 2s\beta \left[1 - 2\ln\frac{sv}{m^2} + \frac{1}{\varepsilon} \right] \},
\end{aligned}$$

where the integrals I_i are given in Appendix C.3.

5.4 Physical Cross Sections

We may obtain the 2+3-jet cross section by adding (5.9), (5.15), (5.21), and (5.27):

$$[\Delta]\frac{d\sigma_{2+3}}{dvdw} = [\Delta]\frac{d\sigma_{\rm LO}}{dvdw} + [\Delta]\frac{d\sigma_{\rm vse}}{dvdw} + [\Delta]\frac{d\sigma_{\rm box}}{dvdw} + [\Delta]\frac{d\sigma_{\rm Br}}{dvdw}. \qquad (5.28)$$

We notice the cancellation of all the $1/\varepsilon$ infrared divergences, leading to a finite, scheme independent result. We also note that the arbitrary mass scale, μ, is no longer *explicitly* present; a byproduct of the on-shell scheme.

At this point it is useful to note that for $s \gg 4m^2$, the LO cross sections (5.9) are large in the forward and backward directions. Since jets going down the beam pipe are difficult to measure experimentally, angular cuts are necessary for $b\bar{b}$ production well above threshold. At the same time, we reduce the $b\bar{b}$ background to the Higgs signal. This also helps eliminate *resolved photon* contributions where the partons within the

photon participate, as opposed to the *direct* contributions, which we present, where the photon is structureless. This is discussed further at the end of this section.

Let θ_3 denote the angle between p_3 and p_1 in the $\gamma\gamma$ c.m.. Then the integrated 2+3-jet cross section, with the constraint $|\cos\theta_3| < \cos\theta_c$, for some θ_c, is given by

$$[\Delta]\sigma_{2+3}(s) = \int_{v_1}^{v_2} dv \int_{w_1}^{1} dw\ \theta(\cos^2\theta_c - \cos^2\theta_3)[\Delta]\frac{d\sigma_{2+3}}{dvdw} \tag{5.29}$$

where

$$v_1 = \frac{1}{2}(1-\beta), \quad v_2 = \frac{1}{2}(1+\beta), \quad w_1(v) = \frac{m^2}{s}\frac{1}{v(1-v)} \tag{5.30}$$

and

$$\cos\theta_3 = \frac{-(1-v-vw)}{\sqrt{(1-v+vw)^2 - 4m^2/s}}. \tag{5.31}$$

Alternatively, we may convert to $d\sigma/d\cos\theta_3 dw$ and integrate directly over θ_3 and w.

The integrated 3-jet cross section is given by

$$\begin{aligned}
[\Delta]\sigma_3(s) &= \frac{K(0)}{(4\pi)^2}\int_{v_1}^{v_2} dv \int_{w_1}^{1} dw\ \theta(\cos^2\theta_c - \cos^2\theta_3)\tilde{f}(0)\int d\Omega(2m)^2[\Delta]|M|^2_{2\to 3} \\
&\times\ \theta((p_3+k)^2 - y_{\rm cut}s)\theta((p_4+k)^2 - y_{\rm cut}s) \\
&= \frac{K(0)}{(4\pi)^2}\int_{v_1}^{v_2} dv \int_{w_1}^{w_2} dw\ \theta(\cos^2\theta_c - \cos^2\theta_3)\tilde{f}(0)\int d\Omega(2m)^2[\Delta]|M|^2_{2\to 3} \\
&\times\ \theta((p_3+k)^2 - y_{\rm cut}s); \qquad w_2 = 1 - \frac{(y_{\rm cut} - m^2/s)}{v}.
\end{aligned} \tag{5.32}$$

The angular integral is given by (5.26) with $\varepsilon = 0$. The dot-products involved may be explicitly expressed as functions of v, w, θ_1 and θ_2 using the parameterizations of Appendix C.1 and Eqs. (5.4). We have imposed the constraints, $(p_3+k)^2 > y_{\rm cut}s$ and $(p_4+k)^2 > y_{\rm cut}s$. With a suitable choice of $y_{\rm cut}$ we may simultaneously cut out events with 2-jet topology and avoid the soft divergence, $w = 1$. We effectively eliminate the soft and collinear gluons from the 3-jet cross section, with the degree of softness and collinearity being specified by $y_{\rm cut}s$.

The desired 2-jet cross section is obtained by the difference

$$[\Delta]\sigma_2(s) = [\Delta]\sigma_{2+3}(s) - [\Delta]\sigma_3(s). \tag{5.33}$$

Since σ_{2+3} and σ_3 are both infrared finite and separately observable quantities, this serves as a reliable and unambiguous method for defining σ_2.

In discussing the numerical results, it will be convenient to split $[\Delta]\sigma_{2+3}$ as follows,

$$[\Delta]\sigma_{2+3} = [\Delta]\sigma_{\rm LO} + [\Delta]\sigma_{\rm S} + [\Delta]\sigma_{\rm H}. \tag{5.34}$$

where $[\Delta]\sigma_{\rm S}$ represents the contribution to the HOC coming from terms proportional to $\delta(1-w)$ and $1/(1-w)_+$, and $[\Delta]\sigma_{\rm H}$ represents the rest. In usual terminology, $[\Delta]\sigma_{\rm S}$ represents virtual and soft contributions whereas $[\Delta]\sigma_{\rm H}$ represents hard radiation.

So far we have only considered direct contributions, i.e. no resolved photon contributions. The reason is the following. Well above the $Q\overline{Q}$ threshold, σ_{2+3} and σ_3 will certainly receive sizable resolved photon contributions. Now, resolved photon events are generally accompanied by a jet making small angles with respect to the beam axis, and carrying a large fraction of the photon's energy. The latter is due to the softness of the photon's gluon distribution,[92] discussed below. For the 2-jet cross section (which is of physical interest), experiment can reject resolved photon events (and other unwanted events) as being those for which the observed jets have total energy measurably lower than $\sqrt{s}$.[85] This is because, due to the angular cuts, either experiment will not observe the jet making small angles and there will be missing energy, or experiment will observe the jet, but it will not qualify as a 2-jet event. Of course, we are assuming a rather well defined initial photon energy, which may be experimentally difficult.

For top-quark production, not too far above threshold, the resolved contributions will be negligible in all the cross sections. This is because the dominant resolved

contribution comes from $g\gamma \to Q\overline{Q}$, where the gluon originates from one of the initial photons, having a fraction x of its momentum. Near threshold, the gluon will have to carry a large fraction of the photon's momentum; and for $x \to 1$, the gluon distribution in the photon is highly suppressed. As well, 3-jet states arising from hard gluonic radiation will be suppressed due to the restricted phase space. The (near) absence of resolved contributions and the non-suppression of the $J_z = 0$ cross section for $2 \to 2$ kinematics, not too far above threshold, implies that we need not worry about whether the events are 2- or 3-jet (even though 3-jet events are either very seldom or none, depending on s). Experimentally, the t-quark will decay before hadronizing, hence the actual number of observed jets will be greater.

5.5 Numerical Results

Here we present numerical results for b- and t-quark production in next-to-leading order. Throughout, we evaluate $\alpha_s(\mu^2)$ (2-loop) with $\mu^2 = s$, $\Lambda = 0.2$ GeV and the number of flavors taken as $N_f = 5$ since we are well above the $b\bar{b}$ threshold. We take $m_b = 4.7$ GeV and $m_t = 174$ GeV.[2] For 3-jet cross sections, we use $y_{\rm cut} = 0.15$. Some justification for this choice of $y_{\rm cut}$ is in order. Experimentally, it is useful to have a small value of $y_{\rm cut}$ so that for the 2-jet cross section we eliminate, as much as possible, events with 3-jet topology via (5.33). Theoretically, there are limitations. If one chooses $y_{\rm cut}$ too small, then the infrared divergence ruins the perturbation expansion, since the 3-jet cross section becomes unphysically large. To control this, an all-orders resummation would be required. We find that $y_{\rm cut} = 0.15$ is the most suitable choice in light of the above considerations.

Fig. 5.4(a) presents $\sigma_{\rm LO}(+,+)$, $\sigma_{2+3}(+,+)$, $\sigma_3(+,+)$ and $\sigma_2(+,+)$ for b-quark production in the range $20 < \sqrt{s} < 200$ GeV with $\theta_c = 30^0$. As expected, the LO

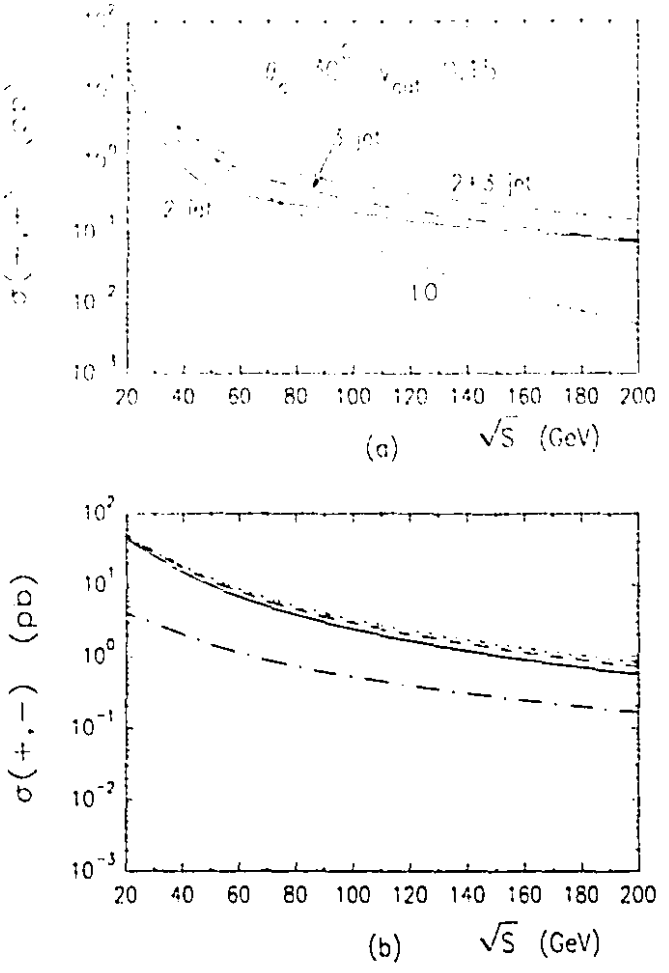

Figure 5.4: Cross sections for $\gamma\gamma \to b\bar{b}(g)$: $\sigma_{\rm LO}$ (dotted line), σ_{2+3} (dashed), σ_3 (dash-dotted) and σ_2 (solid), with $\theta_c = 30^0$ and $y_{\rm cut} = 0.15$ for $20 < \sqrt{s} < 200$ GeV; **(a)** $\sigma(+,+)$; **(b)** $\sigma(+,-)$.

cross section is highly suppressed for large $\sqrt{s}$, but not the 3-jet. In fact $\sigma_3(+,+)$ makes a sizable contribution to $\sigma_{2+3}(+,+)$. Hence $\sigma_2(+,+)$ gets somewhat suppressed relative to $\sigma_{2+3}(+,+)$. For $20 \lesssim \sqrt{s} \lesssim 40$ GeV, the corrections $\sigma_{2+3} - \sigma_{\rm LO}$ are seen to be slightly negative.

Fig. 5.4(b) presents the same cross sections for $J_z = \pm 2$, i.e. $\sigma_{\rm LO}(+,-)$, $\sigma_{2+3}(+,-)$, $\sigma_3(+,-)$ and $\sigma_2(+,-)$. The major difference is that $\sigma_{\rm LO}(+,-)$ and $\sigma_{2+3}(+,-)$ suffer no suppression at large $\sqrt{s}$. Hence the 3-jet contribution to $\sigma_{2+3}(+,-)$ is not so significant and $\sigma_2(+,-)$ remains large. We also notice, $\sigma_{2+3} \lesssim \sigma_{\rm LO}$ throughout. We

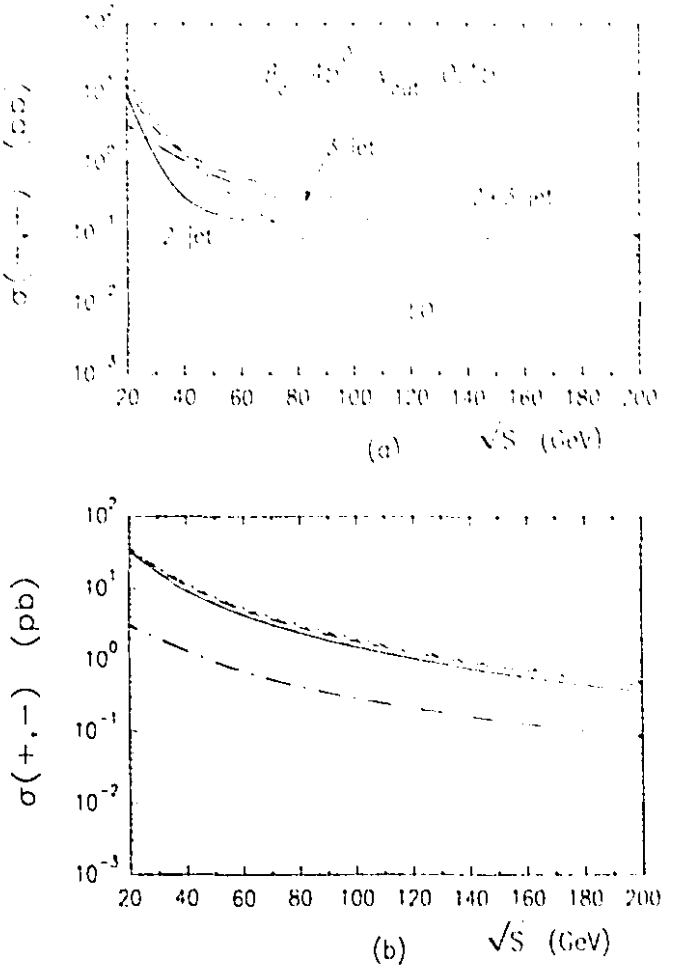

Figure 5.5: Same as Fig. 5.4, except with $\theta_c = 45^0$.

see explicitly that for $J_z = 0$, the 2-jet cross section is suppressed by more than a factor of 10 relative to the $J_z = \pm 2$ case.

Figs. 5.5 (a),(b) present the same quantities as in Figs. 5.4 (a),(b) except with $\theta_c = 45^0$. The major difference is that the cross sections are smaller everywhere and $\sigma_2(+,+)$ is particularly suppressed for $30 \lesssim \sqrt{s} \lesssim 60$ GeV. This reflects the fact that the 2-jet events tend to occur at smaller angles. Since the Higgs cross section is isotropic,[84] $\theta_c = 45^0$ may help to reduce the background to Higgs ratio (at the expense of having less Higgs events).

An interesting feature of the HOC arises for both σ_{2+3} and $\Delta\sigma_{2+3}$. In both cases,

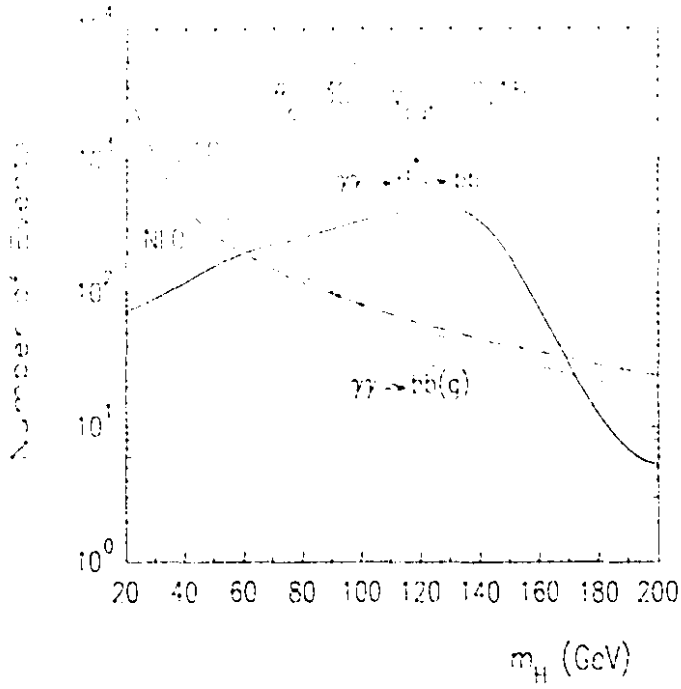

Figure 5.6: Two-jet $b\bar{b}$ background to standard model Higgs decay: $\gamma\gamma \to H^* \to b\bar{b}$ (solid line), σ_{LO} (dotted) and σ_2 (dashed) for $20 < m_H < 200$ GeV. Number of Higgs events taken from Ref. 84. Here $\theta_c = 30^0$, $< \lambda_1\lambda_2 >= 0.8$. The other experimental parameters are described in the text.

σ_S and σ_H are much larger that σ_{LO}, for $s \gg 4m^2$. However, they have opposite sign and are of almost equal magnitude, leading to large cancellations. In other words, the "virtual + soft" part conspires with the "hard" part to yield HOC which are under control.

Fig. 5.6 presents the 2-jet background to the Higgs decay $\gamma\gamma \to H^* \to b\bar{b}$. We have used the standard model Higgs cross section of Ref. 84 which takes $\theta_c = 30^0$ and an average value of $< \lambda_1\lambda_2 >= 0.8$ (i.e. 90% $J_z = 0$, 10% $J_z = \pm 2$). The photons are produced by laser backscattering off electrons (positrons) at a linear e^+e^- collider with $E_{e^+e^-} = 500$ GeV. As well, Ref. 84 uses an effective integrated luminosity of $L_{eff} = 20$ fb^{-1} and a $\gamma\gamma$ energy spread of $\Gamma_{expt} = 5$ GeV; $m_H - \Gamma_{expt}/2 \leq \sqrt{s} \leq$

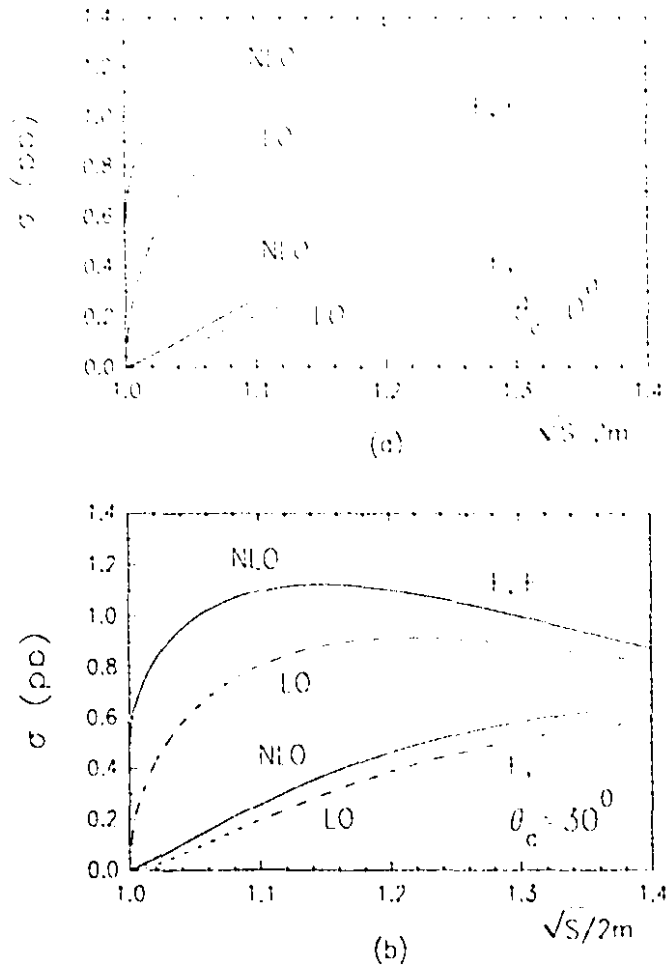

Figure 5.7: Cross sections for $\gamma\gamma \to t\bar{t}(g)$: $\sigma_{\rm LO}(+,-)$ (lower dashed line), $\sigma_{2+3}(+,-)$ (lower solid), $\sigma_{\rm LO}(+,+)$ (upper dashed) and $\sigma_{2+3}(+,+)$ (upper solid) for $1 < \sqrt{s}/2m < 1.4$: **(a)** $\theta_c = 0$; **(b)** $\theta_c = 30^0$.

$m_{\rm H} + \Gamma_{\rm expt}/2$. Using the expression of Ref. 84 for converting the $\gamma\gamma \to b\bar{b}(g)$ cross section into number of events, we obtain the LO and 2-jet next-to-leading order curves shown in Fig. 5.6.

At large $\sqrt{s}$, the increase in $\sigma_2(+,+)$ relative to $\sigma_{\rm LO}(+,+)$ is compensated by a decrease in $\sigma_2(+,-)$ relative to $\sigma_{\rm LO}(+,-)$, so that $\sigma_2(< \lambda_1\lambda_2 >= 0.8)$ does not change radically. In the end, the 2-jet cross section is still well below the Higgs signal for $90 \lesssim m_{\rm H} \lesssim 150$ GeV. With higher degrees of polarization, we could do even better, since for $< \lambda_1\lambda_2 >= 0.8$, the $J_z = \pm 2$ channel still contributes a fair amount.

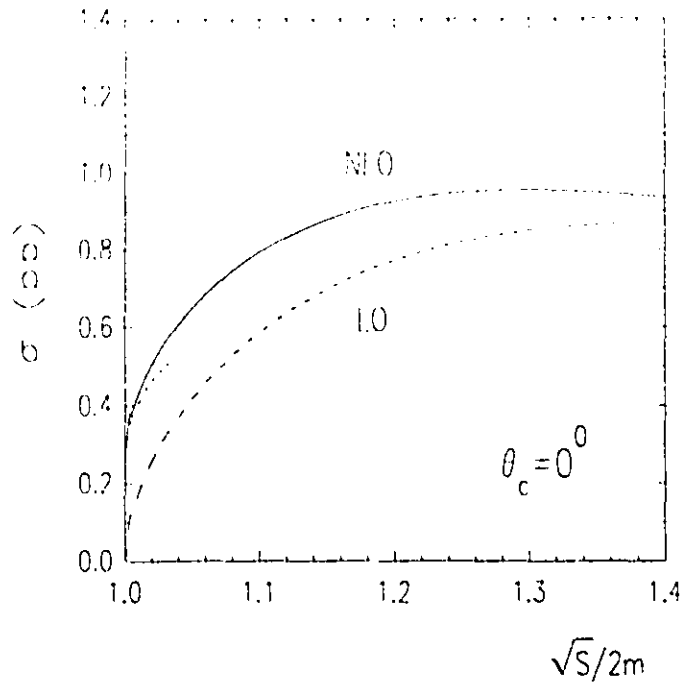

Figure 5.8: Unpolarized cross sections corresponding to Fig. 5.7(a): σ_{2+3} (solid line), $\sigma_{\rm LO}$ (dashed) and the small β approximation (dotted).

Fig. 5.7(a) gives σ_{2+3} and $\sigma_{\rm LO}$ for t-quark production in the range $1 < \sqrt{s}/2m < 1.4$ for $J_z = 0$ and $J_z = \pm 2$, without angular cuts. Fig. 5.7(b) is the same except with $\theta_c = 30^0$. We notice that the angular cuts do not make a big difference. This is because there is no peaked behaviour in the forward/backward directions as for $b\bar{b}$ production. As explained earlier, the (near) absence of resolved contributions makes the angular cuts less important experimentally as well. The most interesting feature of the HOC is that just above threshold, the HOC to $\sigma(+,+)$ completely dominate. There is no similar behaviour from $\sigma(+,-)$. This shows that the $J_z = 0$ channel is ideal for maximizing the top cross section not too far above threshold. At any rate, this drastic spin dependence of the HOC is of theoretical interest by itself and could be tested near the $b\bar{b}$ threshold as well. As the cross section is actually a

function of only $\sqrt{s}/m$ (or β) and $\alpha_s(\mu^2)$ (times an overall factor of e_Q^4/s), the only difference would be an increase in the HOC for $b\bar{b}$ relative to its corresponding LO term, due to an increase in α_s. The exception is right above threshold, where the $b\bar{b}$ pair could form a bound state, unlike in top production where the quarks decay before hadronizing (i.e. $t \to W^+ b$). In fact, the above exception aside, the only ambiguity in the predictions is the choice of scale μ^2 in $\alpha_s(\mu^2)$. Varying μ^2 in the range $s/4 < \mu^2 < 4s$, for $\sqrt{s} = 400$ GeV, gives α_s in the range $0.0878 < \alpha_s < 0.104$ and a corresponding variation in the magnitude of the corrections.

Fig. 5.8 gives the unpolarized cross sections corresponding to Fig. 5.7(a). The unpolarized cross section is somewhat watered down relative to $\sigma(+,+)$ because $\sigma(+,-)$ is relatively small. We also plot the small β (threshold region) approximation of Ref. 82. Our results agree with this approximation just above threshold. We see that the approximation breaks down for $\sqrt{s}/2m \gtrsim 1.02$. As expected, we found that almost all of the correction comes from σ_S, i.e. σ_H is almost negligible not too far above threshold. We found the same was true for $\Delta\sigma_S$, $\Delta\sigma_H$.

5.6 Conclusions

We have obtained complete analytical results for the production of heavy-quark pairs by polarized and unpolarized photons in next-to-leading order. Using these expressions, we computed cross sections for b- and t-quark production by photons having net spin $J_z = 0, \pm 2$. From the $b\bar{b}$ cross sections, we determined the background to $\gamma\gamma \to H^* \to b\bar{b}$ (standard model) coming from $\gamma\gamma \to b\bar{b}(g)$ (2-jet) for $< \lambda_1\lambda_2 >= 0.8$. The HOC to the $J_z = 0$ channel were found to be large for $s \gg 4m^2$, but still a factor of 10 smaller than the $J_z = \pm 2$ channel. For the experimental setup considered, the background was safely below the Higgs signal (but still sizable) for

$90 \lesssim m_H \lesssim 150$ GeV, even after inclusion of HOC. For t-quark production, not too far above threshold, the dominant contribution came from the $J_z = 0$ channel. Just above threshold, the HOC to this channel completely dominate.

Chapter 6

Conclusions

In chapter 3, complete analytical results for the HOC to large-p_T direct photon production in polarized hadronic collisions were presented. Numerical results were given for $\vec{p}\vec{p}$ collisions. The corrections to the cross sections were found to be large (the $\vec{g}\vec{q}$ subprocess dominating), but the asymmetry was found to be rather stable under HOC for the kinematics considered. The large cross sections and asymmetries obtained shall enable a clear determination of the polarized gluon distribution in the proton, $\Delta F_{g/p}$, from RHIC's planned experiments.

In chapter 4, complete analytical results for the HOC to lepton-pair production (Drell-Yan) in transversely polarized hadronic collisions were determined. Numerical results were given for $p_\uparrow p_\uparrow$ collisions. The cross sections received sizeable corrections; nonetheless, the asymmetries exhibited perturbative stability. Measurable cross sections near the Z-peak and also at smaller lepton-pair masses were obtained, thus allowing an accurate determination of the proton's transversity distributions $\Delta_T F_{q/p}$ and $\Delta_T F_{\bar{q}/p}$ from RHIC's planned experiments (assuming $\Delta_T F_{\bar{q}/p}$ isn't too small).

In chapter 5, complete analytical results for the production of heavy quark pairs by polarized and unpolarized photons were presented. The results were shown to be regularization scheme independent. Production of $b\bar{b}$ pairs was considered as a

background to $\gamma\gamma \to H^* \to b\bar{b}$ (standard model). The Higgs signal was safely above the background for $90 \lesssim m_H \lesssim 150$ GeV for the setup considered. Production of $t\bar{t}$ pairs, not too far above threshold was also considered, and the $J_z = 0$ channel was found to dominate.

Some useful information was presented in the Appendixes as well. In Appendix A, convenient scale-dependent parameterizations were given for the longitudinal and transversity parton distributions in the proton. One-loop evolution was used on the inputs, which, at this time, can only be considered as educated guesses (even though the longitudinal distributions still fit the DIS data reasonably well for the x-range of interest).

In Appendix D, a general one-loop counterterm for use with dimensional reduction was derived. It was shown that, after adding this counterterm, the QED Ward identity is satisfied and that no other counterterms are necessary to make the calculations performed here physically consistent.

Appendix A

Parameterizations of the Polarized Parton Distributions

A.1 Longitudinal Distributions

Here we present scale dependent parameterizations of the longitudinally polarized parton distributions of the proton, $\Delta F_i(x,Q^2)$ (also denoted $\Delta F_i(x,M_f^2)$), which were plotted in Sect. 2.1.1. Namely, the inputs of Ref. 27 (sets 1 and 2), evolved using one-loop polarized split functions. For each parton distribution, $\Delta F_i(x,Q^2)$, we will first give the general form, in terms of various parameters. Then we will give the scale dependence of the parameters for sets 1 and 2. The exception is for Set 2 of ΔF_3, which has a different form than Set 1.

Let Q_0 represent the input energy scale. Then we may define the evoution variable, s, by

$$s = \ln\left(\frac{\ln(Q^2/\Lambda^2)}{\ln(Q_0^2/\Lambda^2)}\right), \quad \Lambda = .2 \text{ GeV}, \quad Q_0 = 2 \text{ GeV}, \tag{A.1}$$

in terms of which we present the scale dependent parameterizations:

$$\Delta F_{u_v}(x,Q^2) = Cx^a(1-x)^b \tag{A.2}$$

Set 1:

$$C = 2.137 - .84131s + .16336s^2 \qquad a = .80154 - .26569s + .046293s^2$$

$$b = 2.3966 + .77234s + .11591s^2$$

Set 2:

$$C = 2.9791 - 1.5298s + .34741s^2 \qquad a = .90203 - .31785s + .058446s^2$$

$$b = 3.396 + .80748s + .1469s^2$$

$$\Delta F_{d_v}(x, Q^2) = Cx^a(1-x)^b \tag{A.3}$$

Set 1:

$$C = -.7674 + .36825s - .083881s^2 \qquad a = .80004 - .26831s + .046413s^2$$

$$b = 3.3953 + .84951s + .16853s^2$$

Set 2:

$$C = -1.6096 + .93958s - .23602s^2 \qquad a = .90068 - .31624s + .056336s^2$$

$$b = 4.3948 + .87594s + .19235s^2$$

$$\Delta F_g(x, Q^2) = Cx^a(1-x)^b \tag{A.4}$$

Set 1:

$$C = 16.166 - 40.197s + 55.675s^2 - 38.055s^3 + 9.7801s^4 \quad a = .70309 - 1.2755s + 1.1993s^2$$
$$- .74153s^3 + .18421s^4 \quad b = 7.0135 + .89958s + 3.8745s^2 - .83665s^3 + .098174s^4$$

Set 2:

$$C = 8.8289 - 20.357s + 27.169s^2 - 18.224s^3 + 4.6293s^4 \quad a = .70322 - 1.2518s + 1.1663s^2$$
$$- .72029s^3 + .17987s^4 \qquad b = 6.0125 + 1.0858s + 3.3639s^2 - .80512s^3 + .16765s^4$$

$$\Delta F_{\bar{u}}(x, Q^2) = (d + Cx^a)(1-x)^b \tag{A.5}$$

Set 1: $\Delta F_s(x,Q^2) = \Delta F_d(x,Q^2) = \Delta F_u(x,Q^2)$

$$C = .014303 + 3.2497s - 6.4104s^2 + 4.8053s^3 - 1.2658s^4 \qquad a = 1.3826 - 1.1528s$$
$$+ .26836s^2 \qquad b = 12.164 + .63867s + .64518s^2$$
$$d = 10^{-3} \times (-.20847 - 17.06s + 4.5863s^2 - 3.4677s^3 - 6.0184s^4)$$

Set 2: $\Delta F_d(x,Q^2) = \Delta F_{\bar{u}}(x,Q^2)$

$$C = .020104 + 1.6355s - 3.0584s^2 + 2.1992s^3 - .56124s^4 \qquad a = 1.4059 - 1.165s$$
$$+ .27438s^2 \qquad b = 10.65 + .66548s + .60853s^2$$
$$d = 10^{-3} \times (-.10579 - 10.23s + 2.9632s^2 - 2.3808s^3 - 3.0353s^4)$$

$$\Delta F_s(x,Q^2) = (c_0 + c_1 x + c_2 x^2)(1-x)^b \tag{A.6}$$

$$b(s<1) = 7.8592 + 1.4739s - 40.189s^2 + 174.38s^3 - 220.59s^4 + 103.76s^5$$
$$b(s>1) = 135.28 - 316.41s + 340.22s^2 - 162.32s^3 + 29.282s^4$$
$$c_0 = 10^{-3} \times (-3.7184 - 19.492s + 18.219s^2 - 9.4787s^3 + 5.495s^4)$$
$$c_1 = -.35256 + .72121s + .030831s^2 + .78071s^3 - .45044s^4$$
$$c_2(s<1) = .19644 - .90857s + 8.1439s^2 - 31.34s^3 + 21.542s^4$$
$$c_2(s>1) = .68725 - 1.4574s + .3901s^2.$$

The energy range of validity in the dominant regions (i.e. x-regions where the distributions are not too small to contribute appreciably) is:

$$2 - 3 \text{ GeV}^2 < Q^2 < 10^6 - 10^7 \text{ GeV}^2. \tag{A.7}$$

In general, the valence distributions fit a larger range of Q^2 values. For $Q^2 \gtrsim 10^5 - 10^6$ GeV^2 the gluon and sea quark parameterizations are increasingly larger than the

actual distributions for

$$x \lesssim 5 \times 10^{-4}. \tag{A.8}$$

Note: ideally $F(0) = 0$ for all the distributions, which is not the case for the sea quark parameterizations. Also, for very high energies ($Q^2 \gtrsim 10^4$ GeV^2), the large x behaviour is somewhat unreliable for the gluon and sea quark parameterizations.

A.2 Transversity Distributions

Here we present the scale dependent parameterizations of the transversity distributions of the proton, $\Delta_T F_i(x, Q^2)$, which were plotted in Sect. 2.1.2. More precisely, we perform the one-loop evolution (2.99) on the inputs (2.25) and (2.26).

We may parameterize the scale dependence in terms of the evolution variable, s, defined in (A.1). All the distributions take on the general form,

$$\Delta_T F_{q_i}(x, Q^2) = C x^a (1-x)^b \tag{A.9}$$

with the parameters C, a, b being given by (for each q_i).

u_v

$$\begin{aligned} C &= 2.130709 - .5105464s + .02875147s^2 \\ a &= .8003611 - .1404007s + .01375300s^2 \\ b &= 2.399273 + .8804527s + .09549651s^2 \end{aligned}$$

d_v

$$\begin{aligned} C &= -.7677717 + .2527982s - .03644243s^2 \\ a &= .8002619 - .1541905s + .01903325s^2 \\ b &= 3.397845 + 1.000649s + .1306618s^2 \end{aligned}$$

$$\bar{u} = \bar{d} = \bar{s}$$

$$\begin{aligned} C &= -.2399983 + .05987156s - .004957766s^2 \\ a &= .1000107 - .01771476s - .0006535380s^2 \\ b &= 9.492953 + 2.822821s + .4409071s^2. \end{aligned}$$

Energy range of validity:

$$1 \text{ GeV}^2 \leq Q^2 \leq 10^7 \text{ GeV}^2. \tag{A.10}$$

Valid for all x of interest to within a few percent on average.

Appendix B

Direct Photon Production Details

B.1 Momentum Parameterizations and Phase-Space

For $2 \to 3$ kinematics, working in a frame where p_1 and p_5 are back-to-back, the momenta may be parameterized as follows:

$$\begin{aligned}
p_1 &= \frac{sv}{2\sqrt{s_2}}(1;\, 0, \cdots, 0, 1) \\
p_3 &= \frac{s(1-v+vw)}{2\sqrt{s_2}}(1;\, 0, \cdots, \sin\psi, \cos\psi), \\
p_4 &= \frac{\sqrt{s_2}}{2}(1;\, \cdots, \sin\varphi\sin\theta, \cos\varphi\sin\theta, \cos\theta), \\
p_5 &= \frac{\sqrt{s_2}}{2}(1;\, \cdots, -\sin\varphi\sin\theta, -\cos\varphi\sin\theta, -\cos\theta), \\
p_2 &= \frac{s(1-v+vw)}{2\sqrt{s_2}}\left(\frac{1-vw}{1-v+vw};\, 0, \cdots, \sin\psi, \cos\psi - \frac{v}{1-v+vw}\right),
\end{aligned} \tag{B.1}$$

where

$$\sin\psi = \frac{2\sqrt{w(1-w)(1-v)}}{1-v+vw}, \qquad \cos\psi = \frac{2w-(1-v+vw)}{1-v+vw}. \tag{B.2}$$

For p_1, p_2, p_3 the dots represent zeros. For p_4, p_5 they represent components which depend on the remaining $n-4$ angles of p_5.

We can go to any other frame by making the appropriate changes of momenta. The necessary interchanges we encounter are

$$p_1 \leftrightarrow p_2 \quad \to \quad v \leftrightarrow 1-vw, \quad w \leftrightarrow \frac{1-v}{1-vw}, \quad s \leftrightarrow s \tag{B.3}$$

$$p_1 \to -q \quad \to \quad v \to \frac{1-v+vw}{vw}, \qquad w \to \frac{1}{1-v+vw}, \qquad s \to svw \tag{B.4}$$

$$p_2 \to -q \quad \to \quad v \to \frac{-v}{1-v}, \qquad w \to w, \qquad s \to -s(1-v). \tag{B.5}$$

We now derive the phase space relating $|M|^2_{2\to 3}$ with $E_3 d\sigma/d^3p_3$ for a general $2 \to 3$ (sub)process involving massless particles having momenta

$$p_1 + p_2 \to p_3 + p_4 + p_5, \qquad p_i^2 = 0 \tag{B.6}$$

in terms of which s, t, u and s_2 (or s, v and w) are defined in (3.10).

The total cross section is given by, in n dimensions,

$$\sigma = \frac{F}{2s}\int\frac{d^{n-1}p_3}{(2\pi)^{n-1}2p_{3,0}}\int\frac{d^{n-1}p_5}{(2\pi)^{n-1}2p_{5,0}}\int\frac{d^{n-1}p_4}{(2\pi)^{n-1}2p_{4,0}}|M|^2_{2\to 3}(2\pi)^n\delta^n(p_1+p_2-p_3-p_4-p_5) \tag{B.7}$$

where

$$F = (2^{\#\text{ initial fermions} + \#\text{ final fermions}})/(\#\text{ identical final particles})! \tag{B.8}$$

We note that $|M|^2_{2\to m}$ has dimensions mass$^{4-m(n-2)}$. Using

$$\int\frac{d^{n-1}p}{2p_0} = \int d^n p\,\theta(p_0)\,\delta(p^2 - \overbrace{m^2}^{0}) \tag{B.9}$$

in (B.7) gives, noting $s_2 = 2(p_1+p_2-p_3)\cdot p_5 = 2p_4\cdot p_5$,

$$\begin{aligned}\sigma &= \frac{F}{2s(2\pi)^{2n-3}}\int\frac{d^{n-1}p_3}{2p_{3,0}}\int\frac{d^{n-1}p_5}{2p_{5,0}}\theta(p_{1,0}+p_{2,0}-p_{3,0}-p_{5,0}) \\ &\times \underbrace{\delta[((p_1+p_2)-p_3-p_5)^2]}_{s+t+u-s_2}|M|^2_{2\to 3} \\ &= \frac{F}{2s(2\pi)^{2n-3}}\int\frac{d^{n-1}p_3}{2p_{3,0}}\int\frac{d^{n-1}p_5}{2p_{5,0}}\theta(p_{1,0}+p_{2,0}-p_{3,0}-p_{5,0})|M|^2_{2\to 3}\delta(sv(1-w)-s_2)\end{aligned} \tag{B.10}$$

so

$$\frac{p_{3,0}d\sigma}{d^{n-1}p_3} = \frac{F}{4s(2\pi)^{2n-3}}\int\frac{d^{n-1}p_5}{2p_{5,0}}\theta(p_{1,0}+p_{2,0}-p_{3,0}-p_{5,0})|M|^2_{2\to 3}\delta(sv(1-w)-s_2) \tag{B.11}$$

Now work in a system where $\mathbf{p_5} = -\mathbf{p_4}$ [$(n-1)$-dimensions]. Then

$$s_2 = (p_4 + p_5)^2 = (p_{4,0} + p_{5,0})^2 = (2p_{5,0})^2 = 4p_{5,0}^2 \tag{B.12}$$

so

$$\delta[sv(1-w) - s_2] = \delta[sv(1-w) - 4p_{5,0}^2] = \frac{1}{8p_{5,0}}\delta\left(p_{5,0} - \sqrt{\frac{sv(1-w)}{4}}\right) \tag{B.13}$$

Substituting (B.13) in (B.11) gives

$$\frac{p_{3,0}d\sigma}{d^{n-1}p_3} = \frac{F}{64s(2\pi)^{2n-3}}\left(\frac{sv(1-w)}{4}\right)^{(n-4)/2}\theta[sv(1-w)]\int d^{n-2}\Omega_5|M|^2_{2\to 3}. \tag{B.14}$$

where the θ function now arises since p_5 is only defined for $sv(1-w) > 0$. Since $|M|^2_{2\to 3}$ only depends on the angles θ and φ defined in (B.1), we may trivially integrate over the remaining $n-4$ angles to obtain

$$\int d^{n-2}\Omega_5|M|^2_{2\to 3} = \frac{2^{1-2\varepsilon}}{\pi^\varepsilon}\frac{\Gamma(1-\varepsilon)}{\Gamma(1-2\varepsilon)}\int d\Omega|M|^2_{2\to 3}. \tag{B.15}$$

where

$$\int d\Omega = \int_0^\pi d\theta \sin^{1-2\varepsilon}\theta \int_0^\pi d\varphi \sin^{-2\varepsilon}\varphi. \tag{B.16}$$

Finally, we arrive at, with $E_3 \equiv p_{3,0}$,

$$\frac{E_3 d\sigma}{d^{n-1}p_3} = \frac{F}{64s(2\pi)^{2n-3}}\left(\frac{sv(1-w)}{4}\right)^{-\epsilon}\frac{2^{1-2\epsilon}}{\pi^\epsilon}\frac{\Gamma(1-\varepsilon)}{\Gamma(1-2\varepsilon)}\theta[sv(1-w)]\int d\Omega|M|^2_{2\to 3}. \tag{B.17}$$

Analogously, the $2 \to 2$ phase space, in n dimensions, is given by

$$\begin{aligned}\frac{E_3 d\sigma}{d^{n-1}p_3} &= \frac{F}{4s^2}\frac{1}{(2\pi)^{n-2}}\theta(p_{10}+p_{20}-p_{30})\delta\left(1+\frac{t+u}{s}\right)|M|^2_{2\to 2} \\ &= \frac{F}{4s^2 v}\frac{1}{(2\pi)^{n-2}}\theta(p_{10}+p_{20}-p_{30})\delta(1-w)|M|^2_{2\to 2}.\end{aligned} \tag{B.18}$$

B.2 Coefficients

Here we present the ΔB_{ab} relevant to the Born term (3.30), the coefficients a_1, n relevant to the HOC, Δf, appearing in (3.32), and the overall factor Φ_{ab} relevant to both. Coefficients not given are zero. For the $\vec{q}\vec{q}$ subprocess we have

$$\Phi_{qq} = \frac{1}{4}\alpha\alpha_s c_q^2 C_F, \qquad \Delta B_{qq}(v) = \frac{1}{v} - v. \tag{B.19}$$

Defining

$$Z \equiv 1 - v + vw, \quad \Delta B(v) \equiv \Delta B_{qq}(v), \quad b \equiv (11N_c - 2N_f)/6 \tag{B.20}$$

and using the notation

$$\Delta f_{qq} = C_F \Delta f_{C_F} + N_c \Delta f_{N_c}, \tag{B.21}$$

we have, for Δf_{C_F},

$$\begin{aligned}
a_{1,C_F} &= \left(v + \frac{2}{v}\right)\frac{\pi^2}{3} + 2(1 + v - \pi^2) - \frac{4}{v} - \left(2 - \frac{3}{v}\right)\ln v + \left(2 - \frac{1}{v}\right)(2\ln v \ln(1-v) - \ln^2 v) \\
&\quad + \Delta B(v)\left(\frac{7}{2} - \frac{3}{2}\ln v + \ln^2 v\right) \\
b_{1,C_F} &= \Delta B(v)(2\ln v - 3/2) \\
c_{C_F} &= 2\Delta B(v) \\
a_{2,C_F} &= \Delta B(v)\left(2\ln\frac{v}{1-v} + \frac{3}{2}\right) \\
b_{2,C_F} &= 2\Delta B(v) \\
d_{C_F} &= \frac{2}{w(1-v)} + \frac{3}{w}\left(\frac{1}{v} - 1\right) + \frac{2}{(1-v)Z} - \frac{4}{1-v} + \frac{2v(v-1)}{Z^3} + \frac{2v(1-v)}{Z^2} \\
&\quad + \frac{v^2 - v - 2}{Z} + 2(v - 1/v + 3) \\
e_{C_F} &= d_{C_F} \\
f_{C_F} &= 2\left\{\frac{w}{1-v} - w(1+v) - \frac{1}{w(1-v)} - \frac{1}{wv} - v\right\}
\end{aligned}$$

$$
\begin{aligned}
g_{C_F} &= 2\left\{\frac{1}{w}-\frac{2}{w(1-v)}+\frac{2}{(1-v)Z}+\frac{2v(v-1)}{Z^3}+\frac{2v(1-v)}{Z^2}+\frac{v^2-v-2}{Z}-v\right\}\\
h_{C_F} &= 2\left\{\frac{2}{w(1-v)}+\frac{1}{w}\left(\frac{1}{v}-2\right)-\frac{2}{1-v}+3v+2\right\}\\
i_{C_F} &= 2\left\{-\frac{w}{1-v}+w(1+v)+\frac{1}{w}\left(\frac{1}{v}-1\right)+v\right\}\\
j_{C_F} &= d_{C_F}+2\left\{\frac{w}{1-v}-w(1+v)+\frac{1}{w(1-v)}-\frac{2}{w}+\frac{2}{1-v}+2(1+v)\right\}\\
k_{C_F} &= -\frac{1}{2w}\left(\frac{1}{v}+1\right)+\frac{1}{(1-v)Z}+6\frac{v(1-v)}{Z^3}-5\frac{v(1-v)}{Z^2}+\frac{3v^2-2v-1}{Z}\\
&\quad +v+\frac{3}{v}-6\\
l_{C_F} &= 2(v-2), \qquad m_{C_F}=2\left(\frac{1}{v}-2\right), \qquad n_{C_F}=-2\Delta B(v).
\end{aligned}
$$

For Δf_{N_c}, we have

$$
\begin{aligned}
a_{1,N_c} &= \left(\frac{1}{2}\ln^2(1-v)-2\right)\Delta B(v)+\left(1-\frac{v}{2}\right)(\pi^2+\ln^2 v)+\ln v\\
&+ (v-2)\ln v\ln(1-v)-\frac{b}{N_c}\ln\frac{s}{\mu^2}\Delta B(v)\\
b_{1,N_c} &= 2\Delta B(v)\ln\frac{v}{1-v}\\
c_{N_c} &= 4\Delta B(v)\\
a_{2,N_c} &= b\Delta B(v)/N_c\\
b_{2,N_c} &= 2\Delta B(v)\\
d_{N_c} &= \frac{4}{w(1-v)}+\frac{2}{w}(2\Delta B(v)-v-1)-\frac{4}{(1-v)Z}-\frac{2v}{Z^2}+\frac{2(v+2)}{Z}+v-4\Delta B(v)\\
e_{N_c} &= d_{N_c}\\
f_{N_c} &= -(\Delta B(v)+v-2)\frac{1}{w}\\
g_{N_c} &= \frac{8}{w(1-v)}-\frac{1}{w}(\Delta B(v)+4)-\frac{8}{(1-v)Z}-\frac{4v}{Z^2}+\frac{4(v+2)}{Z}\\
h_{N_c} &= -\left(\frac{1}{w}\Delta B(v)+3v\right)\\
i_{N_c} &= -2vw+\frac{2}{w}(\Delta B(v)-2v)+3v\\
j_{N_c} &= d_{N_c}+2vw+\frac{1}{w}(2-v)-v
\end{aligned}
$$

$$
\begin{aligned}
k_{N_c} &= 9 - \frac{1}{vw} + \frac{3}{v} + \frac{6v}{w} + \frac{4v}{Z^2} - \frac{2v}{Z} - 7v - \frac{2}{w(1-v)} - \frac{5}{w} \\
&\quad + \frac{2}{Z(1-v)} - \frac{2}{Z} \\
l_{N_c} &= -(\Delta B(v) + v - 2), \qquad m_{N_c} = 2 - v, \qquad n_{N_c} = -\Delta B(v)
\end{aligned}
$$

For the $\bar{q}_\alpha \bar{q}_\beta$ subprocess, we have

$$
\Phi_{q_\alpha q_\beta} = \frac{1}{2}\alpha\alpha_s \frac{C_F}{N_c}, \qquad \Delta B_{q_\alpha q_\beta} = 0. \tag{B.22}
$$

Using the notation

$$
\Delta f_{q_\alpha q_\beta} = v\{\Delta f_1 + \delta_{\alpha\beta}(\Delta f_1 - \frac{e_\alpha^2}{3}\Delta f_2)\}(1 - \delta_{\alpha\beta}/2), \tag{B.23}
$$

and defining

$$
\begin{aligned}
Q &\equiv 1 + v - vw, \quad G_1 \equiv 4\frac{1-vw}{1-v} - 2, \quad G_2 \equiv \frac{4}{w} - 2 \\
G_3 &\equiv 4\left[\frac{1-v}{vw} + \frac{2v(1-w)^2}{w(1-v)} + \frac{2v(1-w)}{1-v} + \frac{vw}{1-v} + \frac{2(1-w)}{w} + 2\right] \\
G_4 &\equiv 4\left[\frac{1-3v^2w - v^3(1+w^3)}{v^2w(1-v)(1-vw)Z} - \frac{(1+w) - v(1-w)^2}{vw(1-v)(1-vw)Z} + \frac{v(1+w)+3}{(1-v)(1-vw)Z}\right]
\end{aligned}
$$

we get for Δf_1

$$
\begin{aligned}
d_1 &= e_\alpha^2\left\{\frac{1+v-2vw}{1-v}\left[\frac{1}{(1-vw)^2} - 1\right] + \frac{2-ZQ}{Z^2}\left(1 + \frac{2vw}{1-v}\right)\right\} \\
&\quad + e_\beta^2\left\{\frac{2-w}{w}\left(\frac{1}{v^2} - 1\right) + \frac{2-ZQ}{Z^2}\left(1 + \frac{2(1-v)}{vw}\right)\right\} \\
e_1 &= e_\alpha e_\beta \frac{4(2-vw)}{(1-v)Z} \\
f_1 &= e_\alpha^2 G_1 + e_\alpha e_\beta \frac{-2Q}{vw(1-v)} \\
g_1 &= e_\alpha^2 G_1 + e_\alpha e_\beta \frac{-4Q}{vw(1-v)} + e_\beta^2 G_2 \\
h_1 &= -G_1 e_\alpha^2 + e_\alpha e_\beta \frac{4(1-v)Q}{vw(1-v)Z} \\
i_1 &= -e_\beta^2 G_2 + e_\alpha e_\beta \frac{4Q}{(1-v)Z}
\end{aligned}
$$

$$
\begin{aligned}
j_1 &= e_\alpha e_\beta \cdot 2\left\{\frac{2}{Z}+\frac{Q}{vw(1-v)}\right\} \\
k_1 &= e_\alpha^2\left\{\frac{1}{(1-vw)^2}\left[1-\frac{v^2w(1-w)}{1-v}\right]-\frac{2v^2w(1-w)}{(1-v)Z^2}-\frac{2}{1-v}+\frac{2}{Z^2}\right\} \\
&+ e_\beta^2\left\{-\frac{2(1-v)(1-w)}{wZ^2}-\frac{(1-v)(1-w)}{v^2w}+\frac{2}{Z^2}-\frac{2}{vw}+\frac{1}{v^2}\right\} \\
&+ e_\alpha e_\beta\left\{-\frac{2(1-v)}{vwZ^2}-\frac{1}{v}+\frac{1-w}{w(1-v)(1-vw)}+\frac{1-w}{vw(1-v)}\right. \\
&\left.-\frac{2vw}{(1-v)Z^2}+\frac{1}{1-v}+\frac{4v(1-w)}{Z^2}-\frac{1}{1-vw}+\frac{1}{vw}\right\}.
\end{aligned}
$$

For Δf_2, the result is simply

$$
\begin{aligned}
d_2 &= 4\frac{2-ZQ}{vw(1-v)}, \qquad e_2 = 8\frac{2-ZQ}{(1-v)(1-vw)Z}, \qquad f_2 = 0 \\
g_2 &= -2G_3, \qquad h_2 = G_3+G_4, \qquad i_2 = G_3-G_4 \\
j_2 &= -G_3+G_4+c_2, \qquad k_2 = 0.
\end{aligned}
$$

We note that $\Delta f_{qq}/v$ is symmetric under $1-v \leftrightarrow vw$ (i.e. $t \leftrightarrow u$ or $p_1 \leftrightarrow p_2$); the part $\sim c_\beta^2$ follows from the part $\sim e_\alpha^2$ and the part $\sim e_\alpha e_\beta$ is invariant. This is required by the fact that $e_\alpha \leftrightarrow e_\beta$ is equivalent to $p_1 \leftrightarrow p_2$ in $\Delta|M|^2_{2\to 3}$ and that $\Delta f/v \sim \int d\Omega \Delta|M|^2_{2\to 3}$.

For the $\bar{g}\bar{g}$ subprocess, we have

$$
\Phi_{gg} = \frac{\alpha\alpha_s e_q^2}{8}, \qquad \Delta B_{gg}(v) = 0. \tag{B.24}
$$

Defining

$$
\begin{aligned}
y &= 1-vw, \quad H_1 = 2\left\{\frac{v^3(1-w)^3}{yZ}+\frac{v^2(1+2w^2)}{wyZ}-\frac{v^2[2+(1-w)^2]}{yZ}-\frac{1}{y}\right\} \\
H_2 &= 2\left\{\frac{2}{vwy}-\frac{v}{y}-\frac{v}{1-v}-\frac{(1-v)(1+vw)}{wy}\right\}, \quad H_3 = 2\left\{\frac{-v^2}{yZ}+\frac{v}{(1-v)Z}\right\} \\
H_4 &= 2\left\{\frac{-2}{vw}-\frac{Z}{1-v}+\frac{v}{1-v}\right\}, \quad H_5 = 2\left\{\frac{v}{wZ}-\frac{2}{Z}+y\right\} \\
H_6 &= 2\left\{\frac{2-v}{Z}+\frac{v^2(1-w)}{(1-v)Z}-\frac{y}{1-v}\right\}
\end{aligned}
$$

and using the notation

$$\Delta f_{gg} = C_F \Delta f_{C_F} + N_c \Delta f_{N_c}, \tag{B.25}$$

we have, for Δf_{C_F},

$$\begin{aligned}
d_{C_F} &= -\frac{v}{Z^2}[1+v^2(1-w)^2]\left[\frac{1-v}{vw}+\frac{vw}{1-v}\right] \\
&+ v(2-1/w)[1+1/(1-v)]+v[2-y/(1-v)](1+1/vw) \\
c_{C_F} &= 4\left\{\frac{v(2-v)-2}{wyZ}+\frac{2}{w}\right\} \\
f_{C_F} &= H_1+H_2+H_3+H_4 \\
g_{C_F} &= -\frac{c}{2}+H_3+H_5+H_6+2\left\{\frac{1}{w}-\frac{v(1-v)}{y}\right\} \\
h_{C_F} &= -H_2-H_3-H_4-H_6 \\
i_{C_F} &= \frac{c}{2}-H_4-H_5+2\left\{-\frac{1+(1-v)^2}{vwy}-\frac{2}{w}+\frac{v}{1-v}\right\} \\
j_{C_F} &= -H_1-H_6, \qquad k_{C_F} = -\frac{w}{1-v}+w(1+v)+\frac{v-1}{w} \\
k_{C_F}(DRED) &= 0.
\end{aligned}$$

Define

$$\begin{aligned}
H_1' &= 2\left\{-\frac{(1-v)^2+v^2w^2}{y}+\frac{v[1+(1-v)^2]}{yZ}-4v\right\} \\
H_2' &= 2\left\{-\frac{1-v}{wy}-\frac{2v(1+vw)}{1-v}\right\} \\
H_3' &= 2\left\{-\frac{v(1-v)}{y}+\frac{1-v}{w}+\frac{2v^4w^2(1-w)}{(1-v)yZ}+\frac{v^2wy}{(1-v)Z}\right\} \\
H_4' &= 2\left\{\frac{2vw}{y}+v\frac{1+vw}{1-v}+y\right\}, \quad H_5' = 2\left\{-(1-v)\frac{2-v}{wZ}-\frac{2}{Z}+y\right. \\
&- \left.\frac{v(1+vw)}{1-v}-\frac{1}{wy}\right\}, \quad H_6' = 2\left\{\frac{2(1-v)+v(1+w)+v^2w^2}{Z}-1-2v\right\}.
\end{aligned}$$

Then for Δf_{N_c}, we have

$$d_{N_c} = \frac{v}{Z^4}[1+v^2(1-w)^2][(1-v)^2+v^2w^2]$$

$$
\begin{aligned}
c_{N_c} &= -\frac{1}{2}\left\{c_{C_F} + 4\left[\frac{y}{wZ} - \frac{v(1-v)}{wZ} - \frac{1}{w} + 2v\right]\right\} \\
f_{N_c} &= v - \frac{1}{2}\{H_1' + H_2' + H_3' + H_4'\} \\
g_{N_c} &= 2v - \frac{1}{2}\left\{c_{N_c} + H_3' + H_5' + H_6' + \frac{4}{wy}\right\} \\
h_{N_c} &= -v - \frac{1}{2}\{-H_2' - H_3' - H_4' - H_6'\} \\
i_{N_c} &= -v - \frac{1}{2}\left\{-c_{N_c} - H_4' - H_5' + 2\left[-2\frac{1-v}{w} + \frac{1-v}{wy} - \frac{2}{w}\right]\right\} \\
j_{N_c} &= -\frac{1}{2}\{-H_1' - H_6'\} \\
k_{N_c} &= w(2-v) - 1 - v - \frac{v(2-v)}{y} \\
&+ \frac{2v(1-v)}{y^2} + \frac{2v}{Z} - \frac{2v(7-6v)}{Z^2} + \frac{12v(2-3v+v^2)}{Z^3} - \frac{12v(1-v)^2}{Z^4} \\
k_{N_c}(DRED) &= 2v\left\{-2 + \frac{v}{Z^3}[-(3w^2 - w + 3)(1-w)v^2 - (w^2 + 4w - 4)v \right. \\
&\left. + (2w-1)] - 3\frac{v^2(1-w)^2[(1-v)^2 + v^2w^2]}{Z^4}\right\}.
\end{aligned}
$$

For this subprocess, we have also given the analytical result for DRED, which only differs in the coefficient, k.

We have checked explicitly that $\Delta f_{gg}/v$ is symmetric under $1 - v \leftrightarrow vw$, as it must be since we have two gluons in the initial state. One can readily verify that the coefficients d/v, g/v and k/v are individually symmetric under $1 - v \leftrightarrow vw$, as is necessary.

B.3 Reduction Formulas

Here we give, in the form of a theorem, the reduction formulas necessary to reduce the ratios of products of dot-products arising from the traces into a form suitable for integration via the $2 \to 3$ particle phase space (B.17). In short, we express the dot-products occurring in the numerators in terms of those in the denominators using

the relations given below.

Theorem: Suppose we have 5 four-vectors satisfying $p_1 + p_2 = q + r + k$ and $p_1^2 = p_2^2 = q^2 = r^2 = k^2 = 0$ (for direct photon production, we identify $q = p_3$, $r = p_4$, $k = p_5$). All relations expressing a dot product as a linear combination of three others (there must be *at least* 3) belong to the set

$$\begin{aligned}
\mathcal{R} \;=\; & \{\ [p_1 \cdot (p_1 + p_2 = q + k + r), p_1^2 = 0] && \text{(A)}\\
& \cup\ [p_2 \cdot (\ldots), p_2^2 = 0]\ \cup\ \ldots\ \cup\ [r \cdot (\ldots), r^2 = 0] \\
& \cup\ p_1 \cdot p_2 = q \cdot k + q \cdot r + k \cdot r && \text{(B)}\\
& \cup\ p_1 \cdot p_2 = p_1 \cdot k_a + p_2 \cdot k_a + k_b \cdot k_c; \quad a \neq b, c; \quad k_? \in \{q, r, k\} && \text{(C)}\\
& \cup\ [k_a \cdot k_b = p_1 \cdot k_a + p_1 \cdot k_b - p_2 \cdot k_c; \quad c \neq a, b; && \text{(D)}\\
& \quad k_? \in \{q, r, k\};\ \cup\ (p_1 \leftrightarrow p_2)]\ \}
\end{aligned}$$

(*Note:* Classes (B), (C) and (D) all follow from $(a + b)^2 = (c + d + e)^2$, therefore under $\pm(p/k)_i \leftrightarrow \pm(p/k)_j$, $\{(B),(C),(D)\} \leftrightarrow \{(B),(C),(D)\}$). This may be proved by considering all possible relations and eliminating the ones which lead to contradiction.

Corollary I: Applying the interchanges $p_i \leftrightarrow p_j$, $k_i \leftrightarrow k_j$, $p_i \leftrightarrow -k_j$ to relations which are members of $\mathcal{R}$ yields relations which are members of $\mathcal{R}$, (this is verified by inspection) since these interchanges leave our defining equations: $\sum_i p_i = \sum_i k_i$, $p_i^2 = k_i^2 = 0$ unchanged.

Corollary II: All relations involve s, t, u, or $2k \cdot r \equiv s_2 = s + t + u$ (this is verified by inspection).

Corollary III: There are no other relations (involving 4 dot products) than those listed below.

Class A:

$$p_1 \cdot p_2 = p_1 \cdot q + p_1 \cdot k + p_1 \cdot r \quad \rightarrow \quad s + t = 2p_1 \cdot k + 2p_1 \cdot r \tag{B.i}$$

$$p_2 \cdot p_1 = p_2 \cdot q + p_2 \cdot k + p_2 \cdot r \quad \rightarrow \quad s + u = 2p_2 \cdot k + 2p_2 \cdot r \tag{B.ii}$$

$$p_1 \cdot q + p_2 \cdot q = k \cdot q + r \cdot q \quad \rightarrow \quad -t - u = 2k \cdot q + 2r \cdot q \tag{B.iii}$$

$$p_1 \cdot k + p_2 \cdot k = q \cdot k + r \cdot k \quad \rightarrow \quad s_2 = 2p_1 \cdot k + 2p_2 \cdot k - 2q \cdot k \tag{B.iv}$$

$$p_1 \cdot r + p_2 \cdot r = q \cdot r + k \cdot r \quad \rightarrow \quad s_2 = 2p_1 \cdot r + 2p_2 \cdot r - 2q \cdot r \tag{B.v}$$

Class B:

$$p_1 \cdot p_2 = q \cdot k + q \cdot r + k \cdot r \rightarrow s - s_2 = 2q \cdot k + 2q \cdot r \tag{B.vi}$$

Class C:

$$p_1 \cdot p_2 = p_1 \cdot q + p_2 \cdot q + k \cdot r \quad \rightarrow \quad s_2 = s + t + u \tag{B.vii}$$

$$p_1 \cdot p_2 = p_1 \cdot k + p_2 \cdot k + q \cdot r \quad \rightarrow \quad s = 2p_1 \cdot k + 2p_2 \cdot k + 2q \cdot r \tag{B.viii}$$

$$p_1 \cdot p_2 = p_1 \cdot r + p_2 \cdot r + q \cdot k \quad \rightarrow \quad s = 2p_1 \cdot r + 2p_2 \cdot r + 2q \cdot k \tag{B.ix}$$

Class D:

$$k \cdot r = p_1 \cdot k + p_1 \cdot r - p_2 \cdot q \quad \rightarrow \quad s_2 - u = 2p_1 \cdot k + 2p_1 \cdot r \tag{B.x}$$

$$k \cdot r = p_2 \cdot k + p_2 \cdot r - p_1 \cdot q \quad \rightarrow \quad s_2 - t = 2p_2 \cdot k + 2p_2 \cdot r \tag{B.xi}$$

$$q \cdot r = p_1 \cdot q + p_1 \cdot r - p_2 \cdot k \quad \rightarrow \quad t = 2p_1 \cdot r - 2p_2 \cdot k - 2q \cdot r \tag{B.xii}$$

$$q \cdot r = p_2 \cdot q + p_2 \cdot r - p_1 \cdot k \quad \rightarrow \quad u = 2p_2 \cdot r - 2p_1 \cdot k - 2q \cdot r \tag{B.xiii}$$

$$q \cdot k = p_1 \cdot q + p_1 \cdot k - p_2 \cdot r \quad \rightarrow \quad t = 2p_1 \cdot k - 2p_2 \cdot r - 2q \cdot k \tag{B.xiv}$$

$$q \cdot k = p_2 \cdot q + p_2 \cdot k - p_1 \cdot r \quad \rightarrow \quad u = 2p_2 \cdot k - 2p_1 \cdot r - 2q \cdot k \tag{B.xv}$$

Note: Only 6 of these are *independent* (i.e. (B.i) - (B.v) and any of (B.vi) - (B.xv)) as can be shown.

Note: There are 10 possible dot products. A general relation has the form $\alpha a \cdot b + \beta c \cdot d + \gamma e \cdot f + \delta g \cdot h = 0$. Therefore we can form 210 $(= 10 \times 9 \times 8 \times 7/4!)$ such relations (assuming a unique solution for any permutation of dot products). We see that there are only 15 such relations not having solution $\alpha = \beta = \gamma = \delta = 0$ and each relation has a unique solution having the form $\alpha = \pm\beta = \pm\gamma = \pm\delta$.

Appendix C

Heavy Quark Production Details

C.1 Momentum Parameterizations

Here we present the momentum parameterizations in the frame where p_4 and k are back-to-back. We find

$$\begin{aligned} p_1 &= (\omega_1; 0, \cdots, |\mathbf{p}| \sin\psi, |\mathbf{p}| \cos\psi - \omega_2), \\ p_2 &= (\omega_2; 0, \cdots, 0, \omega_2), \\ k &= (\omega_k; \cdots, \omega_k \sin\theta_1 \cos\theta_2, \omega_k \cos\theta_1), \\ p_4 &= (E_4; \cdots, -\omega_k \sin\theta_1 \cos\theta_2, -\omega_k \cos\theta_1), \\ p_3 &= (E_3; 0, \cdots, |\mathbf{p}| \sin\psi, |\mathbf{p}| \cos\psi). \end{aligned} \tag{C.1}$$

where

$$\begin{aligned} \omega_1 &= \frac{s+t}{2\sqrt{S_2}}, \quad \omega_2 = \frac{s+u}{2\sqrt{S_2}}, \quad \omega_k = \frac{s_2}{2\sqrt{S_2}}, \quad E_4 = \frac{s_2+2m^2}{2\sqrt{S_2}} \\ E_3 &= -\frac{T+U}{2\sqrt{S_2}}, \quad |\mathbf{p}| = \frac{\bar{y}}{2\sqrt{S_2}}, \quad \cos\psi = \frac{us_2 - s(t+2m^2)}{(s+u)\bar{y}} \end{aligned} \tag{C.2}$$

in agreement with Ref. 81. For p_1, p_2, p_3 the dots represent zeros. For k, p_4 they represent components which depend on the remaining $n-4$ angles of k. Since these components do not contribute to $[\Delta]|M|^2_{2\to 3}$, those angles were trivially integrated over in the phase space (5.24).

C.2 Coefficients

In this appendix we list the coefficients for the various cross sections. For $\Delta d\sigma_{\rm vse}/dvdw$ given in Eq. 5.15, the coefficients ΔA_i are

$$\begin{aligned}
\Delta A_1 &= 2[-1 - u/s + u^2/st + m^2 s/tu - 2m^2 u/t^2] \\
\Delta A_2 &= -4[4(6u/t - 4s/u - t/T)m^2/t - 4sT/t^2 - 16s/t + 24u/s + s/T + 4tu/sT]m^2/T \\
\Delta A_3 &= 16[(7s/t + 3 - 3t/u)m^4/t^2 + (4u^2/st + 2t/s - s^2/tu)m^2/t + t/s + u^2/st] \\
\Delta A_4 &= 4[4m^2 u/t^2 - 3s/t + 4u/s]m^2/T
\end{aligned} \tag{C.3}$$

For $d\sigma_{\rm vse}/dvdw$ given in Eq. 5.15, the coefficients A_i are

$$\begin{aligned}
A_1 &= 2[u/t - 2m^2/t + sm^2/tu - 4m^4/tu - 4m^4/t^2] \\
A_2 &= 4[4(12sT/t^2 + t/T + 6)m^4/uT + (s^2/uT - 4s^2/tu - 4s^2T/t^2u \\
&\quad - 12s/t - 2t/T - 8)m^2/T - 4] \\
A_3 &= 16[12m^6 s/t^3 u + (s/t - 14 - 8t/u)m^4/t^2 - (3s/t + 7 + t/u)m^2/t + u/t] \\
A_4 &= -4[4(2s/t + t/T)m^4/tu + (t/T - 4)m^2 s^2/t^2 u + 2t/T - 4]
\end{aligned} \tag{C.4}$$

We note that

$$[\Delta]A_1 + (t \leftrightarrow u) = (2m)^2[\Delta]|M|^2_{\rm LO}/(N_c e^4 c_Q^4 t^{4\epsilon}). \tag{C.5}$$

For $\Delta d\sigma_{\rm box}/dvdw$ given in Eq. 5.21, the coefficients ΔB_i are

$$\begin{aligned}
\Delta B_1 &= \Delta A_1 \\
\Delta B_2 &= 4(s + 4t)m^4/stu + 2(s/u + 4u/s)m^2/s - s^2/tu - 2s/u + t/u - 4u/s \\
\Delta B_3 &= 12m^4/tu + 2m^2(t - u)/tu - s^2/tu - t/u \\
\Delta B_4 &= [8(t - u)/s - 3s/t - s/u]m^2/s + 5u/s - t/s \\
\Delta B_5 &= 4sT/tu + (t/u - 1)m^2 t^2/sT^2 + 4(s^2 - 2t^2)/st - 7tu/sT + t^2(s - 3t)/sTu
\end{aligned}$$

$$\Delta B_6 = 2(s/t-4)m^4/tu - 2m^2(t-u)/tu + s^2/tu + t/u \qquad \text{(C.6)}$$

$$\Delta B_7 = 4(u-4t)m^4/t^2u + 2m^2(u-t)/tu + s^2/tu + t/u; \quad \Delta B_8 = (1+t^2/Ts)(t/u-1)$$

For $d\sigma_{\rm box}/dvdw$ given in Eq. 5.21, the coefficients B_i are

$$B_1 = A_1; \quad B_2 = (2m^2-s)[(2m^2-u)/st - 2/u] - 2m^2(6m^2+t)/su$$

$$B_3 = -4m^4/tu + 2m^2(u-t)/tu + s^2/tu + t/u; \quad B_4 = -2m^2s/tu + 2$$

$$B_5 = 2[(2m^2+s)(2s/t + t/T) - t^3/T^2]/u; \quad B_6 = 8m^4/tu + 2m^2/u - s^2/tu - t/u$$

$$B_7 = -4m^4/tu + 2m^2(t-3u)/tu - s^2/tu - t/u; \quad B_8 = 2(s+t^2/T)/u \qquad \text{(C.7)}$$

For $\Delta|M|^2_{2\to3}$ given in Eq. 5.23 and $\Delta d\sigma_{\rm Br}/dvdw$ given in Eq. 5.27, the coefficients Δc_i are

$$\begin{aligned}
\Delta\tilde{c}_1 &= -16(s/u - s/t - 2)m^4/u - 4[s_2(2 + 2s/u - t/s + u/s + 2t^2/s^2 + 8tu/s^2) + 2s \\
&- 4tu/s]m^2/u + s_2(4s/u - 4 - 8t^2/su - 5t/s) \\
\Delta c_2 &= -4[2m^2(2/s_2u + 2/s_2t + 1/s^2 - u/s^2t) + 6/t - t/s^2 + u^2/s^2t]/u \\
\Delta c_3 &= -2[8m^4(1/tu - 1/s_2u - s/s_2t^2) - 2(4s/s_2 + s/t - 1)m^2/t - 3s/u - 5s/t \\
&- (2s^3/tu - su/t + 3t + 2u + u^2/t)/s_2] \\
\Delta c_4 &= -2(2m^2s/t + 2s + u)m^2/t; \quad \Delta e_5 = 0 \\
\Delta\tilde{c}_6 &= [32m^4/u - 4m^2(t/u + 5 + t^2/su + 5t/s + 2t^3/s^2u + 10t^2/s^2 + 8tu/s^2) \\
&+ 4st/u - 16t - 8t^2s_2/su - 5ts_2/s]/2; \quad \Delta\tilde{e}_7 = -2m^2 \\
\Delta e_8 &= 4m^4(s/tu + 2/u + 1/s) - 2m^2(s^2/tu + 2s_2/u - 1 + t/s) - (s^2/t + s + 3s_2 \\
&+ t^2/s + 3tu/s)s/u; \quad \Delta e_9 = 8(1/u - 1/s_2)/t \\
\Delta e_{10} &= 4[2(1/u + 2s/s_2t - 2/s_2)m^2/u + s_2/tu - 3/s_2 - u/ts_2] \\
\Delta\tilde{e}_{11} &= 8m^4(s/t + t/u + s_2/s) - 2m^2[2s^2/u + 2s^2/t + s + s_2(2t/u + 2 + 4u/t + t/s + u/s)] \\
&- (s^2+t^2)(t+u)/u; \quad \Delta\tilde{e}_{12} = m^2s; \quad \Delta e_{13} = -m^2(4m^2s/t + 2s + u)
\end{aligned}$$

$$\Delta\tilde{c}_{14} = -m^4 s; \quad \Delta c_{15} = 4[2m^2/u - 2m^2/t - t/u + u/t]/s^2 \tag{C.8}$$

$$\Delta c_{16} = a_1 + a_1(t \leftrightarrow u) - 8(m^2 + m^2 t/s - t)/su + 2[t^2(t/u + 2) - u^2(u/t + 2)]/s^2 s_2$$

where

$$a_1 = t[4m^2(7s/t + 1 + 3t/s + 9u/s) - 2s + 6su/t + 4t + u]/s_2 us \tag{C.9}$$

For $|M|^2_{2\to 3}$ given in Eq. 5.23 and $d\sigma_{\rm Br}/dvdw$ given in Eq. 5.27, the coefficients c_i are

$$\begin{aligned}
\tilde{c}_1 &= 2[16m^6(t+u)/tu + 16m^4(s_2/u + s/t + 3) + 2m^2(25s_2 - 2t + 2s_2^2/u) \\
&+ s_2(2s + 5t + 10u)]/u; \quad c_2 = -8[2m^2(t+u)/s_2 t + 3]/tu \\
e_3 &= -2[16m^6(t+u)/s_2 tu + 8(4 + u/t - 2s/s_2)m^4/u + 2m^2(6t/u + 6 - u/t - s/t + s/s_2) \\
&- 2s^2/u - 3st/u - 2s - s_2 + 3st/s_2 - 2t^3/s_2 u]/t \\
e_4 &= 2m^2(2m^2/t + 1)^2; \quad c_5 = -4m^2/u \\
\tilde{e}_6 &= -16m^4/u + 2m^2(5s/u + 7t/u + 11) + t(4s/t - s/u + t/u + 17); \quad \tilde{c}_7 = 2m^2 \\
e_8 &= 8m^6(s/t + 2 + u/s)/su + 4(3s/t + 4 + 2s_2/s)m^4/u + 2m^2(s_2/u - 2 - t/s) \\
&- (s^2/t + s + 3s_2 + t^2/s + 3tu/s)s/u; \quad c_9 = 8(s_2 + u)/ts_2 u \\
e_{10} &= -4[8m^4/u + 2m^2(s/u + 2) - s_2^2/u + 4s + t + 3u]/ts_2 \\
\tilde{e}_{11} &= 16m^6[(t+u)^2/tu + s_2/s]/s + 8m^4[(s-t)/u + t^2/su + 3(t+u)/s + u^2/st] \\
&+ 2m^2[u(s+u)/t + t(t+u)/s - ts_2/u - 7s_2 - 2ts_2/s - us_2/s] + (s^2 + t^2)(t+u)/u \\
\tilde{e}_{12} &= m^2(8m^4/s - 4m^2 - s); \quad e_{13} = m^2(8m^4/t + 4m^2 - t); \quad \tilde{e}_{14} = 2m^6; \quad e_{15} = 0 \\
e_{16} &= -2[22m^2(t+u)/tu + 3t/u + 14 + u/t]/s_2
\end{aligned} \tag{C.10}$$

C.3 Bremsstrahlung Integrals

We give here the bremsstrahlung integrals, I_i, appearing in Eq. (5.27). They are defined as

$$I_i = \frac{1}{2\pi}\int d\Omega f_i : \qquad (2m)^2[\Delta]|M|^2_{2\to 3} \equiv C\sum_i [\Delta]c_i f_i/s_2^{n_i} \tag{C.11}$$

(see (5.23)). The f_i may be explicitly expressed as functions of θ_1 and θ_2 using the expressions in Appendix A. All the integrals here are 4-dimensional (i.e. $\varepsilon = 0$ in (5.26)) and are determined using the general forms given in Ref. 81.

First we list the four basic integrals.

$$\begin{aligned}
I_6 &= \frac{2S_2}{s_2\bar{y}}\ln\frac{T+U-\bar{y}}{T+U+\bar{y}}, \qquad I_6' \equiv \frac{2S_2}{s_2(s+t)}\ln\frac{S_2}{m^2} \\
I_8 &= \frac{4S_2}{s_2\sqrt{s}}\frac{1}{\sqrt{x_8}}\ln\frac{x_8+s_2^2 s+2s_2\sqrt{sx_8}}{x_8+s_2^2 s-2s_2\sqrt{sx_8}}, \quad x_8 \equiv 4m^2(s_2 s+tu)+s_2^2 s \\
I_{11} &= \frac{4S_2}{s_2\sqrt{stx_{11}}}\ln\frac{x_{11}+st-2\sqrt{stx_{11}}}{x_{11}+st+2\sqrt{stx_{11}}}, \quad x_{11} \equiv 4m^2(s_2-t)+st
\end{aligned} \tag{C.12}$$

Define,

$$z_1 \equiv 2m^2 s+s_2 s-tu, \quad z_2 \equiv s_2 u-2m^2 s-st, \quad z_3 \equiv m^2 s-tu, \quad z_4 \equiv 2m^2 s-tu, \quad z_5 \equiv 2m^2+t \tag{C.13}$$

We may now express the remaining integrals in terms of those listed above:

$$\begin{aligned}
I_5 &= -\frac{2S_2 z_4}{m^2(s+t)^3}+\frac{I_6' z_1}{(s+t)^2} \\
I_9 &= \frac{1}{4S_2(s+t)^3}\{2z_1(s_2-t)(s+t)s_2-(z_1^2+2z_3 S_2 s)(2m^2+s_2)\}+\frac{I_6'}{4(s+t)^2}(z_4^2+2m^2 s z_3) \\
I_{10} &= \frac{z_1}{(s+t)^2}-\frac{I_6' z_4}{2(s+t)}; \quad I_{12} = \frac{8S_2}{m^2 s_2 t}\left(\frac{z_5}{x_{11}}-\frac{1}{s_2}\right)-2I_{11}\frac{z_5(s_2-t)}{x_{11}t} \\
I_{13} &= -\frac{8S_2 z_5}{x_{11}(s_2-t)m^2 t}-2\frac{I_{11}}{t}\left(1-\frac{s_2 z_5}{x_{11}}\right) \\
I_{14} &= \frac{16S_2}{stx_{11}}\left(\frac{12z_3}{x_{11}t}+\frac{\bar{y}^2+s_2^2}{s_2^2 m^2}\right)-\frac{4I_{11}}{x_{11}st}\{s_2 u-sz_5-3z_5(s_2-t)\frac{s}{t}\left(1-\frac{s_2 z_5}{x_{11}}\right)\}
\end{aligned}$$

$$
\begin{aligned}
I_{15} &= \frac{s_2}{4S_2\bar{y}^4}\{(z_2^2+2S_2sz_3)(U+T)+2\bar{y}^2z_2(s_2-t)\}+\frac{I_6s_2^2}{4y^4}\{(z_4-u^2)^2+2m^2sz_3\} \\
I_{16} &= \frac{z_2}{\bar{y}^2}-\frac{I_6s_2(z_4-u^2)}{2\bar{y}^2}
\end{aligned}
\tag{C.14}
$$

The integrals were put into the above form using REDUCE. The integrals not listed here (including the n-dimensional ones not given in Ref. 81) are straightforward and have been substituted directly in (5.27). As an aside, we point out that $x_{11}(t \rightarrow u)$ vanishes for $v = 1/2$, $w = w_1$. Hence one must avoid reaching *exactly* the lower bound (as for the upper) of the w integral, in numerical calculations.

Appendix D

Dimensional Reduction Counterterms

In this appendix we derive the DRED counterterm which must be added to the electron-photon vertex at the 1-loop level, then we generalize to the quark-photon and quark-Z vertices. This counterterm is necessary in order that the vertex have the correct Lorentz structure, as we will show in the next section. Having added the counterterm, we will show that the QED Ward identity is satisfied and also that the correct value for the anomalous magnetic moment results.

D.1 The Fermion-Photon Vertex

Let us consider the scattering of an electron off a static external field as shown in Fig D.1. The Born amplitude is

$$M_0 = -ie\mu^\varepsilon \bar{u}(p_2)\gamma^\mu u(p_1)A_\mu(q) \tag{D.1}$$

where $A^\mu(q)$ represents a static external electromagnetic field (actually, its Fourier transform, evaluated at $q = p_2 - p_1$). We will take the limit $p_2 = p_1$ at the end.

Making use of the Gordon identity

$$\bar{u}(p_2)(p_2 + p_1)^\mu u(p_1) = \bar{u}(p_2)[2m\gamma^\mu - i\sigma^{\mu\nu}(p_2 - p_1)_\nu]u(p_1) \tag{D.2}$$

Figure D.1: The scattering of an electron off an external field: (a) leading order graph, M_0; (b) one-loop vertex correction, M_V.

where

$$\sigma^{\mu\nu} \equiv \frac{i}{2}(\gamma^\mu\gamma^\nu - \gamma^\nu\gamma^\mu), \qquad p_1^2 = p_2^2 = m^2 \tag{D.3}$$

as well as Lorentz covariance and the Lorentz (axial) gauge condition

$$q \cdot A(q) = 0 \tag{D.4}$$

we see that the most general form for the corrected amplitude is, to all orders in DRED,

$$\begin{aligned} M_V &= -ie\mu^\varepsilon \bar{u}(p_2)\left\{\gamma^\mu F_1(q^2) + \gamma_\varepsilon^\mu \hat{F}_1(q^2) + \frac{i}{2m}\sigma^{\mu\nu}q_\nu F_2(q^2)\right\} u(p_1) A_\mu(q) \\ &\equiv -ie\mu^\varepsilon \bar{u}(p_2)\Lambda^\mu(p_2,p_1)u(p_1)A_\mu(q). \end{aligned} \tag{D.5}$$

The term $\sim \gamma_\varepsilon^\mu$ is possible in DRED because the momenta are in n dimensions and the gamma matrices are in 4 dimensions. But since virtual-loop integrations produce the term $g_n^{\mu\nu}$, which is contracted with 4-dimensional gamma matrices, the unphysical ε-dimensional Lorentz structure appears manifestly. Additionally, this term manifestly violates the QED Ward identity, as will be explained in the next section. Hence we

remove it with a counterterm, $\gamma_\mu\delta$, satisfying

$$\delta = -\hat{F}_1. \tag{D.6}$$

Explicit calculations have shown that $\hat{F}_1$ does not depend on q^2, hence we may take the limit $q^2 \to 0$.

An alternate method of deriving such counterterms is to consider the difference in the DREG and DRED Lagrangians and attribute the counterterm to renormalization of fictitious scalars, called ε-scalars, which arise from the difference in the two Lagrangians[44,87]. We do not intend to convert from DRED to DREG in this work, though. Rather, we only add the counterterms necessary to make DRED physically consistent.

Define

$$\int\!\mathcal{D}k = \frac{\mu^{2\varepsilon}}{i}\int\frac{d^nk}{(2\pi)^n}, \quad D = k^2[(k+p_1)^2 - m^2][(k+p_2)^2 - m^2]. \tag{D.7}$$

Then we have

$$\begin{aligned}
M_V &= \bar{u}(p_2)(-ie\gamma^\alpha\mu^\varepsilon)\int\frac{d^nk}{(2\pi)^n}i\frac{\not{k}+\not{p}_2+m}{(k+p_2)^2-m^2}\frac{(-ie\gamma^\mu\mu^\varepsilon)}{ik^2} \\
&\times\ i\frac{\not{k}+\not{p}_1+m}{(k+p_1)^2-m^2}(-ie\gamma_\alpha\mu^\varepsilon)u(p_1)A_\mu(q) \\
&= -ie^3\mu^\varepsilon\bar{u}(p_2)\left\{\underbrace{\gamma^\alpha\gamma^\rho\gamma^\mu\gamma^\sigma\gamma_\alpha}_{-2\gamma^\sigma\gamma^\mu\gamma^\rho}\left[\int\!\mathcal{D}k\frac{(k_\rho+p_{2\rho})(k_\sigma+p_{1\sigma})}{D}\right]\right. \\
&+\ m\overbrace{\gamma^\alpha\gamma^\rho\gamma^\mu\gamma_\alpha}^{4g^{\rho\mu}}\left[\int\!\mathcal{D}k\frac{(k_\rho+p_{2\rho})}{D}\right] + m\underbrace{\gamma^\alpha\gamma^\mu\gamma^\sigma\gamma_\alpha}_{4g^{\mu\sigma}} \\
&+\ \left.m^2\overbrace{\gamma^\alpha\gamma^\mu\gamma_\alpha}^{-2\gamma^\mu}\left[\int\!\mathcal{D}k\frac{1}{D}\right]\right\}u(p_1)A_\mu(q) \\
&= -ie^3\mu^\varepsilon\bar{u}(p_2)\{-2\gamma^\sigma\gamma^\mu\gamma^\rho(C_{\rho\sigma}+p_{1\sigma}C_\rho+p_{2\rho}C_\sigma+p_{2\rho}p_{1\sigma}C_0) \\
&+\ 4mg^{\mu\sigma}[(p_{1\sigma}+p_{2\sigma})C_0+2C_\sigma] - 2m^2\gamma^\mu C_0\}u(p_1)A_\mu(q),
\end{aligned} \tag{D.8}$$

where, in the limit $p_1 \to p_2$,

$$\begin{aligned}
C_0 &\equiv \int \mathcal{D}k \frac{1}{D} \to B_0 = C_\varepsilon \frac{1}{m^2} \frac{1}{2\varepsilon} \\
C^\sigma &\equiv \int \mathcal{D}k \frac{k^\sigma}{D} = C_{11} p_1^\sigma + C_{12} p_2^\sigma \to \frac{B_{11}}{2}(p_1^\sigma + p_2^\sigma), \qquad B_{11} = \frac{C_\varepsilon}{m^2} \\
C^{\sigma\rho} &\equiv \int \mathcal{D}k \frac{k^\sigma k^\rho}{D} = C_{21} p_1^\sigma p_1^\rho + C_{22} p_2^\sigma p_2^\rho + C_{23}(p_1^\sigma p_2^\rho + p_2^\sigma p_1^\rho) + C_{24} g_m^{\sigma\rho} \\
&\to \frac{B_{21}}{4}(p_1^\sigma p_1^\rho + p_2^\sigma p_2^\rho + p_1^\sigma p_2^\rho + p_2^\sigma p_1^\rho) + B_{22} g_m^{\sigma\rho} \\
&\quad (B_{21} = -\frac{1}{2m^2} C_\varepsilon, \qquad B_{22} = \frac{C_\varepsilon}{4} \left\{ \frac{1}{\varepsilon'} \frac{1}{(1-\varepsilon')} \right\}),
\end{aligned} \tag{D.9}$$

where the B_{ij} are calculated (and C_ε is defined) at the end in Appendix D.3. The justification for making the above replacements is that in the limit $p_2 \to p_1$, the 3-point functions reduce to 2-point functions and the coefficients of p_1^σ, p_2^σ must be equal. We still distinguish between p_1 and p_2 at this stage.

Using the relation

$$g_{\sigma\rho}^n \gamma^\sigma \gamma^\mu \gamma^\rho = (2-n)\gamma^\mu - 2\gamma_\varepsilon^\mu \tag{D.10}$$

we may immediately identify

$$\delta = -\hat{F}_1 = -e^2 C_\varepsilon \frac{1}{\varepsilon'} = -\frac{e^2}{(4\pi)^2} \frac{1}{\varepsilon'} + \mathcal{O}(1). \tag{D.11}$$

We may drop the $\mathcal{O}(1)$ term since it multiplies γ_ε^μ, which vanishes in the limit $\varepsilon \to 0$. In higher orders, one might have to keep it though.

We may write explicitly the counterterm for the e-γ vertex graph

$$\gamma^\mu \to -\frac{e^2}{(4\pi)^2} \frac{1}{\varepsilon'} \gamma_\varepsilon^\mu \tag{D.12}$$

(i.e. the Feynman rule for the counterterm is obtained by making the above substitution in the usual rule). For the q-γ vertex, the gluon loop simply gives an overall color factor, C_F:

$$\gamma^\mu \to -C_F \frac{g^2}{(4\pi)^2} \frac{1}{\varepsilon'} \gamma_\varepsilon^\mu \tag{D.13}$$

It is easy to show that the above counterterms hold also for the c-Z and q-Z vertices, respectively.

Let us further evaluate $M_{\rm V}$. Using (D.8) (D.10) and (D.12) (or (D.11)) gives

$$\begin{aligned} M_{\rm V} &= -ic^3\mu^\epsilon \bar{u}(p_2)\{-2\gamma_\sigma\gamma^\mu\gamma_\rho[p_1^\sigma p_2^\rho(\frac{B_{21}}{4}+B_{11}+B_0) \\ &+ p_2^\sigma p_1^\rho(\frac{B_{21}}{4}) + p_1^\sigma p_1^\rho(\frac{B_{21}}{4}+\frac{B_{11}}{2}) + p_2^\sigma p_2^\rho(\frac{B_{21}}{4}+\frac{B_{11}}{2}) + g_n^{\rho\sigma}B_{22}] \\ &- \frac{1}{(4\pi)^2}\frac{1}{\varepsilon'}\gamma_\xi^\mu + 4m(p_1+p_2)^\mu(B_0+B_{11}) - 2m^2\gamma^\mu B_0\}u(p_1)A_\mu(q) \end{aligned} \tag{D.14}$$

We note that

$$\begin{aligned} \gamma^\sigma\gamma^\mu\gamma^\rho &= \gamma^\sigma(-\gamma^\rho\gamma^\mu+2g^{\mu\rho}) = 2\gamma^\sigma g^{\mu\rho} - 2g^{\sigma\rho}\gamma^\mu + \gamma^\rho\gamma^\sigma\gamma^\mu \\ &= 2\gamma^\sigma g^{\mu\rho} - 2g^{\sigma\rho}\gamma^\mu + 2g^{\mu\sigma}\gamma^\rho - \gamma^\rho\gamma^\mu\gamma^\sigma, \end{aligned} \tag{D.15}$$

so that, for general p,

$$\not{p}\gamma^\mu\not{p} = 2\not{p}p^\mu - p^2\gamma^\mu \tag{D.16}$$

and

$$\not{p}_1\gamma^\mu\not{p}_2 = -\not{p}_2\gamma^\mu\not{p}_1 + \underbrace{2\not{p}_1 p_2^\mu + 2\not{p}_2 p_1^\mu}_{-2m(p_1^\mu+p_2^\mu)} - \overbrace{2p_1\cdot p_2}^{-2m^2}\gamma^\mu. \tag{D.17}$$

Using (D.16), (D.17), (D.10) and (D.2) in (D.14) gives

$$\begin{aligned} M_{\rm V} &= 2ic^3\mu^\epsilon\bar{u}(p_2)\{(\frac{B_{21}}{4}+B_{11}+B_0)[(-m^2+4m^2-2m^2)\gamma^\mu + \frac{i}{2m}\sigma^{\mu\nu}q_\nu(-4m^2)] \\ &+ (\frac{B_{21}}{4})(m^2) + (\frac{B_{21}}{4}+\frac{B_{11}}{2})[(4m^2-2m^2)\gamma^\mu + \frac{i}{2m}\sigma^{\mu\nu}q_\nu(-4m^2)] \\ &+ B_{22}(2-n)\gamma^\mu - \frac{1}{2}(B_0+B_{11})[8m^2\gamma^\mu + \frac{i}{2m}\sigma^{\mu\nu}q_\nu(-8m^2)] \\ &+ m^2B_0\gamma^\mu\}u(p_1)A_\mu(q), \end{aligned} \tag{D.18}$$

where we made use of the Dirac equation

$$\bar{u}(\not{p}-m) = (\not{p}-m)u(p) = 0. \tag{D.19}$$

We may write (D.18) in the form

$$\begin{aligned} M_V &= -ie\mu^\varepsilon \bar{u}(p_2)\{(-2e^2)\gamma^\mu[(\frac{B_{21}}{4})(4m^2) \\ &+ B_{11}(-2m^2) + B_0(-2m^2) - 2B_{22}(1-\varepsilon)] \\ &+ (-2e^2)\frac{i}{2m}\sigma^{\mu\nu}q_\nu[(\frac{B_{21}}{4})(-8m^2) + B_{11}(-2m^2)]\}u(p_1)A_\mu(q) \\ &= -ie\mu^\varepsilon \bar{u}(p_2)\{(-2e^2C_\varepsilon)\gamma^\mu\left(-\frac{1}{2} - 2 - \frac{1}{\varepsilon} - \frac{2(1-\varepsilon)}{4\varepsilon'(3-\varepsilon')}\right) \\ &+ (-2e^2C_\varepsilon)\frac{i}{2m}\sigma^{\mu\nu}q_\nu(1-2)\}u(p_1)A_\mu(q) \qquad \text{(D.20)} \\ &= -ie\mu^\varepsilon \bar{u}(p_2)\{\gamma^\mu[e^2C_\varepsilon(\frac{1}{\varepsilon'} + 5 + \frac{2}{\varepsilon})] + \frac{i}{2m}\sigma^{\mu\nu}q_\nu(\frac{\alpha}{2\pi})\}u(p_1)A_\mu(q). \end{aligned}$$

Comparing with (D.5), we obtain

$$F_1(0) = e^2C_\varepsilon(\frac{1}{\varepsilon'} + 5 + \frac{2}{\varepsilon}) \qquad \text{(D.21)}$$

and

$$F_2(0) = \frac{\alpha}{2\pi}. \qquad \text{(D.22)}$$

D.2 Applications: The QED Ward Identity and Electron Anomalous Magnetic Moment

Firstly, we wish to verify the satisfaction fo the QED Ward identity[76]

$$\Lambda_\mu(p,p) = \left.\frac{\partial\Sigma(p)}{\partial p^\mu}\right|_{p^2=m^2} \qquad \text{(D.23)}$$

where $\Sigma(p)$ is the all orders corrected electron self-energy. In 4 dimensions, or in dimensional regularization, the above identity is automatically satisfied by direct differentiation of $\Sigma(p)$. Not so in DRED since the RHS is only defined for $\mu \leq n$, while the LHS is defined for all μ. This means that (D.23) will be satisfied for the first n dimensions, but Λ_μ may have the incorrect structure for the remaining $4-n$ dimensions. $\Lambda_\mu(p,p)$ is required to be proportional to γ_μ since it is γ_μ which occurs in

the vertex *before* corrections and the corrections must preserve that structure to all orders. In the other regularizations, the vertex structure is automatically preserved. For DRED, we must add the counterterm (D.12).

Having eliminated the term $\sim \gamma^\mu$ in (D.5), we may write

$$\bar{u}(p)\Lambda^\mu(p,p)u(p) = F_1(0)\bar{u}(p)\gamma^\mu u(p). \tag{D.24}$$

Hence we associate $F_1(0)$ with the vertex renormalization constant by

$$F_1(0) = -(Z_1 - 1). \tag{D.25}$$

upon definition.

We also know that,

$$\Sigma(p^2 = m^2) + (\text{mass renormalization}) = -(Z_2 - 1)(\not{p} - m). \tag{D.26}$$

Hence (D.23) implies

$$Z_1 = Z_2. \tag{D.27}$$

A direct calculation of $\Sigma(p)$, Taylor expanding about $p^2 = m^2$ (before integrations), lead to

$$Z_2 = 1 - e^2 C_\varepsilon(\frac{1}{\varepsilon'} + 5 + \frac{2}{\varepsilon}). \tag{D.28}$$

Substituting (D.21) in (D.25), we see that the Ward identity (D.27) is indeed satisfied.

Also, $F_2(0)$ is just the anomalous magnetic moment of the electron. From Eq. D.22, the value is seen to be the correct one.

D.3 Necessary Integrals

Here we derive the integrals used in this appendix. Define

$$B_{0,\mu,\mu\nu} = \frac{\mu^{2\varepsilon}}{i}\int \frac{d^n q}{(2\pi)^n} \frac{1, q_\mu, q_\mu q_\nu}{q^2[(p+q)^2 - m^2]^2}, \quad p^2 = m^2. \tag{D.29}$$

Using Feynman parameters, we may write

$$\begin{aligned}\frac{1}{q^2[(p+q)^2-m^2]^2} &= 2\int_0^1 dy\, y \int_0^1 dx \frac{1}{[(2q\cdot p+q^2)yx+q^2(1-y)+(2q\cdot p+q^2)y(1-x)]^3} \\ &= 2\int_0^1 dy\, y \int_0^1 dx \frac{1}{[q^2+q'_\mu(2p^\mu y)]^3} \\ &= 2\int_0^1 dy\, y \frac{1}{(q'^2-m^2y^2)^3}, \quad q'_\mu \equiv q_\mu + p_\mu y. \end{aligned} \tag{D.30}$$

Defining

$$B_\mu = B_{11}p_\mu, \quad B_{\mu\nu} = p_\mu p_\nu B_{21} + g''_{\mu\nu}B_{22}, \tag{D.31}$$

we see that

$$\begin{aligned} B_0, B_{11}, B_{21} &= 2\int_0^1 dy\, y\{1,-y,y^2\}\left[\frac{\mu^{2\varepsilon}}{i}\int\frac{d^nq'}{(2\pi)^n}\frac{1}{(q'^2-m^2y^2)^3}\right] \\ &= 2\int_0^1 dy\, y\{1,-y,y^2\}\left[-\frac{1}{(4\pi)^2}\left(\frac{4\pi\mu^2}{m^2}\right)^\varepsilon \frac{1}{m^2y^{2+2\varepsilon}}\frac{1}{2}\Gamma(1+\varepsilon)\right] \\ &= -\frac{1}{(4\pi)^2}\left(\frac{4\pi\mu^2}{m^2}\right)^\varepsilon \frac{1}{m^2}\Gamma(1+\varepsilon)\int_0^1 dy\{\underbrace{y^{-1-2\varepsilon}}_{-1/2\varepsilon}, \underbrace{-y^{-2\varepsilon}}_{-1/(1-2\varepsilon)}, \underbrace{y^{1-2\varepsilon}}_{1/2(1-\varepsilon)}\}. \end{aligned} \tag{D.32}$$

Thus

$$B_0, B_{11}, B_{21} = \overbrace{\frac{1}{(4\pi)^2}\left(\frac{4\pi\mu^2}{m^2}\right)^\varepsilon \Gamma(1+\varepsilon)}^{C_\varepsilon}\frac{1}{m^2}\left\{\frac{1}{2\varepsilon}, \frac{1}{1-2\varepsilon}, \frac{-1}{2(1-\varepsilon)}\right\}. \tag{D.33}$$

Also

$$\begin{aligned} B_{22} &= \frac{2}{n}\int_0^1 dyy\left[\frac{\mu^{2\varepsilon}}{i}\int\frac{d^nq'}{(2\pi)^n}\frac{q'^2}{(q'^2-m^2y^2)^3}\right] = \frac{2}{n}\int_0^1 dyy\left[\frac{1}{(4\pi)^2}\left(\frac{4\pi\mu^2}{m^2}\right)^\varepsilon y^{-2\varepsilon}\right. \\ &\times \left.\underbrace{\Gamma(3-\varepsilon)\Gamma(\varepsilon)/\Gamma(2-\varepsilon)}_{(2-\varepsilon)\Gamma(1+\varepsilon)/\varepsilon}\frac{1}{2}\right], \end{aligned} \tag{D.34}$$

giving

$$B_{22} = \frac{C_\varepsilon}{4}\left\{\frac{1}{\varepsilon'}\frac{1}{(1-\varepsilon')}\right\}. \tag{D.35}$$

References

[1] Review of Particle Properties, *Phys. Rev.* **D50** (1994) 1.

[2] F. Abe et al. (CDF Collab.), Phys. Rev. **D50** (1994) 2966; Phys. Rev. Lett. **73** (1994) 225; **74** (1995) 2626; S. Abachi et. al. (D0 Collab.), *ibid* **74** (1995) 2632.

[3] C. Itzykson and J.B. Zuber, *Quantum Field Theory* (McGraw–Hill, 1980).

[4] L.D. Faddeev and V.N. Popov, *Phys. Lett.* **B25** (1967) 29.

[5] R.P. Feynman, *Rev. Mod. Phys.* **20** (1948) 367; P.A.M. Dirac, *Rev. Mod. Phys.* **17** (1945) 195.

[6] W. Heisenberg and W. Pauli, *Z. Phys.* **56** (1929) 1; **59** (1930) 168.

[7] C. Becchi, A. Rouet and R. Stora, *Ann. Phys.* **98** (1976) 287.

[8] J.D. Bjorken, *Phys. Rev.* **179** (1969) 1547.

[9] J.D. Bjorken and E.A. Paschos, *Phys. Rev.* **185** (1969) 1975.

[10] R.P. Feynman, *Photon–Hadron Interactions* (Benjamin, New York 1972).

[11] J. Ashman et al. (European Muon Collab.), *Phys. Lett.* **B206** (1988) 364; *Nucl. Phys.* **B328** (1989) 1.

[12] M.J. Alguard et al., *Phys. Rev. Lett.* **37** (1976) 1261; **41** (1978) 70; G. Baum et al., *Phys. Rev. Lett.* **51** (1983) 1135.

[13] B.L. Ioffe, V.A. Khoze and L.N. Lipatov, *Hard Processes, Vol1, Phenomenology / Quark-Parton Model* (North Holland, 1984).

[14] E. Leader and E. Predazzi, *An Introduction to Gauge Theories and The New Physics* (Cambridge University Press, 1982).

[15] J.D. Bjorken, *Phys. Rev.* **148** (1966) 1467; **D1** (1970) 1376.

[16] S.A. Larin and J.A.M. Vermaseren, *Phys. Lett.* **B259** (1991) 345 and references therein.

[17] J. Ellis and R. Jaffe, *Phys. Rev.* **D9** (1974) 1444; erratum **D10** (1974) 1669.

[18] F.E. Close and R.G. Roberts, *Phys. Lett.* **B316** (1993) 165.

[19] S.A. Larin, *Phys. Lett.* **B334** (1994) 192.

[20] B. Adeva et al., *Phys. Lett.* **B302** (1993) 533.

[21] D.L. Anthony et al., *Phys. Rev. Lett.* **71** (1993) 959.

[22] B. Adeva et al., *Phys. Lett.* **B320** (1994) 400.

[23] RHIC Spin Collaboration, Updated Proposal, September 1993.

[24] H. Huang et al., *Phys. Rev. Lett.* **73** (1994) 2982. A second run achieved 25 GeV.

[25] Proceedings of the LC '92 ECFA Workshop on e^+e^- Linear Colliders (July 25 - August 2, 1993, Germany), MPI-PhE/93-14, ECFA 93-154.

[26] E.L. Saldin et al., DESY 94-243 and references therein.

[27] G. Altarelli and W.J. Stirling, *Particle World* **1** (1989) 40.

[28] T. Gehrmann and W.J. Stirling, Durham report DTP/94/82.

[29] J. Morfin and W.K. Tung, *Z. Phys.* **C52** (1991) 13.

[30] F. Bloch and A. Nordsieck, *Phys. Rev.* **52** (1937) 54; A. Nordsieck, *Phys. Rev.* **52** (1937) 59.

[31] W. Vogelsang, *Z. Phys.* **C50** (1991) 275.

[32] W. Pauli and F. Villars, *Rev. Mod. Phys.* **21** (1949) 434.

[33] G. t'Hooft, *Nucl. Phys.* **B33** (1971) 173.

[34] E.R. Speer, *J. Math. Phys.* **9** (1968) 1404; E.R. Speer, *Generalized Feynman Amplitudes* (Princeton Univ. Press, 1969); C.G. Bollini, J.J. Giambiagi and A. Gonzales Dominguez, *Nuovo Cim.* **31** (1964) 550.

[35] W.J. Marciano, *Phys. Rev.* **D12** (1975) 3861.

[36] G. 't Hooft and M. Veltman, *Nucl. Phys.* **B44** (1972) 189.

[37] C.G. Bollini and J.J. Giambiagi, *Nuovo Cim.* **B12** (1972) 20; *Phys. Lett.* **B40** (1972) 566.

[38] A.P. Contogouris, S. Papadopoulos and F.V. Tkachov, *Phys. Rev.* **D46** (1992) 2846 and *Proceed. of Joint Internat. Lepton-Photon Symposium & Europhysics Conf. on H.E. Physics*, Geneva, 1991 (World Scientific, 1992), Vol. 1, p. 450.

[39] M. Chanowitz, M. Furman and I. Hinchliffe, *Nucl. Phys.* **B159** (1979) 225.

[40] P. Breitenlohner and D. Maison, *Commun. Math. Phys.* **52** (1977) 11.

[41] M. Jamin and M.E. Lautenbacher, *Tracer* (Version 1.1), TU München report TUM-T31-20/91.

[42] W. Siegel, *Phys. Lett.* **B84** (1979) 193.

[43] W. Siegel, *Phys. Lett.* **B94** (1980) 37; R. Grigjanis, P.J. O'Donnell, H. Navelet and M. Sutherland, *ibid* **B237** (1990) 252; L. Adveev and A. Vladimirov, *Nucl. Phys.* **B219** (1983) 262.

[44] I. Jack, D.R.T. Jones and K.L. Roberts, *Z. Phys.* **C62** (1994) 161; **C63** (1994) 151; M. Cinchini, E. Franco, L. Reina, and L. Silvestrini, *Nucl. Phys.* **B421** (1994) 41.

[45] T. Kinoshita, *J. Math. Phys.* **3** (1962) 650; T.D. Lee and M. Nauenberg, *Phys. Rev.* **133** (1964) B1549.

[46] F.J. Dyson, *Phys. Rev.* **75** (1949) 1736.

[47] T. Muta, *Foundations of Quantum Chromodynamics* (World Scientific, 1987).

[48] J.C. Taylor, *Nucl. Phys.* **B33** (1971) 436; A.A. Slavnov, *Teor. Mat. Fiz.* **10** (1972) 153 [*Theor. Math. Phys.* **10** (1972) 99)].

[49] G. 't Hooft, *Nucl. Phys.* **B61** (1973) 455.

[50] W.A. Bardeen, A.J. Buras, D.W. Duke and T. Muta, *Phys. Rev.* **D18** (1978) 3998.

[51] R.K. Ellis, M.A. Furman, H.E. Haber, and I. Hinchliffe, *Nucl. Phys.* **B173** (1980) 397.

[52] S. Weinberg, *Phys. Rev.* **D8** (1973) 3497; M.J. Holwerda, W.L. van Neerven and R.P. van Royen, *Nucl. Phys.* **B75** (1974) 302; J.C. Collins and A.J. Macfarlane, *Phys. Rev.* **D10** (1974) 1201.

[53] G. Altarelli and G. Parisi, *Nucl. Phys.* **B126** (1977) 298.

[54] X. Artru and M. Mekhfi, *Z. Phys.* **C45** (1990) 669.

[55] V.N. Gribov and L.N. Lipatov, *Yad. Fiz.* **15** (1972) 781, 1218 [*Sov. J. of Nucl. Phys.* **15** (1972) 438, 675]; L.N. Lipatov, *Yad. Fiz.* **20** (1975) 181 [*Sov. J. of Nucl. Phys.* **20** (1975) 94]; Yu. L. Dokshitzer, *ZhETF* **73** (1977) 1216 [*JETP* **46** (1977) 641].

[56] J. Huston, *Proceed. of XIV Internat. Symposium on Lepton and Photon Interactions at H.E.*, Stanford, California, 1989, ed. M. Riordan (World Scientific, Singapore, 1990); *Proceed. of Advanced Research Workshop on QCD Hard Hadronic Processes*, St. Croix, 1987, ed. B. Cox (Plenum, New York, 1987), pp. 81, 519.

[57] P. Ratcliffe, *Nucl. Phys.* **B223** (1983) 45.

[58] A. Efremov and O. Terayev, Dubna report E2-88-287 (unpublished); *Phys. Lett.* **B240** (1990) 200; G. Altarelli and G. Ross, *Phys. Lett.* **B212** (1988) 391; R. Carlitz, J. Collins and A. Mueller, *Phys. Lett.* **B214** (1988) 229.

[59] E. Berger and J. Qiu, *Phys. Rev.* **D40** (1989) 778 and 3128; S. Gupta, D. Indumathi and M. Murthy, *Z. Phys.* **C42** (1989) 493; H.-Y. Cheng and S.-N. Lai, *Phys. Rev.* **D41** (1990) 91; A.P. Contogouris, S. Papadopoulos and B. Kamal, *Nucl. Phys.* (Proc. Suppl.) **B23** (1991) 119.

[60] A.P. Contogouris and S. Papadopoulos, *Phys. Lett.* **B260** (1991) 204.

[61] A.P. Contogouris, S. Papadopoulos and B. Kamal, *Phys. Lett.* **B246** (1990) 523; M. Doncheski and R. Robinett, *Phys. Lett.* **B248** (1990) 188; J.L. Cortes and B. Pire, *Phys. Rev.* **D38** (1988) 3586; M.A. Doncheski and R.W. Robinett, *Z. Phys.* **C63** (1994) 611.

[62] A.D. Watson, *Z. Phys.* **C12** (1982) 123; J. Ph. Guillet, *Z. Phys.* **C39** (1988) 75; M. Glück and E. Reya, *Z. Phys.* **C39** (1988) 569; M. Glück, E. Reya and W. Vogelsang, *Nucl. Phys.* **B351** (1991) 579.

[63] J.J. Peralta, A.P. Contogouris, B. Kamal and F. Lebessis, *Phys. Rev.* **D49** (1994) 3148.

[64] N.S. Craigie, K. Hikada, M. Jacob, A. Penzo and J. Soffer, *Nucl. Phys.* **B204** (1982) 365; W. Vogelsang, *Phys. Rev.* **D50** (1994) 4436.

[65] A.P. Contogouris, B. Kamal, Z. Merebashvili and F.V. Tkachov, *Phys. Lett.* **B304** (1993) 329; *Phys. Rev.* **D48** (1993) 4092.

[66] L.E. Gordon and W. Vogelsang, *Phys. Rev.* **D48** (1993) 3136; **D49** (1994) 170.

[67] P. Aurenche et al., *Nucl. Phys.* **B286** (1987) 553; **B297** (1988) 661; *Phys. Rev.* **D42** (1990) 1440 and computer outputs.

[68] A.P. Contogouris, S. Papadopoulos et al. (a) *Int. J. Mod. Phys.* **A5** (1990) 1951; (b) *Mod. Phys. Lett.* **A5** (1990) 901; (c) *Theoret. and Mathem. Phys.* **87** (1991) 62.

[69] F. Berends et al. *Phys. Lett.* **B103** (1981) 124.

[70] F. Berends et al., *Nucl. Phys.* **B206** (1982) 61; I. Avaliani, Z. Merebashvili and L. Slepchenko, *Z. Phys.* **C50** (1991) 473; V. Matveev et al., *Phys. Lett.* **B206** (1988) 127.

[71] M. Gluck, E. Reya and A. Vogt, *Phys. Rev.* **D48** (1993) 116.

[72] W. Vogelsang, private communication.

[73] X. Ji, *Phys. Lett.* **B284** (1992) 137; J. Ralston and D. Soper, *Nucl. Phys.* **B152** (1979) 109; J. Cortes et al, *Z. Phys.* **C55** (1992) 409; G. Bunce et al., *Particle World* **3** (1992) 1; and references cited therein.

[74] W. Vogelsang and A. Weber, *Phys. Rev.* **D48** (1993) 2073.

[75] A.P. Contogouris, B. Kamal and Z. Merebashvili, *Phys. Lett.* **B337** (1994) 169.

[76] J.C. Ward, *Phys. Rev.* **78** (1950) 182.

[77] G. Altarelli, R.K. Ellis and G. Martinelli, *Nucl. Phys.* **B157** (1979) 461.

[78] J. Soffer, *Phys. Rev. Lett.* **74** (1995) 1292.

[79] G.R. Goldstein, R.L. Jaffe and X. Ji, MIT report MIT-CTP-2402.

[80] P. Nason, S. Dawson, and R.K. Ellis, *Nucl. Phys.* **B303** (1988) 607; **B327** (1989) 49 and erratum **B335** (1990) 260.

[81] W. Beenakker, H. Kuijf, W.L. van Neerven, and J. Smith, *Phys. Rev.* **D40** (1989) 54; W. Beenakker, W.L. van Neerven, R. Meng, G.A. Schuler and J. Smith, *Nucl. Phys.* **B351** (1991) 507.

[82] J. Smith and W.L. van Neerven, *Nucl. Phys.* **B374** (1992) 36; J.H. Kühn, E. Mirkes, and J. Steegborn, *Z. Phys.* **C57** (1993) 615; M. Drees, M. Krämer, J. Zunft, and P.M. Zerwas, *Phys. Lett.* **B306** (1993) 371.

[83] B. Kamal, Z. Merebashvili and A.P. Contogouris, *Phys. Rev.* **D51** (1995) 4808.

[84] J.F. Gunion and H.E. Haber, *Phys. Rev.* **D48** (1993) 5109.

[85] D.L. Borden, V.A. Khoze, J. Ohnemus, and W.J. Stirling, *Phys. Rev.* **D50** (1994) 4499.

[86] A.P. Contogouris, O. Korakianitis, F. Lebessis, and Z. Merebashvili, *Phys. Lett.* **B344** (1995) 370.

[87] G.A. Schuler, S. Sakakibara, and J.G. Körner, *Phys. Lett.* **B194** (1987) 125; J.G. Körner and M.M. Tung, *Z. Phys.* **C64** (1994) 255.

[88] P.J. O'Donnell and H.K. Tung, *Phys. Rev.* **D45** (1992) 4342.

[89] G. Passarino and M. Veltman, *Nucl. Phys.* **B160** (1979) 151.

[90] J. Vermaseren, FORM User's Manual, NIKHEF-H, Amsterdam, 1990.

[91] A.C. Hearn, REDUCE User's Manual Version 3.3 (Rand Corporation, Santa Monica, CA, 1987).

[92] TOPAZ Collab., M. Iwasaki et al., KEK report 94-109, October 1994.